Theses and Dissertations

August 2017

A Theoretical Analysis on the Zintl-klemm Concept and Its Extensions

Sandra Maria Simon
University of Wisconsin-Milwaukee

Recommended Citation

A THEORETICAL ANALYSIS ON THE ZINTL-KLEMM CONCEPT AND ITS EXTENSIONS

by

Sandra Maria Simon

A Dissertation Submitted in

Partial Fulfillment of the

Requirements for the Degree of

Doctor of Philosophy

in Chemistry

at

The University of Wisconsin-Milwaukee

August 2017

ABSTRACT

A THEORETICAL ANALYSIS ON THE ZINTL-KLEMM CONCEPT AND ITS EXTENSIONS

by

Sandra Maria Simon

The University of Wisconsin-Milwaukee, 2017
Under the Supervision of Dennis W. Bennett

The desire to rationalize and explain the complex structures that form in solid states has motivated many to explore collections of structures with similar topologies but with differing compositions in order to determine whether or not similar chemical bonding was responsible for the structures. The Zintl-Klemm Concept, the Extended Zintl-Klemm Concept Model-1, and the Extended Zintl-Klemm Concept Model-2 attempt to rationalize and predict the structure of a group of intermetallics, referred to as Zintl Compounds, and their oxides based on simple electron counting schemes and with the introduction of pseudo-atoms. This study looks at the electronic structure of a set of Zintl Compounds and their oxides in order to determine if the internal electronic structure of these solids mirror the predictive models used to rationalize their structure and the behavior exhibited in terms of the pseudo-atom approach used to arrive at the physical structure of the solid. The electronic structure was attained by analyzing the charge density from three *ab initio* DFT programs via the Laplacian, the Bader Charges (by applying Bader's Atoms in Molecules Analysis), and difference charge densities. The three programs utilized in this study were: FLAIR, CRYSTAL14, and VASP. Both FLAIR and CRYSTAL14 are all-electron programs that take advantage of a crystal's symmetry to arrive at convergence. While FLAIR is a Full-potential Linearized Augmented Plane Wave (FLAPW) program, CRYSTAL14 is a molecular orbital computational program, using atomic basis sets to model the atoms in the crystal and calculate the wave functions. VASP, while also using plane wave basis sets, approximates the core electron

density with pseudo-potentials – therefore using only the valence electrons when calculating the electron density. These three programs were used to verify if computational bias was present within the results attained in the analysis of these solids. The comparison between programs demonstrated that even though different computational methods were used, the information was largely equivalent, imparting the same information for the solids compared. The theoretical analysis on the concepts determined that the Zintl-Klemm Concept and the Extended Zintl-Klemm Concept Model-1 were able to adequately rationalize the bonding and pseudo-atom behavior proposed, but that when examining the oxides the bonding posited by the Extended Zintl-Klemm Concept Model-2 was not seen. In other words, the electronic structure in the solids analyzed with the Zintl-Klemm Concept and the Extended Zintl-Klemm Concept Model-1 mirrored the rationalizations used to explain the physical structure of these solids and their behavior. While assessing these solids, unexpected and unusual behavior was observed with solids containing calcium. The calcium atoms within the structures seemed to acquire charge, becoming anionic. This behavior was seen even in the presence of oxygen.

Dedicated To:

The memory of my father and to

my mother, who has been a constant

in my life.

TABLE OF CONTENTS

LIST OF FIGURES

LIST OF TABLES

ACKNOWLEDGMENTS

The journey to become a scientist is a long and challenging one, though not one that is navigated alone. Although this was a path I chose, I could could not have accomplished it without support.

I would first like to thank my Professor, Dr. Bennett. I look at the years I have been under his tutelage and feel that I could not have gotten anyone better. He has always been what a mentor should be: supportive, yet always challenging me in the ways I needed to be so that I could develop both professionally and personally. I will always be appreciative because I would not be who I am today without the time and effort he expended on my behalf.

I would also like to thank the rest of my committee, Dr. Dietz, Dr. Geissinger, Dr. Pacheco, and Dr. Woehl, who have not only supported me throughout this project but have also been my Professors through the majority of the chemistry courses I have taken since I first decided to study chemistry. It was in their classes that I learned to love chemistry. That is something without measure, so thank you for providing the opportunity for me to learn and love science.

Along with my committee I owe the department my gratitude. In the years I have been here, the department has been my other home. The unending support I have received provided me with the ability to complete my academic career. Dr. Sorensen was always ready to lend a hand or an ear and would go from putting my computer back together to listening to my life crises. He was always there for when I needed advice and, as a grad student, it seemed to cover a realm of topics.

In the Physics Department, I would like to thank Dr. Weinert for all his help and support with FLAIR. To the CRYSTAL14 team who patiently answered all my questions even from across the globe, thank you.

Thanks are also due to the wonderful staff in the UWM Writing Center, who as I type are checking for any grammatical mistakes. The writing of this dissertation would have been a more harrowing experience without them.

As for the financial burden that fell on me during this process, I would like to thank the Chemistry Department and the Life Impact Program.

On a personal note, I would like to thank my friends and family. My sister and my mother have been constant supporters of my goals. They kept me grounded and focused, and I could not have done it without their amazing cheerleading skills. My son, who is an

absolute angel, has been my inspiration since the day he was born. He is beyond amazing and it is because of him that I was inspired to be and do more. To my friends, Veronica Marco and Shalini Srinivasan, you guys are the absolute best. I look back at all those nights we spent studying, researching, brainstorming, grading, *et cetera* while eating pizza, watching those amazingly hilarious awful movies in the background (e.g. *Nazis at the Center of the Earth*...reviewers say, "If I could give it zero stars, I would!"), and drinking so much coffee that we didn't have to sleep for days. I know that it is because of you guys that grad school was so much fun.

Chapter 1

Introduction

Chemical bonding is the central tenet of chemical science. Original models for chemical bonding began with elegant and simple electron counting schemes that have served as the basis for many of the predictive tools still used in chemistry today.

Over the past 20 years, modern quantum chemistry has served to update, explain, modify, and sometimes replace these models for molecular systems. Until recently, the complexity of extended systems, covalent, metallic, and ionic solids, has made it difficult to apply rigorous quantum computational analysis, but the advent of more powerful software and vastly more powerful computers has changed all of that. For the first time, modern computational models are allowing us to peer inside these extended structures and analyze their relationships to the simpler bonding models that have been applied to them over the years, just as we have been able to do with molecules.

This dissertation is a report of the results of an application of these new quantum mechanical tools to an important class of compounds known as Zintl compounds. These compounds do not fit neatly into the currently accepted "covalent", "metallic", and "ionic" bonding classifications, and research attempting to explain their behavior has resulted in schemes analogous to those used for molecular systems. The most famous of these is known as the Zintl-Klemm concept. This document reports an analysis of the Zintl-Klemm concept and its extensions using modern quantum chemistry tools.

In order to explain the Zintl compounds, scientists have had to use a combination of the simple bonding formalisms to adequately describe the bonding and behavior these compounds exhibit. The concept of bonding is essential to chemistry, with all bonds originating from electrostatic forces – forces described quantitatively by Coulomb's Law – undoubtedly the central law of chemistry. As such, the bonding formalisms, commonly known as ionic, covalent, polar covalent, and metallic, all describe the various ways the negative charge and positive charge interact within a bond. When using these formalisms to explain complicated

structures, these formalisms must be used qualitatively and in terms of their idealized definition, such that if one were to classify a structure as ionic, it is understood that electronic charge is being completely transferred from cation to anion. However, even though this is not the case, as even our idealized ionic structures (e.g. NaCl) are not completely ionic, this method of assuming ideal circumstances helps one understand the mechanism of the bonds within the structure and predict physical properties. Hence, structures identified as covalent extended solids assume that charge is not being transferred but is gathered between nuclei and both nuclei are then held together by an equal "sharing" of the localized charge. Polar covalent bonding indicates that while there is charge gathered between the two nuclei, it is not shared equally but that one atom in the bonding pair has the electronic charge gathered more closely around it than the other. Lastly, metallic charges, similar to covalent bonds, have charge gathered between the metal nuclei with less localization, which allows for the metallic property of conductivity. Some idealized extended solids, such as sodium chloride, diamond, or copper, can be easily classified as ionic, covalent, or metallic, respectively, and the physical properties exhibited by these solids correspond to the representative behavior of these classifications. However, many solids are not so easily classified and display behavior that falls within a spectrum of these simple bonding formalisms. This can be visualized by the Van Arkel-Ketelaar triangle.
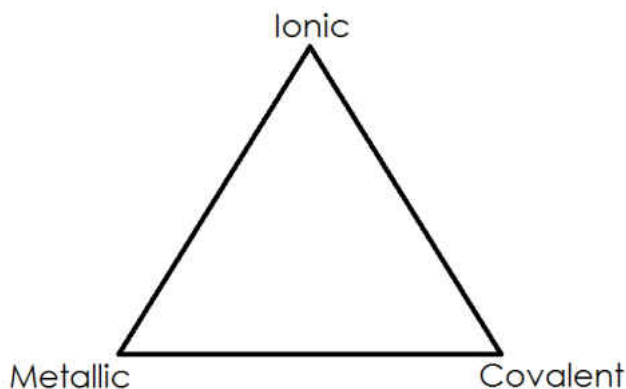
Figure 1.1: Van Arkel-Ketelaar Triangle

Therefore, in order to understand some of the more complicated extended systems, like the Zintl compounds, a combination of the traditional formalisms must be used to describe these solids. One can see in figure 1.2, that these solids lie between the idealized metal and ionic solid.
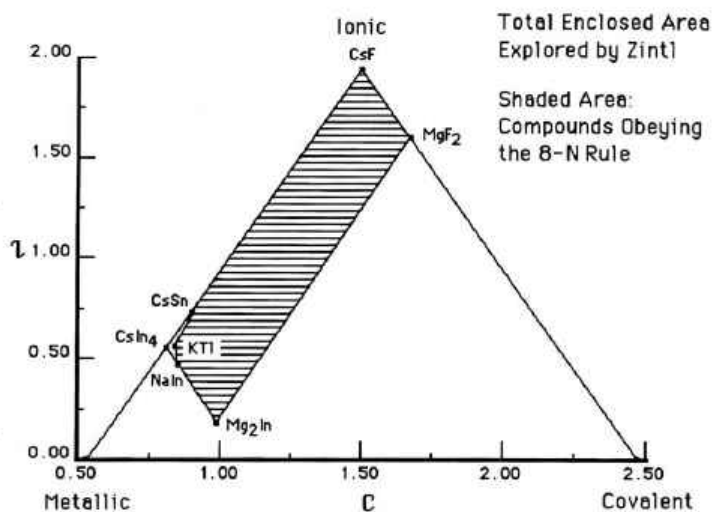
Figure 1.2: Van Arkel-Ketelaar Triangle[46]

These Zintl-Klemm compounds were first studied because of the behavioral discrepancies seen in comparison to other intermetallics. These compounds, comprised of only metals, usually Group I or Group II with metals from Group XIII and XIV, are generally semiconductors and can dissolve in polar basic solvents[48]. Since these were properties not found in traditionally characterized metallic compounds, the Zintl-Klemm Concept was introduced to explain, rationalize and even predict these structures. Following on the success of the Zintl-Klemm concept, attempts have been made to extend this concept and encompass other intermetallics and their oxides.

However, the problem lies in being able to assess the connection between the internal electronic structure and these simple bonding formalisms in relation to the the Zintl-Klemm Concept and its extensions. While, these concepts attempt to rationalize and predict the external structure of the extended solid, and successfully, in many documented cases[31,101], the internal electronic structure has not been given enough of a focus in comparison to the amount of literature published on the external structures. With modern quantum mechanical tools we can now begin the task of investigating the concept's ability to predict the external structure of a solid, in terms of the internal electronic structure, which should logically mirror the predictive measures that were used to determine and rationalize its external structure, giving better insight into the bonding found within.

Chapter 2

Literature Review

This chapter will describe and explain the formation of the Zintl Klemm Concept(ZKC), the original extension of this concept, the Extended Zintl-Klemm Model 1 (EZKC-1) and the second extension to this extension, the Extended Zintl-Klemm Model 2 (EZKC-2), and how they relate to extended solids. There is a substantial body of literature that forms the basis for the work described here; this chapter will summarize the essential elements of that literature.

Since the inception of the Zintl-Klemm Concept and its extensions, there has been some disorganization in connecting the correct concept to the correctly classified extended solid. The confusion is compounded at the existence of two different extensions to the Zintl-Klemm concept but both are named the same, implying that both concepts' criteria are the same and that they function the same way as well. An example of this can be seen in the article "Revisiting the Zintl–Klemm Concept: A2AuBi (A= Li or Na)"[105], which is investigating ternary intermetallics that include a transition metal and a late main group metal. Based on each model's criteria, these intermetallics classify under the purview of the Extended Zintl-Klemm Concept Model 1, yet the study being performed suggests that it will be analyzed as being part of the original Zintl-Klemm concept and being examined under the parameters set by that particular concept. A goal for this literature review is to help dispel any confusion about what classifies an extended solid for each particular model. Since the objective of this project is to examine the internal electronic structure in terms of these concepts, it is essential that this review also covers the mathematical tools, and their application in relation to the chemical bond, being used to assess each extended solid under review. Therefore, the literature review will clarify the need to use Bader's Atom in Molecules Theory, the Laplacian of the Charge Density, and the Charge Difference Density to inspect and understand these solids.

2.1 Zintl-Klemm Concept

Before the Zintl-Klemm Concept (ZKC) was introduced, a few things occurred that led to the birth of this concept. First, dating back to 1891[17], A. Joannis reported structures of $NaPb_4$ and $NaPb_2$, products of sodium in ammonia with other metals, a procedure that would come to be used frequently when synthesizing what are known as Zintl compounds from Zintl anions[63]. The next development occurred in 1916, when Gilbert N. Lewis published his article "The Atom and the Molecule"[54]. He introduced the idea of the (8-N) rule, a conceptual electron valence counting scheme that allows for a simplified, yet useful, mechanism for predicting the possible structures of molecules. This would become "indispensable" to the Zintl-Klemm concept and its extensions[67]. By 1929, Eduard Zintl began to study a class of binary intermetallics that consisted of Group I or Group II with metals from Group XIII and XIV (known as the Zintl border)[64]. He proposed the idea that, in these extended binary solids, there was a charge transfer between the least electronegative metal to the more electronegative metal. These intermetallics have come to be known as Zintl compounds. However, it was not until Klemm formalized Zintl's idea to encompass the (8-N) rule and introduce the concept of the pseudo-atom, that today's Zintl-Klemm Concept (ZKC) became what we know it as today. ZKC attempts to explain, rationalize and predict structures based on the (8-N) rule and the pseudo-atom approach, and while it might be a "fuzzy approach"[64], as stated in the literature, it is functional. Its ability to be functional, while still remaining relatively simple to apply, can be supported by the many structures stated to be successfully predicted in studies that involve the synthesis of Zintl compounds when implementing the (8-N) rule, and there is a general consensus that the predictive aspect of the concept works.

The ZKC ascertains that there is an electronic transfer, like in a traditional ionic solid, where the less electronegative element donates its electrons to the more electronegative element, which then becomes anionic. In the case of these intermetallics, the metal from Group I or II donates to the metal in either Group XIII and XIV, also known as Zintl anions. This transfer constitutes the ionic part of the bonding in these extended solids. However, the (8-N) rule and the pseudo-atom approach highlight the covalent bonding aspect found within these solids. The first exercise that must be undertaken is to determine the pseudo-atom that the Zintl anion will pack and bond like. This determination can be accomplished by looking at the isoelectronic nonmetal/metalloid of the Zintl anion, with the closest electronegativity to that exhibited by the anionic metal. For example, if considering the compound LiAl, the lithium would donate the traditional one electron to make an aluminum anion, Al^{-1}. The aluminum anion, isoelectronic to the elements in Group XIV, is considered a pseudo-silicon,

since silicon, with an electronegativity of 1.8, is closest in value to aluminum's electronegativity value of 1.5. The figure 2.1 depicts how a pseudo-atom becomes isoelectronic with different elements as electrons get transferred to it.
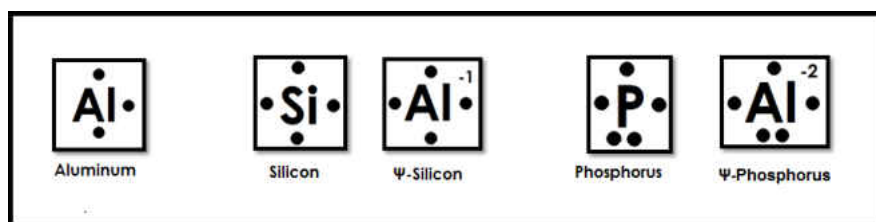
Figure 2.1: Pseudo-Atom

Once the pseudo-atom has been determined, the lattice formed within the extended solid by the Zintl anion will both pack and bond like the described pseudo-atom. So following the LiAl example, the aluminum which becomes a pseudo-silicon because of its -1 charge, will contain an aluminum lattice that is structurally similar to that of elemental silicon and will form covalent bonds similar to those found between silicon-silicon structures.

This concept, conceived as a response to intermetallics that exhibited unlikely behaviors, has proven successful, especially in its simplicity yet functionality. The only disadvantage that this concept has suffered from was that at the time of its creation, other than examining the physical structure, analysis on the internal electronic structure was not possible. The lack of available technology forced this concept and future extensions to shift the focus from expanding on the bonding theories posed by Zintl & Klemm to the ability to predict the external structure, where the structural information was used as a guide for predictive measures. The shift in focus to the physical structure of the extended solids can be be seen as the effect of the success of the technological and chemical advances of the time that emphasize the external structure such as, "The results of X-ray crystal structure determinations [that] have assumed a great significance in discussions of the bonding in these phases.[48]", due to 30 years (1960-1990) of successful synthesis of Zintl phases[64].

However, by the mid 1980's, scientists performed quantum calculations on Zintl compounds, allowing more complicated Zintl systems to be better understood. Unfortunately, these calculations were hindered by the lack of computational power of the time. These calculations originally were performed on both cluster and band structures[64]. More recently, there has been a growing interest in modeling these solids using atom/molecule computational methods to gather more insight into these solids and the concepts behind them; most recently studies have been presented by Miller and Wang[106,105] and Evers[25]. They performed VASP, LMTO, and IDOS calculations on a variety of compounds that fall within the Zintl-Klemm concept in assessment of the concept and its application to those solids.

Miller and Wand performed total energy calculations, which were then partitioned, in order to calculate the electronic contribution and to determine the metallic character of the bond. The conclusion, supporting what many in the literature stated, was that was that while the ZKC is simplistic, it does an adequate job at rationalizing many structures. However, there are notable exceptions found within the study, such as LiTl and KTl[95,98]. It was determined that while there is a covalent nature to the bonds, these structures should not be rationalized solely on the covalent aspect of the concept but in terms of the metallic and ionic effects as well.[106].

2.2   Extended Zintl-Klemm Concept

Traditionally, Zintl compounds have been primarily binary in composition and classified as semi conductors, but this idea was expanded to include ternary compounds as well as compounds with more metallic properties between the mid 1980's and mid 1990's[17,90,99]. Since the Zintl-Klemm concept was successful in predicting and explaining many extended solids, extending the concept to include other intermetallics appeared to be like a natural progression. This began by the inclusion of ternary compounds, which allowed polyatomic zintl anions as well as transition metals and heavy post transition metals, to be considered, which would eventually lead to the concept being officially extended by Hoffman[64,44] into 'The Extended Zintl-Klemm Concept' Model 1 (EZKC-1); Wade and Mingos actually had begun this extension years prior[107]. The second 'Extended Zintl-Klemm Concept' Model 2 (EZKC-2) is attributed to Vegas[101] and his works, which includes traditional Zintl compounds as well as many of their oxides. This inclusion by Hoffman and Vegas widened what had been a very small class of compounds into a wide range of solids, which now include non-metals. This expansion of what classifies a Zintl compound has been part of a confusing transition since what was once the specific name 'Zintl compound' has become generic. Along with vagueness that is found in the name 'Zintl compounds', the differing extensions (that are both named identically) claim to be part of the same extension. This confusion can be exacerbated by the varying criteria each extension utilizes to classify the types of Zintl compound as part of their Extended Zintl-Klemm Concept Model. It is also compounded by the differing method of utilizing the 'pseudo-atom approach'. Because of this confusion, compounds that might fall within the Extended Zintl-Klemm Model 1 are considered occasionally part of the Zintl-Klemm Concept, blurring the lines between the original concept and the first extension (by Hoffman) because of the existence of the second extension (by Vegas), named exactly like the first extension of the ZKC.

2.2.1 Extended Zintl-Klemm Concept: Model 1

This extension is based on Hoffman and Papoian's work[67], which goes into great detail about the extension. Below is a recounting of the similarities and differences between the original Zintl-Klemm Concept and this Extension and how it applies to the explanation, rationalization, and prediction of the extended solids under investigation with the new modifications.

While some basic ideas remain the same, such as the idea that the more electronegative element(s) acquires the transferred electrons and that only metals make up the composition of the extended solids, other aspects have been overhauled completely while still others have just had minor modifications. In the ZKC, the metals to take part in this class of compounds were limited to Group I and II with Metals from Group XIII and XIV, however this criteria has been modified and expanded to include transition metals and heavy late group metals. Another change to the original concept is the inclusion of ternary and quaternary compounds, allowing for a much larger group of compounds to be assessed in comparison to the Zintl-Klemm concept, which just examined binary zintl compounds. Due to the larger group of compounds, the (8-N) rule was modified to include electron-rich hypervalent phases and according to Hoffman is "indispensable" when analyzing the structure 'retrotheoretically', a method of structural analysis added to this extension. This marks a shift in focus from the internal behavior of the chemical species to the external structure since 'retrotheoretical' analysis places more emphasis on structural formations and electron counting. This will be discussed in more detail in an example below.

Another more subtle, yet fundamental, change is the difference in how one utilizes the pseudo-atom approach. While in the ZKC, the pseudo-atom's elemental form was used as the predictor for the anionic lattice structure, such that in LiAl, where the aluminum is considered a pseudo-silicon, one would look towards the structure of elemental silicon to determine the lattice formed by the anionic aluminum. This new modification does not use the pseudo-atom's elemental form, but rather the structure formed between the metal donating the electrons with the pseudo-atom that forms. For example, in the $FeSb_2$, $CrSb_2$, $CoSb_2$, $NiSb_2$, compounds in which the antimony, which is the more electronegative element, is the one accepting electrons from the donating transition metals. In this case, because there could be multiple oxidation states, chemical knowledge into the species being assessed is key. When assessing the oxidation state of the transition metal, one must pose that it would be unreasonable to give the transition metals an oxidation state of +4, as that is not the most stable oxidation state for many of them, which leaves the very stable oxidation state of +2, which is shared by the all transition metals in the compounds listed above. If the oxidation state for the transition metal is +2, this in turns gives each antimony a -1 charge transfer. Antimony pertains to Group XV, but with an extra electron its valence electrons would be

isoelectronic to the elements in Group XVI, making antimony a pseudo-sulfur.

In the ZKC, one would have been guided by the elemental form of sulfur to determine the anionic lattice, however what determines the bonding and structure of the solids that fall within this extension is the structure between the pseudo-atom and the transition metal. In this case, $Fe\Psi-S_2$, a known and existing compound, where sulfur is the pseudo-atom for antimony, will be used to predict the types of chains, lattice, sub-lattices, or clusters that may form when the the transitions metals are bound to antimony. Though not directly stated in the literature, compound $Fe\Psi-S_2$ should also provide insight on the bonding that should be found within $FeSb_2$, $CrSb_2$, $CoSb_2$, and $NiSb_2$.

Hoffman's motivation to choose Sulfur instead of another element in Group XVI was not directly stated in the literature. It could be that he believed that it that one could look at either Sulfur or selenium as the possible pseudo-atom for Antimony because, if being guided by ZKC, one must look at the electronegativity of both elements. Unfortunately, both electronegativity values are very similar. So upon reflection, it would seem pertinent that one should look at the elemental structures as well as the already known structures between the transition metals and the possible pseudo-atom. When determining which pseudo-atom to choose, a closer look revealed that both $FeSe_2$, and FeS_2 share the same space group Pnnm (58), a space group also shared by $FeSb_2$, $CrSb_2$, $CoSb_2$, and $NiSb_2$. Still making both, sulfur and selenium, possible pseudo atoms. However, while, both $FeSe_2$ and FeS_2 have the same space group, it was only when looking at their elemental form that one found that only elemental Sulfur has a space group of Pnnm (58), making Ψ-S in $Fe\Psi-S_2$the ideal pseudo-atom for Antimony. So that in examining FeS_2, one can then predict the type of bonding seen in these antimony Zintl compounds.

The image 2.2 is given to clarify the possible types of bonds that Antimony could form, as electrons are acquired from less electronegative metals. Bond lengths between Sb-Sb are stated to range between 2.64Å - 3.24Å, depending on the geometry within the structures.

While EZCK-1 does describe bonding by way of extended Hückel calculations within the structures with the "assumption of weak π interactions and weak (although, still significant) s-p mixing", there is an overwhelming focus on the new 'retrotheoretical analysis' method introduced in an earlier paper[66], which shifts the attention of the concept to the external structure versus the internal electronic structure. This method, which will play a role in the next extension of the ZKC, is utilized to gather information on a crystal structure by decomposing the structures into simpler substructures, which can then be analyzed and finally reassembled. This is used to understand larger and more complex intermetallic structures. The key example used to demonstrate this method is $La_{12}Mn_2Sb_{30}$, described in two papers by Hoffmann and Papoian[67,66]. An image of this crystal can be seen in figure 2.3.
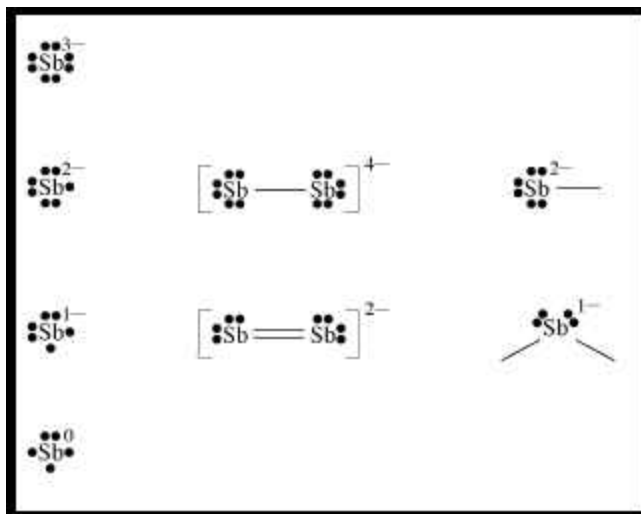
Figure 2.2: Bonding Schemes for Sb[67]
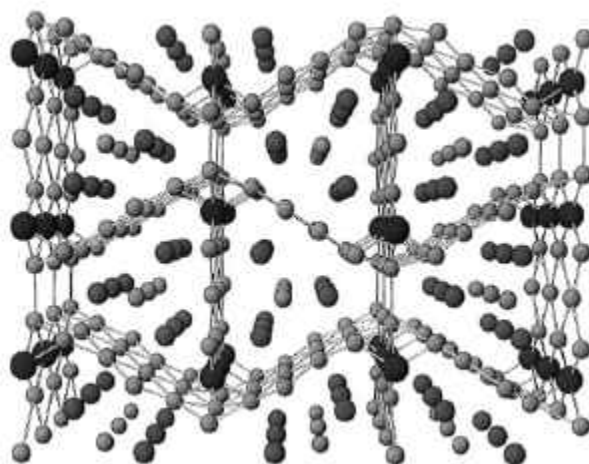
Figure 2.3: "Perspective view of the crystal structure of $La_{12}Mn_2Sb_{30}$–Sb, small spheres; La, medium spheres; Mn, large spheres." [66]

This structure, while complicated, can then be decomposed by removing the Lanthanum and Manganese atoms, as they are the atoms donating the electrons. This leaves one of the anionic substructures, the 3D net, in the compound seen in figure 2.4.

By removing the lanthanum and manganese atoms, and decomposing the 3D net, the kinked sheets that can make up the substructure can be clearly seen in 2.4. This decomposition of the substructures can then be used to find similar structures in pseudo atoms. The modification to the electron count for this compound goes as follows: La is assumed to donate 3 electrons, making it a +3, Mn is assumed to be dipositive, making it a +2, which mean the number of electrons transferred to the Sb lattice is $(12 \times 3) + (2 \times 2) = 40$ electrons.
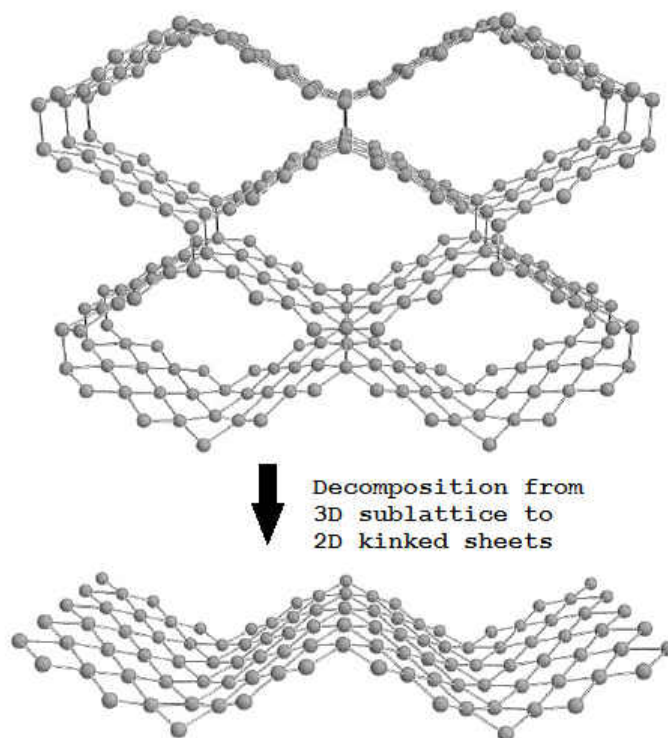
Figure 2.4: "Three dimensional Sb_{20} substructure" [66]

Looking at the substructure in figure 2.4, this was determined to only be part of the Sb_{30}. The totality of Sb_{30}, when decomposed into simpler sub structures, is made of of one Sb_{20}–a 3D net, two Sb_6–1D strips and four Sb_4–atoms. It is then assumed that the lone Sb atoms are assigned a -3 charge, the charge assigned to the 1D strip (as a whole) is a -5 charge, and the charge on the 3D net is a -16. This assignation of electrons allows for atoms to have a partial electronic charge. When added together, $(-3 \times 4) + (-5 \times 2) + (-16 \times 1) = -38$, 2 electrons short of the assumed -40 charge. There is a mild disregard for the inability to account for all the electrons and it is disregarded because "The disposition of the last two electrons (from a total of 200 electrons in a unit cell) is a matter of some interest, and is no doubt related to the conducting properties of the material.[67]"

The study concluded successfully by applying these new tools, such as the new method of the pseudo-atom approach, retrotheoretical analysis on a crystal's substructures, and the application of Zintl-Klemm electron counting scheme to a variety of crystals. However, a year later, while looking at tin compounds, such as LiSn, Hoffmann and Papoain were unable to acquire either the sublattice or the electron count predicted when analyzed by Hoffmann's extension of the Zintl-Klemm concept [41]. The LiSn structure was theorized to

form a 3-dimensional lattice composed of the Sn anions, yet the structure is arranged such that it consists of a series of infinite 2-dimensional tin (with bonding distances up to 3.18Å) layers that are intercalated by the lithium atoms[41]. This study also included the elements from Group XVI and Group XVII, and led to the general conclusion that "s,p mixing will diminish as one moves across the period"[41]. This conclusion, while drawing some doubt about the role retrotheoretical analysis has in predicting structures, supports the bonding of anionic metals closer to the traditional Zintl border, metals found in Group XIV and Group XV. However, retrotheoretical analysis has still proven effective when analyzing structures such as $La_{12}Mn_2Sb_{30}$. Its pseudo-atom approach is a successful modification as it provides insight into the types of bonding that can be found in these structures, helping to better understand these solids. Another revelation about these solids that was brought to light was the very long range interactions these anionic metals can form, a range between 2.64Å - 3.24Å. This allows the consideration that bonding could be occurring where, previously, it would not have been thought possible due to the long distances.

2.2.2   Extended Zintl-Klemm Concept: Model 2

This extension of the Zintl-Klemm concept, primarily driven by Angel Vegas, is an extension on Hoffman and Papoian's Extended Zintl-Klemm concept, which can be seen as another development in this expanding theory. The development of this model starts off where the other model ended and depends heavily on the idea introduced in the EZKC Model 1, the idea of retrotheoretical analysis, and the long bonding distances between the anionic metal substructures. While the previous concepts attempted to explain the bonding aspects of the chemical species, this concept focuses on using the structural patterns, long range bonding distances, and the modified (8-N) counting scheme proposed in EZKC-1 in an attempt to predict crystal structures. By focusing on the metallic substructures within the solid, as well as the distances of the metals, and the use of data mining of structural databases, it has become easier to identify extended solids that have similar structural patterns and similar metal-metal distances[99,44].

With the focus straying from the type of bonding found within the solid, to the external structure, there have been some added changes to the EZKC-l . In EZKC-1 and in the ZKC, the extended solid under scrutiny stayed within the realm of intermetallics (binary, ternary, or quaternary). However, the Extended Zintl-Klemm Concept Model 2 (EZKC-2) has extended this to include nonmetals as part of these extended solids, as well as intermetallics. That means that the term 'Zintl compounds', in the literature, now extends to binary, ternary, and quaternary intermetallics as well as their oxides and other compounds that include

other nonmetals. This, as stated before, compounds the problem of correctly identifying the correct concept to utilize when analyzing these solids. During the course of this extension the use of data mining has helped in the introduction of new compounds, so while the vague 'Zintl compound' term is beginning to buckle under the weight of the many types of solids it encompasses, shedding light on all these new solids is a step in better understanding the unusual behaviors that caught Zintl's intrigue.

By using data mining as a source for many different structures, the use of of retrotheoretical analysis is crucial to this extension. With parameters set for certain metal-metal distances and the types of elements present, this concept is now firmly entrenched in the physicality of the structure versus the chemical insight that was used/gathered by the previous ZKC and the EZKC-1. However, its claimed ability to predict and rationalize structures will be tested, along with the other concepts, when viewing the extended solids that each concept claims in terms of its internal electronic structure. With its focus on the physical external structure, retrotheoretical analysis becomes fundamental in assessing these solids and understanding EZKC-2. An example from one of Vega's earlier papers[44] highlights what appears to be the exception of his extension of the ZK concept while exemplifying the EZKC-2 method. The example first looks at the Tl-Tl distances in the pure metal and finds that these distances are maintained in both Tl_2O_3 and in $AgTlO_2$. The idea proposed is that since the oxygen does not change the metal-metal distance, then the oxygens can be classified as simply "stuffed" into the lattice, making this compound a 'stuffed oxide'. The oxygens would be contained in Tl_2O_3 and in $AgTlO_2$, without disrupting the Tl-Tl distances, which suggests that there might be an incomplete electronic transfer between thallium and oxygen. This concludes that the oxygens might have significant covalent interactions with each other which results in enough electronic charge on the metal to still maintain metal-metal interactions[44]. Based on similar metal-metal distances, Vegas and others have argued that the model has bridged the gap between zintl compounds and their oxides[100,90]. We will examine this hypothesis in the chapters that follow.

Another major change in the ZKC is a significant extension of what constitutes a pseudo-atom. While in both the EZKC-1 and ZKC, the least electronegative atom(s) would donate to the more electronegative atom or zintl polyanionic metals, in the EZKC-2 this has become a rationalizing tool independent of electronegativity, as explained in detail below and in one of Vega's paper[101] when looking at the many different pseudo-atom cases when analyzing the Li_3AlN_2 structure and creating pseudo-compounds.

In order to understand all the possible pseudo-atoms, based on how the electrons are redistributed in the EZKC-2 for Li_3AlN_2, refer to figure 2.5.

As one can see from Figure 2.5, electronegativity no longer plays a role in deciding which

Electron donation			Atom	Electron acceptance		
3	2	1		1	2	3
N^{+3} = (Ψ-Be)	N^{+2} = (Ψ-B)	N^{+1} = (Ψ-C)	N^0	N^{-1} = (Ψ-O)	N^{-2} = (Ψ-F)	N^{-3} = (Ψ-Ne)
	Li^{+2} = (Ψ-H)	Li^{+1} = (Ψ-He)	Li^0	Li^{-1} = (Ψ-Be)	Li^{-2} = (Ψ-B)	Li^{-3} = (Ψ-C)
Al^{+3} = (Ψ-Ne)	Al^{+2} = (Ψ-Na)	Al^{+1} = (Ψ-Mg)	Al^0	Al^{-1} = (Ψ-Si)	Al^{-2} = (Ψ-P)	Al^{-3} = (Ψ-S)
V^{+3} = (Ψ-Ca)	V^{+2} = (Ψ-Sc)	V^{+1} = (Ψ-Ti)	V^0	V^{-1} = (Ψ-Cr)	V^{-2} = (Ψ-Mn)	V^{-3} = (Ψ-Fe)

Figure 2.5: All possible pseudo-atoms for Li_3AlN_2[101]

element acquires electrons as one posits possible scenarios to explain and rationalize possible structural predictions, providing that each scenario can be tied back to the current structure by using justifications such as similar substructures, lattices, and any other similarity. In this scenario there are three possible cases, but only two cases will be discussed as that will be sufficient to highlight how the pseudo-atom approach is handled in this concept.

In case 1: Lithium would donate one electron, so Li would now be a Ψ-He and would result in the formation of $[AlN_2]^{-3}$; assuming 2 of those electrons were to be donated to the Nitrogens, then Nitrogen would then be a Ψ-O and the last electron would be donated to the Aluminum making it a Ψ-Si. This creates the pseudo-compound $(\Psi-He)_3(\Psi-Si)(\Psi-O)_2$ where $[AlN_2]^{-3}$ becomes effectively $(\Psi-SiO_2)$, which forms a similar substructure to that of the AlN_4 tetrahedra found within this structure. Showing this structure as a Al stuffed Li_3N_2.

In case 2: Aluminum donates its 3 electrons to the three Lithiums creating 3 Li^{-1} which are then considered to be Ψ-Be. The Al^{+3} is then considered a Ψ-Ne, and Nitrogen remains unchanged and acts as elemental N^0. This results in a hypothetical $(\Psi-Ne)$-stuffed $(\Psi-Be_3N_2)$ were $(\Psi-Be_3N_2)$ forms the same structure as Li_3N_2 making this essentially an Al stuffed Li_3N_2.

Both cases seem to have arrived at the structure of the compound in question. While this methods seems to be successful in predicting structures as noted in the various literature[100,73,99,90,96,97], the chemical insight into bonding that was generated by the ZKC and the EZKC-1, has been replaced with an elaborate electron counting scheme. A counting scheme that contains enough pseudo-atom permutations could naturally find a structure similar to the structure being rationalized. During the course of this study, various crystals will be examined in terms of their metal-metal interactions to discover if some of these pseudo-atoms and pseudo-compounds are possible and maybe bring insight into the ever expanding concept.

2.3 Analytical Methods

These concepts are based on the idea that charge transfer occurs and covalent bonds form betwixt the species acquiring the electronic charge. However, in order to examine these concepts, it is essential to peer into the extended solids and examine the electronic structure found within. To achieve this goal, it is essential to consider the use of quantum calculations. In the past, extended systems have been too complex to be modeled effectively with quantum chemistry software. By the mid 1980's these structures had been analyzed using Extended Hückel calculations, band structure calculations, ELF calculations, total energy calculations, and charge density maps. However, in recent years, increasing computer power and the creation of accurate density functionals has made it possible to analyze these systems more thoroughly. In this work, three *ab initio* programs, all using density functional theory to calculate the charge density of a specific class of solids known as Zintl compounds and their extensions, are compared. The programs chosen for the quantum calculations are Flair[108,19], an all-electron full-potential linearized augmented plane wave program that uses muffin tin approximations for the core electrons. VASP[52], also using plain wave basis sets, approximates the core electron density with pseudo-potentials, therefore using only the valence electrons when calculating the electron density. CRYSTAL14[22], an all-electron molecular orbital computational program, uses atomic basis sets to model the atoms in the crystal and calculate the wave functions to obtain the charge density. Both Flair and CRYSTAL14 take advantage of a crystal's symmetry to arrive at convergence, making the calculations more efficient by requiring fewer operations to compute both the charge density and the total energy. By comparing the results, we can determine whether or not these fundamentally different approaches effectively model the same charge density and properties of extended systems.

Another area of advancement that has occurred with increasing computing ability is the creation of better visualization programs. These programs aid in the analysis of the computed data by constructing a 3D representation of the crystal and of the data making it easy to display; while there are many programs that perform this function, the visualization program chosen was VESTA[61]. These programs will be described and discussed in detail in the Comparison of Methods chapter. However, once the programs for both the calculation and visualization of the data was decided, the question that remained was: what would be the best method to examine the charge density? Since all three concepts involves charge transfer, the ionic nature in these extended solids needs to be explored. Therefore, finding the charge on each species seemed pertinent and Bader's 'Atoms in Molecules[4]' (AIM) theory was chosen as the first part in the assessment of these solids. While this theory is discussed

in great detail in Bader's book, for the purposes of this study, only the essentials will be discussed. The next goal was to assess the covalent character in these solids. While there seems no way to quantify the covalency of these solids, one can qualitatively appraise these solids by viewing the Laplacian of the charge density. Another method of analysis, while also qualitative, though no less powerful, is to examine the difference charge density maps of the charge density.

One of the biggest challenges when partitioning charge density is that it can be quite arbitrary and many differing methods exits. For this study, the theory of Atoms in Molecules (AIM) was chosen because of its innate intuitiveness in dividing the atoms from the molecule. This is accomplished by first calculating the gradient vector field of the charge density. After that has been calculated, one takes an initial point and the path of steepest ascent if followed between the 26 neighboring grid points along the charge density gradient. This path is followed until it reaches a local maxima (usually, but not necessarily, the nuclei of an atom). This continues to cycle until all the grid points are assigned to a maxima. The Bader volume is assigned by creating a surface boundary where the trajectories do not intersect and create a zero flux.[88] This volume is then integrated over the charge density of the assigned grid points within the dividing Bader surface. Once integrated, this gives us a charge for each atomic species. Figure 2.6 illustrates the trajectories and how the volume and surface are designated.
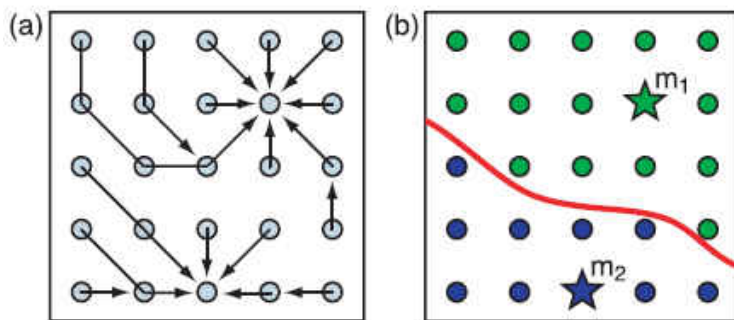
Figure 2.6: "An illustration of the steepest ascent paths (a) on a charge density grid to find the Bader volumes...Each trajectory terminates at a new charge density maximum, m_i, or at a grid point which has already been assigned. For all grid points assigned (b), the set of points which terminate at each maximum (green to m_1 and blue to m_2) constitute that Bader volume. The Bader surfaces (red curved line) separates the volumes."[88]

While the AIM theory does provide a method to quantify the charge on an atom and hints to the bonding within the structure, there is still a need for more information on the extended solid's internal electronic structure. That need was assuaged by information garnered from calculating and looking at the charge density difference maps. These maps

provide a clear 3D picture of the movement of the charge between the atomic species within the extended solid. This is done by calculating the charge density of the atomic species within the extended solid before they have been allowed to interact and then subtracting this charge density from the charge density after convergence. By doing this subtraction, one can see where the electron density has migrated to and from, giving a clear picture of the formation of ions and bonds. This can be seen when one interprets an image based on the simple formalisms of what constitutes as ionic or covalent bonds. In any image, a build up of charge density between two nuclei consists of a covalent bond, while a spherical loss or a spherical gain of charge density around an atom, without any charge density build up between itself and another species, would indicate that there has been charge transfer and that the atom has now become an ion. In this work, difference electron density was observed to be much more sensitive to electron migration than the Laplacian.

The information the charge density difference reveals can be verified by computing the Laplacian of the charge density for the crystals with smaller atoms. In this case, by computing the Laplacian of the charge density (a scalar field), the Laplacian reflects the geometry[85] of the location of the electrons within the crystal. This is done by taking the second partial derivative of the density at each point of the charge density 3D grid such that:

$$\vec{\nabla}^2 f(x,y,z) = \nabla \cdot \nabla f(x,y,z) = \frac{d^2 f}{dx^2} + \frac{d^2 f}{dy^2} + \frac{d^2 f}{dz^2} \tag{2.3.1}$$

This serves as an averaging property, so that when, at given point r_0, if the value is the same as the others, it vanishes. This reflection of the geometry around each point is able to demonstrate that there is an accumulation of charge density at a given point. This occurs because at any point on the grid, the Laplacian acts like an averaging function, where it is positive when electrons are no longer present, and is negative where the electrons have migrated. The information provided by the Laplacian corroborates the information seen in the charge density difference maps.

While it has been claimed that the concepts explored have been able to predict structures, these concepts delve into more than just the physical nature of the extended solids under their purview. These concepts' ability to predict these solids fall back onto their ability to explain the mechanism behind the bonding within each solid; one key example is the unique pseudo-atom approach each concept adopts. The ability to predict these solids must then be explored in terms of the electronic structure within as to gain insight into the bonding each theory alleges to exist.

Chapter 3

Theoretical Analysis of the Zintl-Klemm Concept

As previously detailed, the Zintl-Klemm Concept (ZKC) is based on simple electron counting schemes. We will analyze the concept here in terms of the charge density distributions of a subset of Zintl Compounds that fulfill the original concept's criteria. This criteria is based on solids that are binary and form between Group I & II metals with those from Group XIII & XIV. While previous studies of the ZKC investigated these extended solids, those studies failed to account for many of the possible compounds within each class of compounds. This study will examine Zintl Compounds with varying stoichiometric ratios. It will also examine any trends found within these compounds formed from Group I/Group II (Li, Na, K, Be, Mg & Ca) and with metals from Group XIII (Al, Ga, In, & Tl). For instance, in terms of stoichiometric ratios, LiAl falls within the ZKC criteria, but then so do compounds such as $LiAl_3$ and Li_3Al_2. Theoretically, if the bonding mechanism proposed by the ZKC applies to the compound LiAl, then the bonding mechanism should also apply in all of its binary forms. Therefore, a more comprehensive set of Zintl Compounds will be investigated, compounds formed from Group I/Group II (Li, Na, K, Be, Mg & Ca) and with metals from Group XIII (Al, Ga, In, & Tl), as will any trend found within these compounds. By including compounds with metals from Group XIII, this study hopes to find similar trends, as one would inherently expect. The extended solids investigated in this study are presented in table 3.1. The cells in the table have been color coded and colored cells indicate a deviation from the Zintl-Klemm Concept. While the majority of crystal structures do demonstrate the bonding mechanism proposed, a few of the extended solids do not, and they have been separated into a few categories to help indicate the type of bonding found within the structure. The blue cells indicate that the structure is mainly ionic in nature, while the yellow cells indicate more traditional metallic behavior. The green cells indicate unusual behavior by the Group

II metal, while the salmon colored cells indicate a phenomena yet unresearched in terms of calcium's bonding mechanism. Calcium, unless in a structure where it is the minority, stoichiometrically, gains charge at the expense of the more electronegative metal.This goes directly against the Zintl-Klemm Concept in terms of how charge is transferred between metal species in Zintl Compounds. These deviations from the ZKC will be discussed more extensively at the end of the chapter.

LiAl

The first structure that was analyzed was LiAl. In this structure, according to the ZKC, lithium should be donating one electron to aluminum (assuming formal charges). By accepting a -1 charge, aluminum would become isoelectronic to Group XIV causing aluminum to behave like silicon. Silicon is chosen over carbon because it is the closest in electronegativity to aluminum and contains the same amount of electrons as the anionic aluminum in LiAl. Since aluminum atoms packing and bonding changes to match silicon, aluminum can now be referred to as pseudo-silicon, which can be written like Ψ-Si. By looking at the way aluminum metal packs, in figure 3.1,
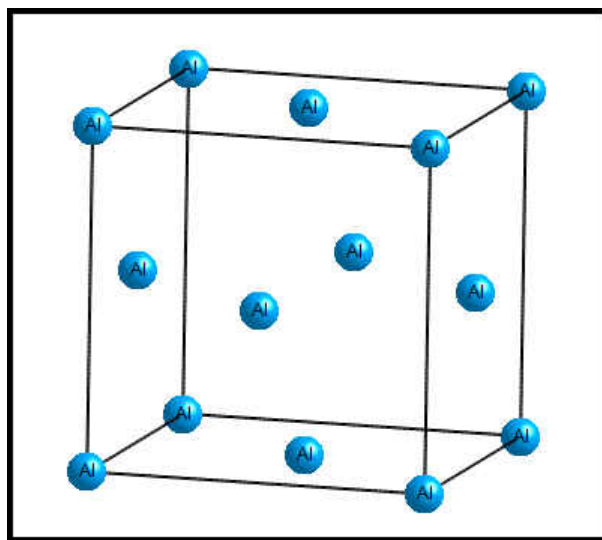
Figure 3.1: Unit cell of aluminum metal.

one can more easily discern the change in packing by aluminum metal when compared to aluminum atoms in LiAl. The ZKC states that aluminum would not only pack but also form bonds similar to those formed by its pseudo-atom. If aluminum atoms in LiAl pack like elemental silicon, then this gives credence to the predictive aspect of the ZKC. As point of reference, the structure of elemental silicon is shown in figures 3.2 and 3.3.

Zintl Compounds				
Group I/II Metal	Aluminum	Gallium	Indium	Thallium
Lithium	LiAl	LiGa	LiIn	LiTl
	LiAl$_3$	Li$_2$Ga	Li$_2$In	Li$_2$Tl
	Li$_3$Al$_2$	Li$_3$Ga$_2$	Li$_3$In$_2$	Li$_3$Tl
	Li$_9$Al$_4$	Li$_5$Ga$_4$	Li$_5$In$_4$	Li$_5$Tl$_2$
		Li$_2$Ga$_7$		
Sodium		NaGa$_4$	NaIn	NaTl
			Na$_2$In	Na$_2$Tl
Potassium		KGa$_3$	KIn$_4$	KTl(64)
		K$_2$Ga$_3$		KTl(227)
Magnesium	MgAl$_2$	MgGa	MgIn	MgTl
		Mg$_5$Ga$_2$	Mg$_5$In$_2$	Mg$_5$Tl$_2$
		Mg$_2$Ga$_5$	Mg$_2$In	Mg$_2$Tl
		MgGa$_2$(194)	Mg$_3$In	
		MgGa$_2$(55)	MgIn$_3$	
		Mg$_2$Ga		
Calcium	CaAl$_2$	CaGa	CaIn	CaTl
	CaAl$_4$	CaGa$_2$	CaIn$_2$	CaTl$_3$
		CaGa$_4$		Ca$_3$Tl
		Ca$_3$Ga$_5$		
		Ca$_5$Ga$_3$		

Table 3.1: Comprehensive List of Zintl Compounds.The numbers in parenthesis indicate the different space groups.
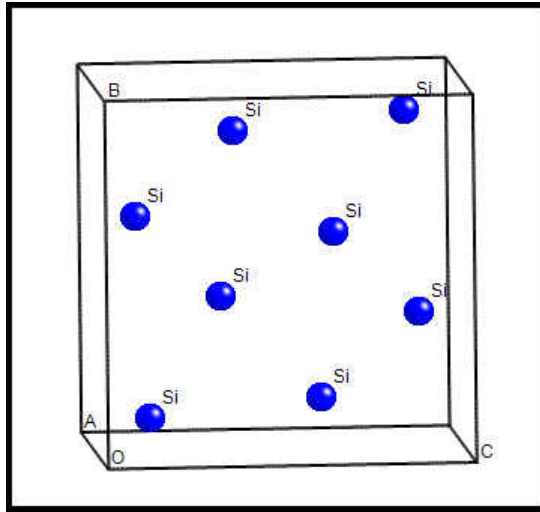
Figure 3.2: Unit cell of Elemental silicon.
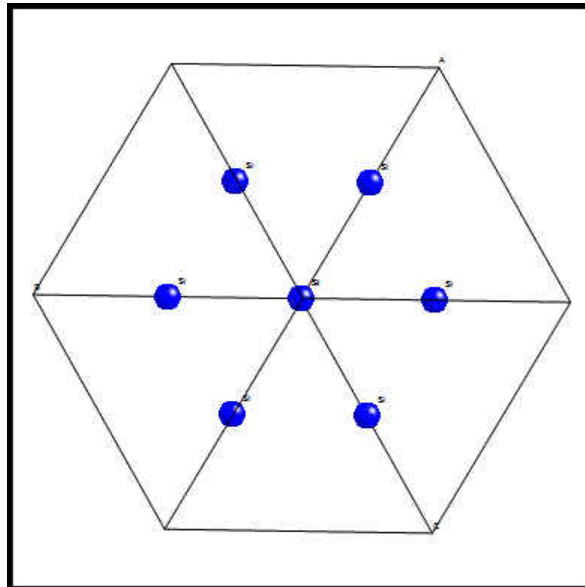
Figure 3.3: Unit cell of Elemental silicon- Hexagonal.
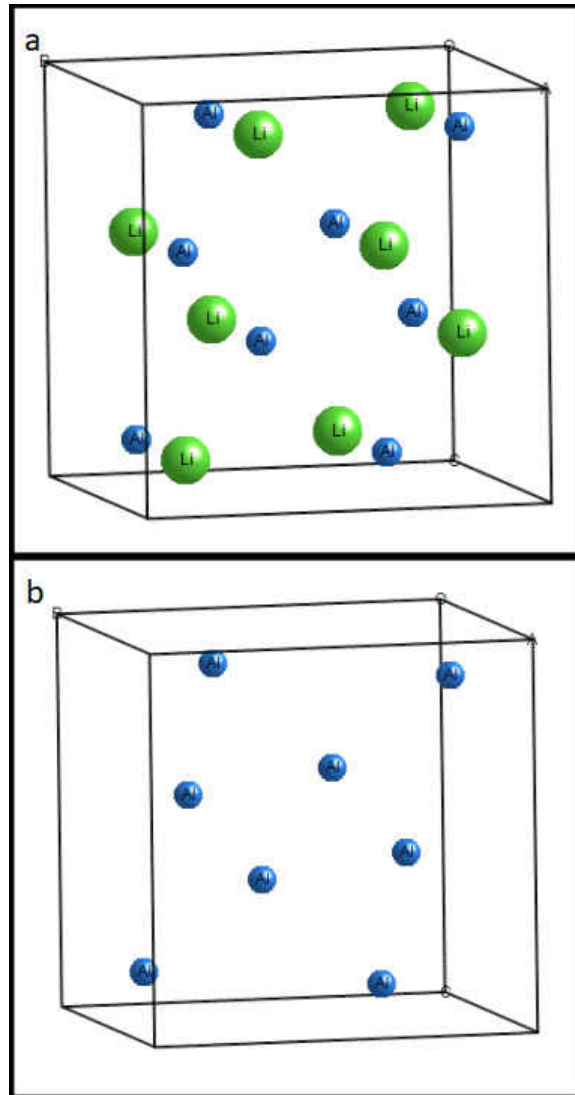
Figure 3.4: LiAl Structure.

The first step in the analysis was to view the packing of aluminum atoms in LiAl[53] to determine if they pack like that of silicon. The packing of aluminum in LiAl can be seen in figure 3.4, where (a) is the unit cell of LiAl and by removing the lithium atoms from view, the structure (b) reveals the packing of aluminum atoms within the structure.

By comparing the structures in figures 3.2 and 3.4, it can be clearly seen that aluminum inLiAl packs like elemental silicon, affirming the ZKC's hypothesis that the metal in question would pack like its pseudo-atom. With the packing of aluminum established like that of silicon, the bonding within LiAl must be assessed in order to determine if the aluminum atoms bonds like elemental silicon. To be able to determine if aluminum demonstrates Ψ-Si bonding behavior, it was necessary to first compute the charge density of the silicon crystal
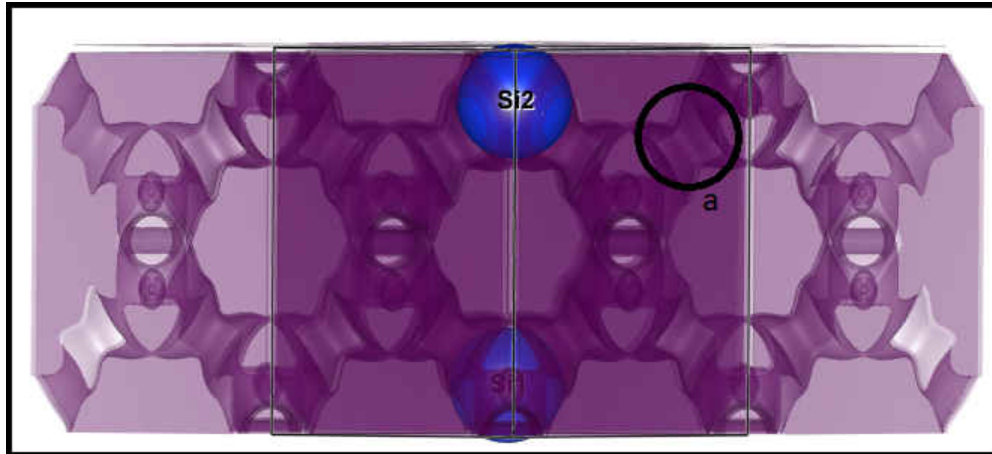
Figure 3.5: Laplacian of the charge density of Silicon.

and take both the Laplacian and the charge density difference of silicon. The Laplacian, the second partial derivative of the charge density, is presented below in figure 3.5.

In figure 3.5, (a) reveals the electrons between silicon atoms, clearly displaying the covalent bonding between silicon atoms. The bonding between silicon atoms form a hexagonal shape, similar to the way silicon packed in figure 3.3. However, calculating the Laplacian was not a consistently viable method. While the Laplacian does provide the location of the electrons, it is also very sensitive to grid size, making the calculations impractical due to the lengthy calculation time needed for bigger solids since they would require bigger grids. A more robust approach was to systematically examine the difference in the charge density between the atoms before and after the formation of bonds – the difference electron density.

Throughout this chapter (and throughout this dissertation), the extended solids under scrutiny will be examined by looking at the charge density difference (CDD) maps. The figures produced from the calculated data show less sensitivity to grid size, unlike the Laplacian, making it the ideal method to assess the charge density distribution in these solids. The information present in the CDD maps corroborates the information the Laplacian provides, as will be shown below, meaning that there will be no loss of information when examining these extended solids. An added benefit these CDD maps provide is information on the polarization of the charge density. In order to make the analysis of the solids more straightforward, all the charge density difference maps are presented with the same color scheme throughout this dissertation. The color scheme used is as follows: blue signifies positive charge density, indicating where charge density has been gained (where it has migrated to); while pink signifies negative charge density, where there has been a loss of charge density (where it has migrated from). Figure 3.6, is the charge density difference map of silicon where (a) reveals where the charge density has been gained between nuclei and (b) indicates

24
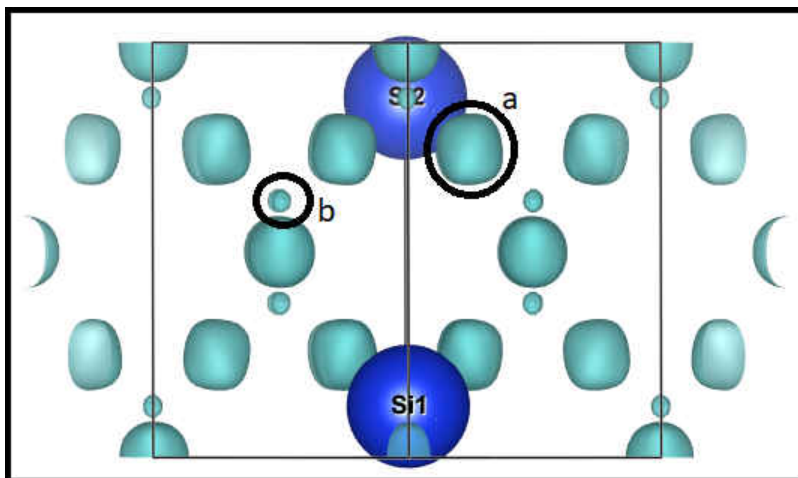
Figure 3.6: Charge Density Difference of Si.

the center of the silicon atoms. Only the charge density gain (blue) is present, since this allows for the bonds between the silicon atoms in the figure to be easier to see.The CDD map of elemental silicon clearly demonstrates that charge density is accumulating between silicon nuclei, indicative of a covalent bond between the atoms, corroborating the information that was garnered from the Laplacian.

With the charge density difference of silicon calculated, the CDD of LiAl was compared to silicon to verify if the bonding seen between silicon atoms is seen between aluminum atoms. The charge density difference of LiAl is presented in figure 3.7.
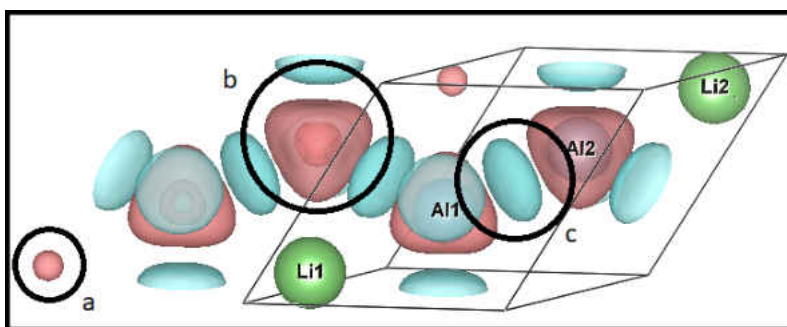
Figure 3.7: The Parts of LiAl

Figure 3.7, representative of all charge density difference maps included in this work, identifies the different areas of interest in its map. The areas marked show the different points of electronic migration within the extended solid. In almost all figures presented, the unit cell of the extended solid illustrates placement atoms which are there to help the reader determine which atom is which. These placement atoms can be seen in figure 3.7. However, they can mask the CDD maps' information. As a result, in many occasions the unit cell is

extended as in the case of this figure for better clarity. The figure contains a lithium cation (a), which is pink, and has no charge density increase around it, which indicates that it has lost charge and contracted. This is the behavior one would expect from a cation, including the spherical loss of charge. The aluminum atom (b), which is also pink, has lost charge density around itself but has gained charge density (blue) between itself and its aluminum neighbors creating charge density accumulation (c) such that aluminum atoms have formed covalent bonds. Expanding the CDD map we get the following in figure 3.8:
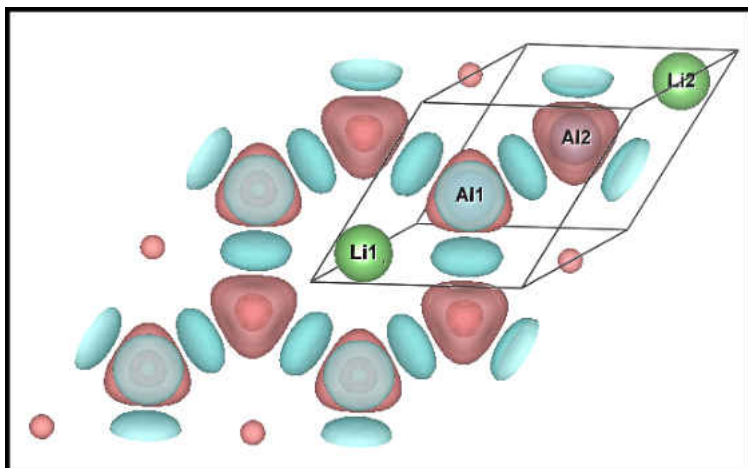
Figure 3.8: Charge Density Difference of LiAl.

Figure 3.9: Charge Density Difference Gain in LiAl.

In figure 3.9, the charge density loss (the pink) was removed, leaving only where the charge density migrated to (blue). The charge density difference map reveals that aluminum atoms have formed covalent bonds with neighboring aluminum atoms while also

having charge density accumulation gather around their nuclei, expanding outside of the tight cores. This expansion of charge density around the cores signify that aluminum atoms have acquired enough charge density to become anions, while still forming covalent bonds with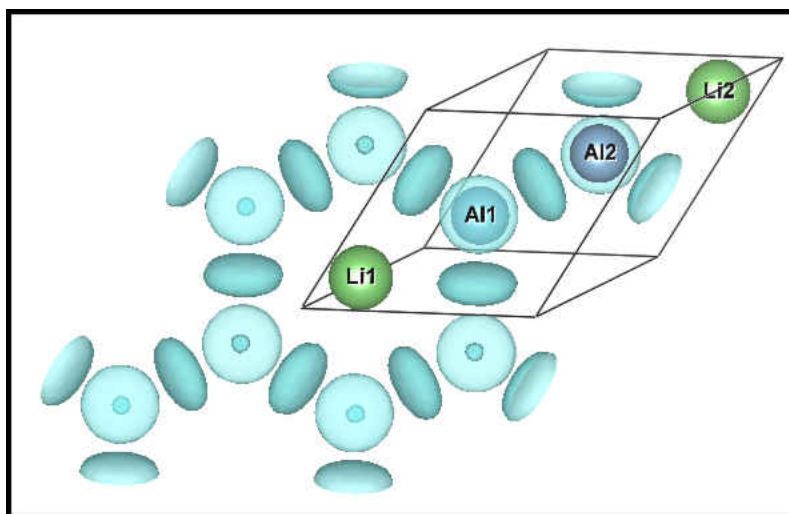 other aluminum atoms, as predicted by the ZKC. Comparing figures 3.9 and 3.8 with figures 3.5 and 3.6, the can see that the anionic lattice formed by the aluminum anions are similar, in both bonding and packing, to that of its pseudo-atom silicon. After analyzing the charge density difference maps, one must recognize the success in the ZKC ability to predict both structure and bonding of this compound by way of a simple counting scheme, since the behavior theorized in the ZKC was seen to occur in LiAl. Since the CDD maps show that a charge transfer occurred, it seemed pertinent to attempt to quantify the charge transfer. In order to accomplish this task, Bader's Atoms in Molecule theory was applied to LiAl's charge density. While this method is also grid size dependent, much like the Laplacian, LiAl's small size allows for analysis with this approach. Therefore, the Bader Charges on both lithium and aluminum atoms were calculated and presented in table 3.2. The charges given, while not quite a ± 1 charge transfer, seems to be sufficient to have had the ionic charge transfer effect the ZKC expected.

LiAl - Bader Charges	
Li	+0.83
Al	−0.83

Table 3.2: Bader Charges of LiAl charge density.

3.1 Compounds of Li and Al with Different Stoichiometric Ratios

With the success of the ZKC in explaining LiAl, this study will explore compounds that are still binary in nature but have different stoichiometric ratios. The compounds that will be analyzed will be $LiAl_3$, Li_3Al_2, and Li_9Al_4 since each Li-Al compound contains a differing fractional amount of lithium. These three compounds present an opportunity to examine the effect the varying percentage of lithium, within the stoichiometric ratio of the compound, has on the behavior of the Group XIII metal, in this case aluminum. The percentage of lithium in the compounds stoichiometric ratio display a wide range, from 25 percent in $LiAl_3$ to 70 percent in Li_9Al_4 and with Li_3Al_2 very close to LiAl.

27

LiAl₃[110]

Looking at $LiAl_3$ in figure 3.10, whose stoichiometric ratio is 25 percent lithium,
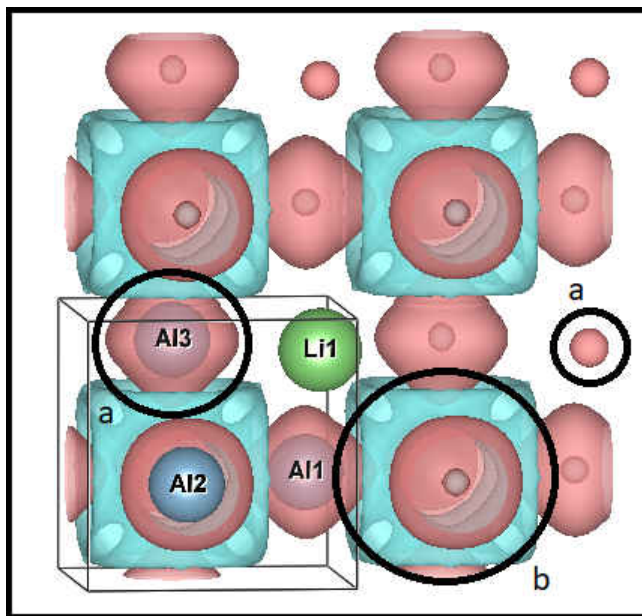
Figure 3.10: Charge Density Difference of $LiAl_3$

we find that both lithium and aluminum atoms lose charge density. However, the charge density is concentrated between aluminum atoms in discreet cuboids, which is distinctly a covalent bonding construct. While this is not a formation found in elemental silicon, it is found in elemental carbon[57], still within Group XIV. It would seem that in the case of aluminum even a small fractional amount of charge transfer from lithium is enough to cause a distortion in the the packing of aluminum. The bonding suggests that instead of acting like a Ψ-Si it might be behaving like a Ψ-C (still within the neighboring Group XIV). The pseudo-carbon behavior exhibited by aluminum can be rationalized if the charge transferred was incomplete, such as a fractional charge transfer, that the collective electronegativity of aluminum causes aluminum atoms to behave like a much more electronegative neighbor, carbon. Taking the Bader Charges of this compound , found in table 3.3

LiAl₃ - Bader Charges	
Li	+0.9
Al	−0.3

Table 3.3: Bader Charges of $LiAl_3$ charge density.

one finds that lithium has donated almost a full electron and the resulting charge transfer is then shared equally between aluminum atoms, giving them a fractional charge. With a fractional charge of -0.3 on aluminum atoms, aluminum in $LiAl_3$ seems to behave like a pseudo-carbon, which is more electronegative than silicon, but still within the neighboring group. The covalent bonds present in the charge density difference of $LiAl_3$ mimic those found in the neighboring group, and the charge transfered from lithium, further confirm the ZKC's premise that charge transfer and covalent bonding within the anionic metals occurs at the expense of the least electronegative element.

Li_3Al_2[89]

When examining Li_3Al_2, with a Li:Al ratio close to that of LiAl, we find that
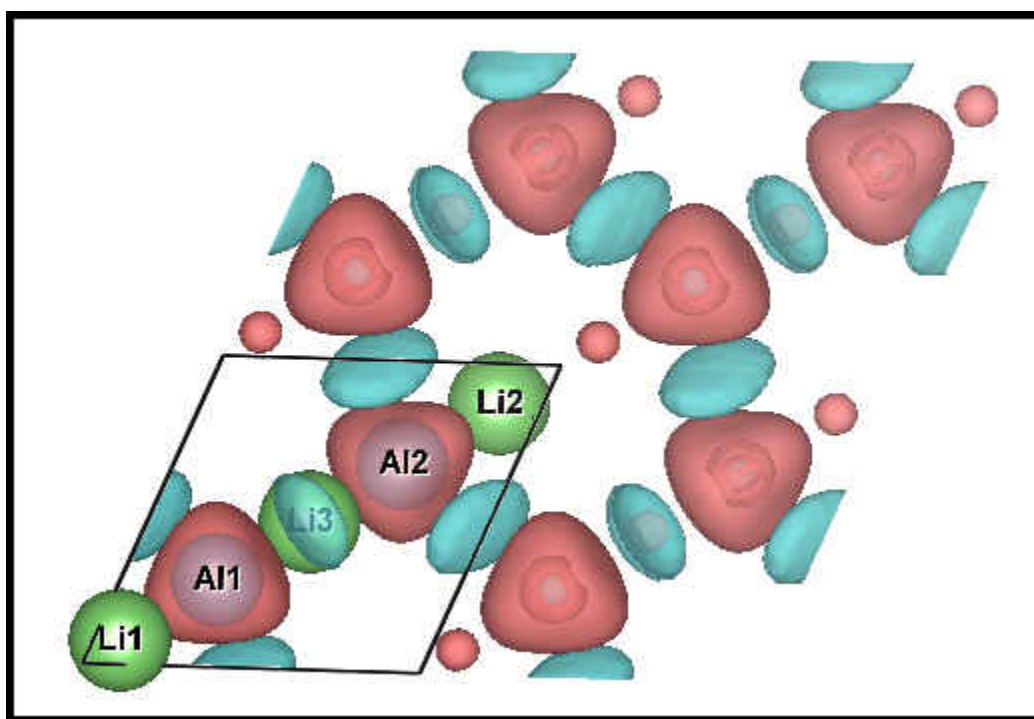
Figure 3.11: Charge Density Difference of Li_3Al_2.

the overall structural packing of aluminum, just like in LiAl, packs and bonds is the same way as elemental silicon, which confirms the bonding mechanism proposed by the ZKC. Lithium atoms lose charge density and aluminum atoms show electron density build up between each other. The similarity between LiAl and Li_3Al_2 seems to imply that there is very little difference in a compound where the stoichiometric ratio between the Group I Metals, with similar electronegativities, lie between 50 to 60 percent in comparison with

Group XIII metals. This, 50-60%, stoichiometric ratio will be examined in the next section as we investigate compounds with lithium in similar ratios with metals from Group XIII.

Li_9Al_4[33]

The next compound, Li_9Al_4, has almost 70 percent of its stoichiometric ratio comprised of lithium atoms. In this compound, lithium atoms donate electrons to aluminum atoms, as seen in figure 3.12. Using formal charges as our guide, each aluminum atom would acquire about -2.25 charge. This amount of charge would make the aluminum atoms' valence electron count closer to that of sulfur/selenium versus phosphorus. The charge transferred to aluminum which could place it beyond Group XV and into Group XVI is very small, with a fractional formal charge acquisition of an additional -0.25. Still, a similar amount of charge was enough to distort $LiAl_3$ and create bonding similar to carbon, which is found in Group XIV. Looking at figure 3.12,
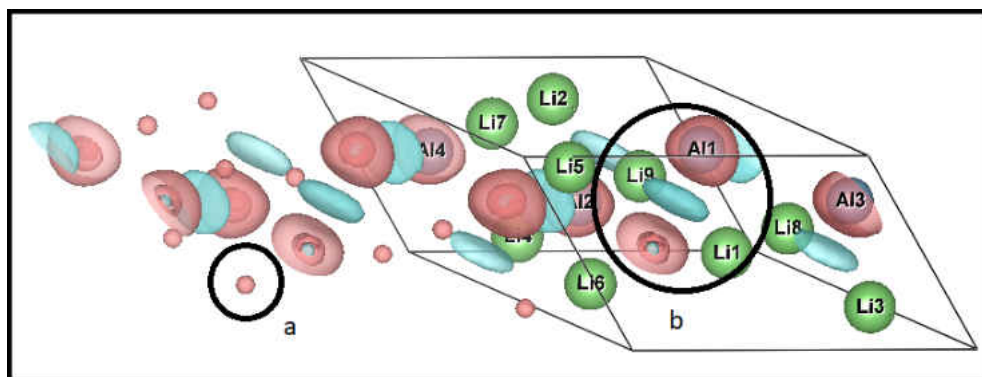
Figure 3.12: Charge Density Difference of Li_9Al_4.

it can be seen that (a) lithium atoms lose charge density while (b) aluminum atoms gain charge density between themselves. In figure 3.13, only the charge density gain is shown and it can be seen that aluminum atoms, which gain charge density between themselves, create planar zig-zag chains found in elemental selenium[83,10]. Once again, demonstrating that this solid follows the ZKC.
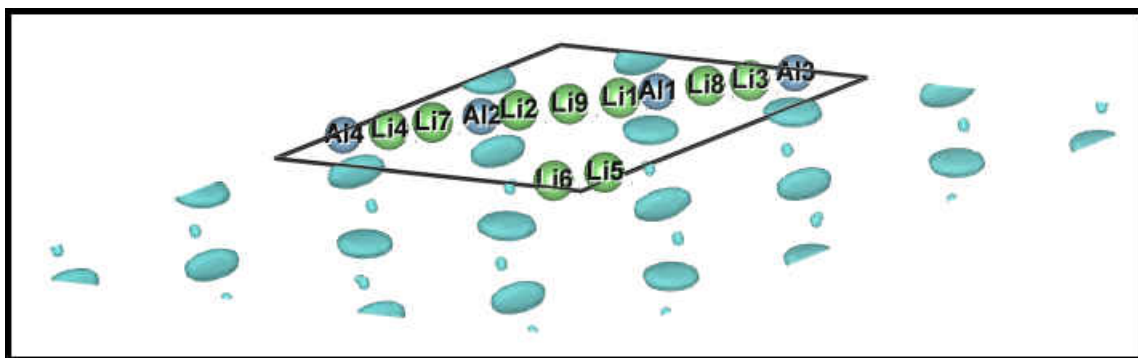
30

Figure 3.13: Charge Density Difference of Li_9Al_4.

It would seem that the ability to gain charge must cap at some point and the Group XIII metal would have enough charge that it could no longer need to create covalent bonds, but at almost 70 percent lithium in the stoichiometric ratio of Li_9Al_4, it does not seem that cap has been met. In all four lithium compounds with aluminum, the ZKC was successful in predicting and rationalizing these structures, both physically and electronically.

3.2 Compounds of Li with Ga, In, and Tl

The ZKC concept appears to be able to explain solids with various stoichiometric ratios. The next step, which will be explored, in this section is to determine if the ZKC can be used to successfully explain solids as lithium forms compounds with other Group XIII metals. The first solid analyzed was LiAl (see figure 3.8), by keeping lithium the same but descending down Group XIII, one can test the trend on how the anionic metal should pack and bond. The ZKC bonding mechanism should remain the same since in these structures one can assumes a formal charge transfer of -1 per lithium atom to the Group XIII metal. Luckily, LiGa[45], LiIn[?] , & LiTl[68] extended solids exist which provide an excellent opportunity to discover if a trend exists since all the compounds listed above exhibit a 1:1 ratio between Lithium and the Group XIII. The structures should bond and pack much like the aluminum in LiAl, making them Ψ-Si, as predicted by the ZKC. In past studies, it has been stated that LiTl[95] did not conform to the ZKC, however this study will show that is not the case.

LiGa[45]

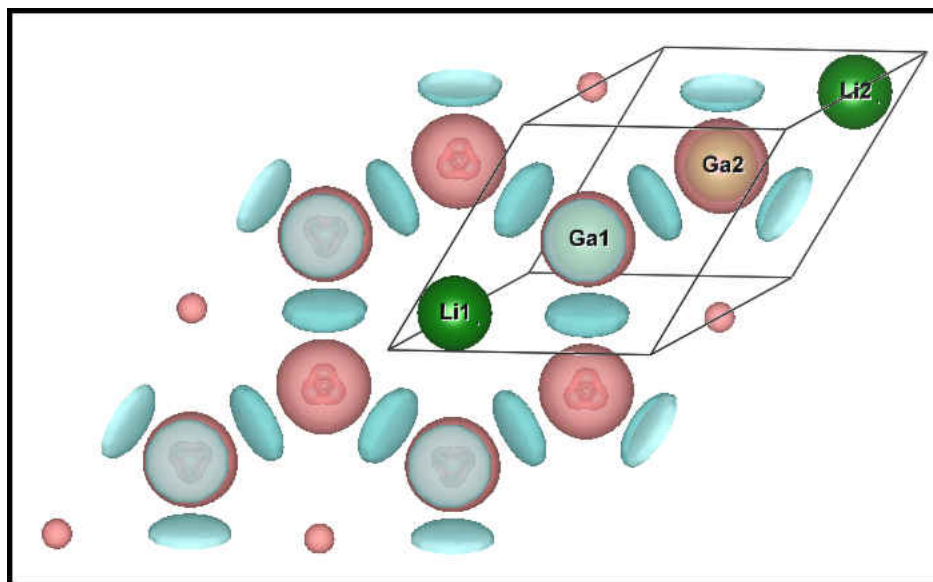The charge density difference for LiGa is presented in figure 3.14, below.

Figure 3.14: Charge Density Difference of LiGa·

In LiGa, lithium atoms have lost charge density and there is now charge density accumulation between gallium atoms, creating covalent bonds. Gallium atoms, just like aluminum in LiAl, pack and show bonding similar to that of elemental silicon.
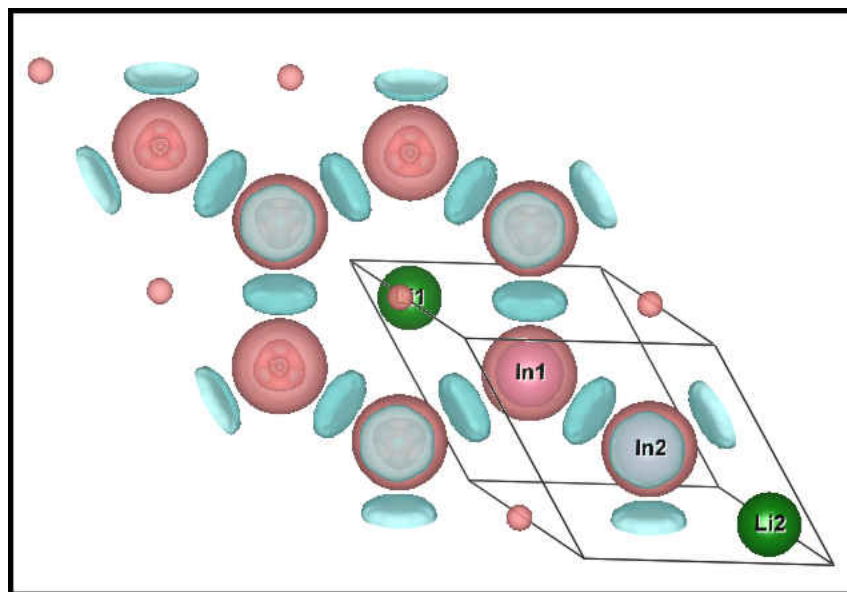
LiIn?

The charge density difference for LiIn:

Figure 3.15:

In LiIn, lithium atoms have lost charge density and indium atoms have charge density accumulation between their neighboring indium atoms, just like aluminum in LiAl and gallium in LiGa, which pack and show bonding similar to that of elemental silicon.

As one can see in both structures, LiGa and LiIn, the charge density difference maps show that lithium atoms have lost charge density while the more electronegative element has gained it, giving credence to the idea of pseudo-atom behavior since both structures pack and bond like LiAl, which in turn packs and bonds like elemental silicon, in accordance to the ZKC.

LiTl[68]

While the previous structures have packed and bonded as predicted, the question resides with the structure LiTl since LiTl has been stated to being an exception to the ZKC. The charge density difference map of this extended solid is pictured below in figure 3.16.
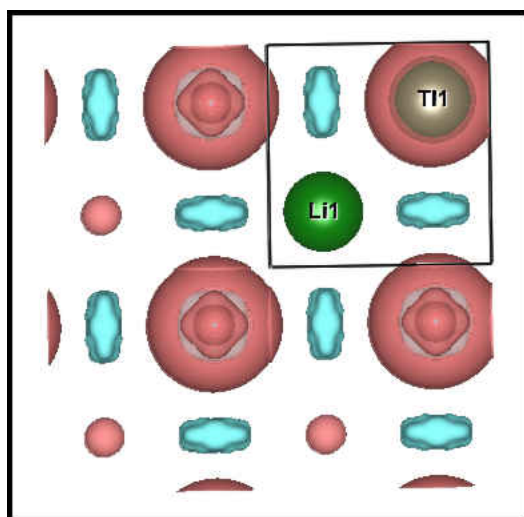
Figure 3.16: Charge Density Difference of LiTl.

Looking at figure 3.16, one can see that in this structure lithium atoms have lost charge density while charge density accumulated between thallium atoms. Since thallium atoms have charge density between each other, indicating the formation of covalent bonds, one would expect this structure to coincide with the ZKC. However, the packing of the thallium atoms in this structure does not conform to elemental silicon, which may be the reason this structure was said to not follow the ZKC in precious studies. However, if the ZKC concept is correct in terms of the bonding, perhaps the formal charge assumed transferred by lithium atoms might be incorrect. In this structure, lithium atoms might be donating more than a +1 charge due to thallium's lanthanide contraction allowing for more charge to be accepted

by thallium atoms. It has already been noted, in structures like $LiAl_3$ and Li_9Al_4, that a fraction of a charge can shift the packing and bonding into a neighboring Group. If lithium donated a fraction over a +1 charge it would throw thallium's valence count into Group XV, making thallium a Ψ-As, since it is closest to thallium in electronegativity. By examining the packing of arsenic atoms in figure 3.17,
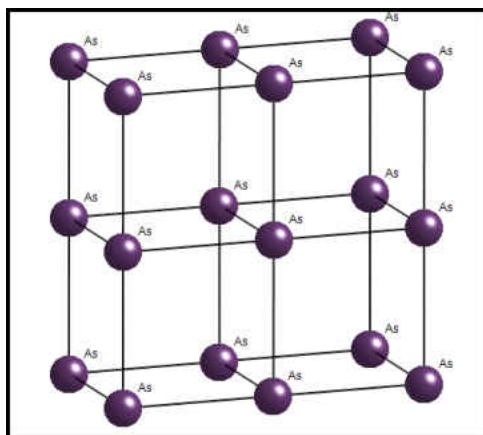
Figure 3.17: The structure of arsenic.

to the packing of thallium atoms in LiTl, one can come to the conclusion that thallium does pack like elemental arsenic. Calculating the charge difference density map of arsenic provided us with figure 3.18.
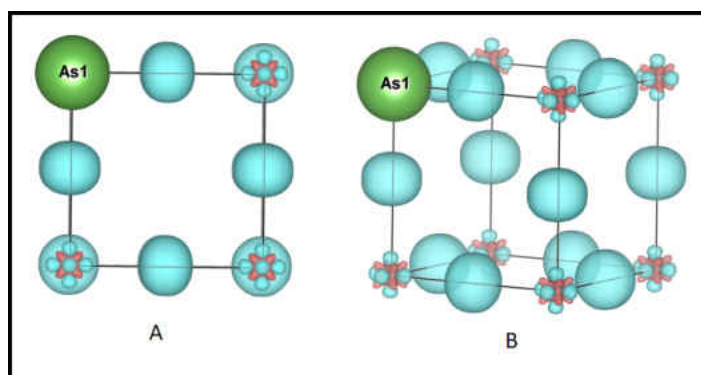
Figure 3.18: Charge Density Difference of As.

Looking at the charge density difference map of arsenic, where (A) is a top view and (B) is a skewed view, one can see that there is charge accumulation between arsenic atoms in much the same way that charge accumulates between thallium atoms in LiTl, indicating a similar covalent bond. With both the packing and bonding of thallium apparently similar to arsenic, one can not only gain insight on lithium atoms ability to donate more than a

-1 charge and thallium's ability to accept more charge, but also that the ZKC was able to successful predict and rationalize this extended solid. This indicates that while LiTl might look different than LiAl, LiGa, and LiIn, it does follow the ZKC in both how it packs and bonds.

3.3   Group I Relationships

Similarities

Group I metals in structures with Group XIII metals present a series of similarities as one travels down the group, as expected. However, due to diminishing electronegativity and the addition of the d subenergy to the atomic composition the the elements in period 3 and 4, one can find that while lithium and potassium contain similar bonding and structural patterns, lithium and sodium do not (unless the sodium structure is a high pressure phase). In contrast, potassium and sodium do contain similar structural and bonding patterns. As stated, this deviation in behavior between lithium and sodium could be due to the change in electronegativity and/or the addition of a 3d subenergy level to potassium, something that lithium is too small to have.

$50\% \geq$ or $\leq 60\%$ Ratio - lithium and sodium

Earlier in this chapter, compounds whose stoichiometric ratios contained 50 to 60 percent lithium (minus LiTl), transferred charge to the Group XIII metal to make the Group XIII metal behave like a Ψ-Si. This behavior, predicted by the ZKC, appears to be true for compounds containing lithium or sodium with gallium, indium and thallium, when maintaining a 50-60 percent stoichiometric ratio. Presented below are a series on charge density difference maps of structures that behave like the ZKC predicted and bond and pack similar to that of silicon, and where lithium or sodium donate their electrons to the Group XIII metal.

Lithium compounds

The first set of compounds in this section contain 55 percent lithium within their stoichiometric ratio. This set includes Li_5Ga_4 and Li_5In_4. These compounds, shown in figures 3.19 and 3.20, show lithium atoms losing charge density and charge density accumulating between the gallium atoms and indium atoms, forming covalent bonds. The bonding group XIII metals exhibit is as predicted and bond just like aluminum in Li_3Al_2, which packs and bonds similar to elemental silicon.
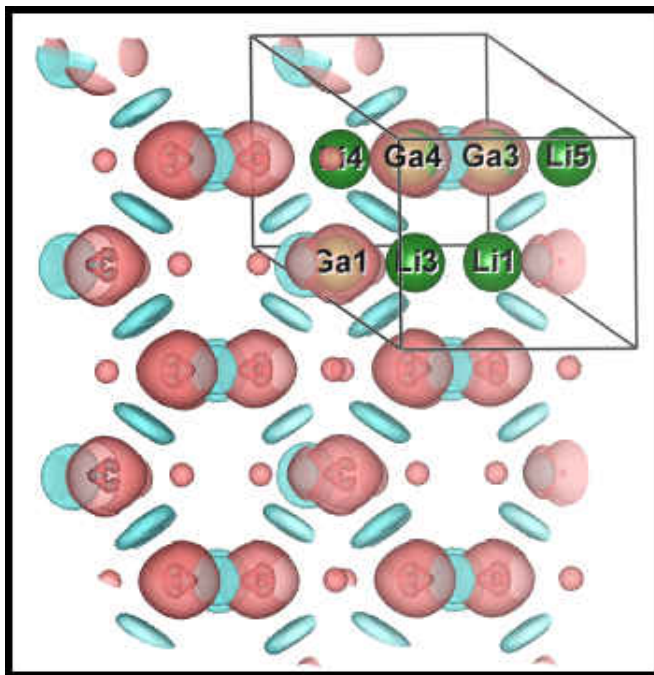
Li$_5$Ga$_4$[84]

Figure 3.19: Charge Density Difference of Li$_5$Ga$_4$.
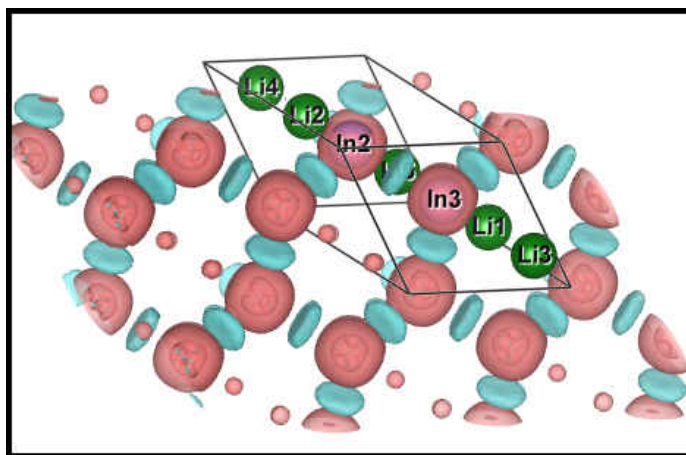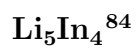
Li$_5$In$_4$[84]

Figure 3.20: Charge Density Difference of Li$_5$In$_4$.

The next two structures Li$_3$Ga$_2$ and Li$_3$In$_2$, also like Li$_3$Al$_2$, contain 60 percent lithium in their stoichiometric ratios. These two structures also bond and pack just like Li$_3$Al$_2$, which in turn packs and bonds like elemental silicon. The structures of these compounds can be seen in figures 3.21 and 3.22.
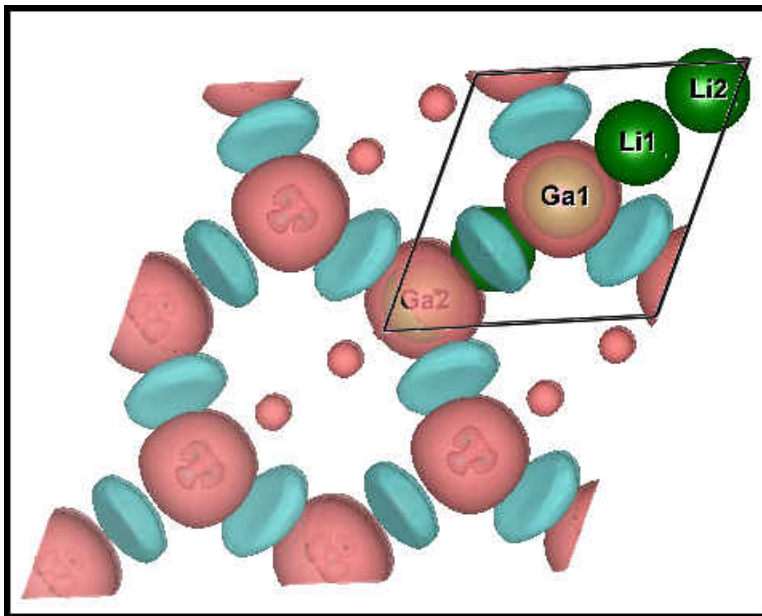
Li$_3$Ga$_2$[84]

Figure 3.21: Charge Density Difference of Li$_3$Ga$_2$.
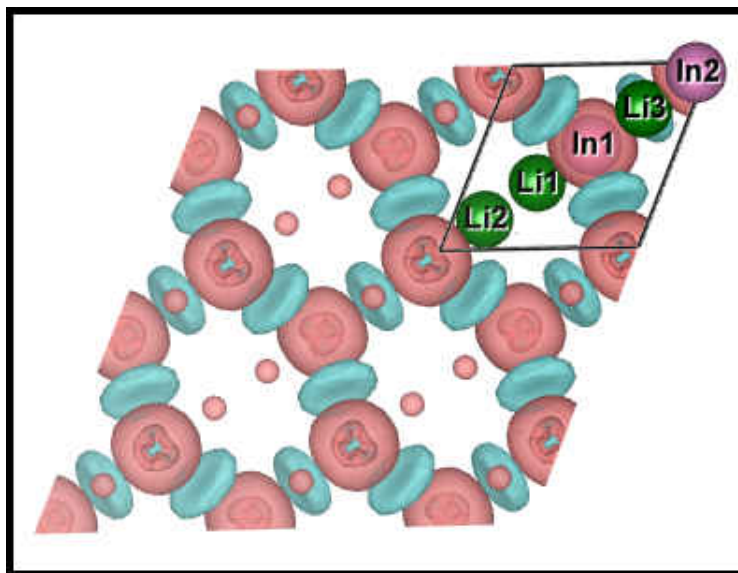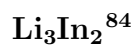
Li$_3$In$_2$[84]

Figure 3.22: Charge Density Difference of Li$_3$In$_2$.

As can be seen in the charge density difference maps of the lithium compounds in this section, the packing and bonding displayed of the Group XIII metals mirror the bonding of their pseudo-atom, silicon, as the ZKC predicted.

Sodium Compounds

Both structures below have a 1:1 ratio between sodium and Group XIII metals.

NaIn[116]
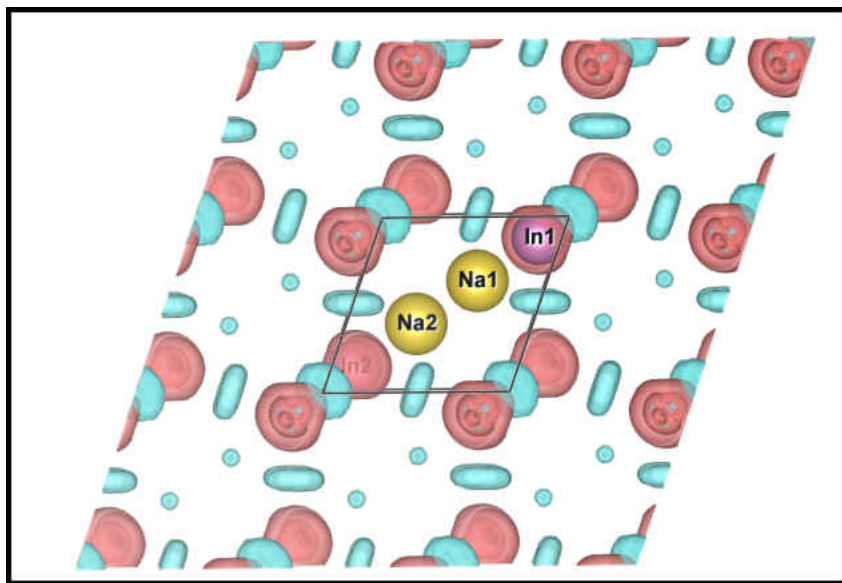
Figure 3.23: [Charge Density Difference of NaIn.

Figure 3.23, NaIn shows charge density accumulation between indium atoms, and displaying that indium packs and bonds like elemental silicon. Structures with matching anionic lattices are Li_3Al_2, Li_3Ga_2, Li_3In_2, Li_5Ga_4, Li_5In_4 and NaTl (seen below in figure 3.24). This is under the assumption that both, indium and thallium atoms, if gaining a -1 charge should bond and pack like silicon, in accordance to the ZKC.

NaTl[76]
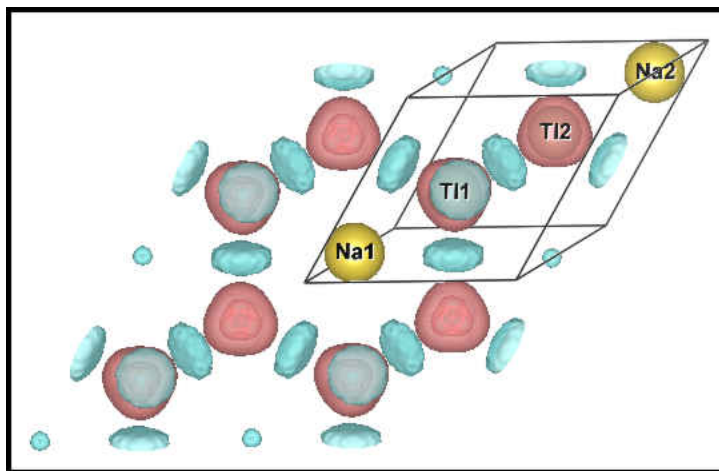
Figure 3.24: Charge Density Difference of NaTl.

Potassium Compounds

As stated previously, the Zintl Compounds containing sodium have similarities to both lithium and potassium Zintl Compounds, but potassium Zintl Compounds do not have many packing similarities to Zintl Compounds that contain lithium, unless in a high pressure phase or if the Group I metal is in the minority (stoichiometrically). While the potassium Zintl Compounds do seem to follow the ZKC, a deviation from the expected packing of the Group XIII metal can be noted when looking at KTl (space group Cmca (64)) versus KTl (space group Fd-3m (227)).

In figure 3.25, the structure of space group Fd-3m (227), is in a high pressure phase of KTl. The figure shows that potassium atoms have lost charge density and there is now charge density accumulation between thallium atoms. The structure formed by KTl (227) is similar to LiAl, LiGa, LiIn, NaIn, and NaTl with the anionic metal packing and bonding similar to that of elemental silicon and follows the ZKC.

KTl-1[26]
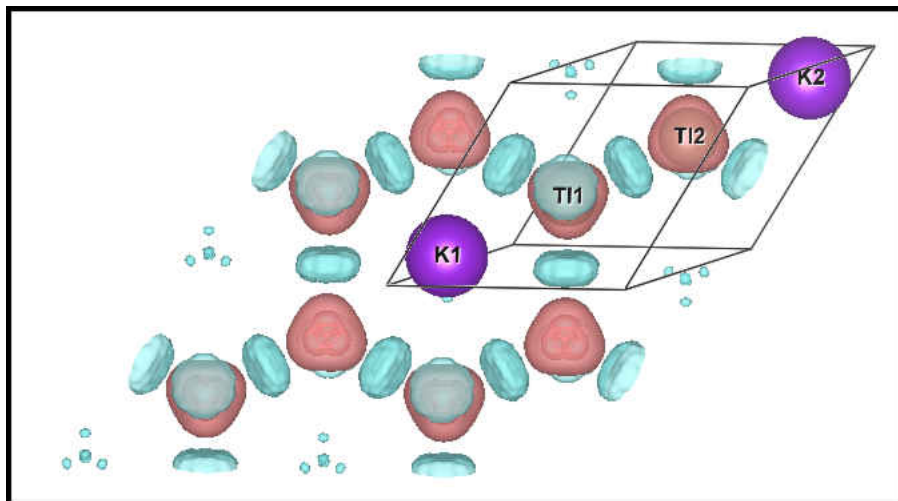
Figure 3.25: Charge Density Difference of KTl (227).

KTl-2[21]

In the room temperature stable structure of KTl, found in figure 3.26, with space group of Cmca (64), does not have thallium atoms packing like the expected pseudo-atom, silicon. much like LiTl, KTl presents with a different packing structure which can cause doubt on whether it does follow the the ZKC. In this structure's charge density difference, potassium atoms have lost charge density and charge density accumulation is seen between thallium atoms, creating the covalent bond predicted by the ZKC. In this case, thallium atoms form discreet Tl_6 octahedral clusters separated by potassium ions. The ZKC seems to also apply to this compound since the formation of covalent bonds can be seen, as well as charge transfer from the less electronegative metal. The inability to assess the correct charge transfer from potassium could be at the crux of why this compound was said to deviate from the ZKC. Guided by previously observed behavior in LiTl, one could pose that if potassium were donating a fraction more than a -1 charge then thallium would be a pseudo arsenic, a behavior noted in the compound LiTl. That would mean that the thallium would once again be acting as a Ψ-As and the discreet Tl_6 octahedral clusters should be found in elemental arsenic. The clusters found in KTl have been found in elemental arsenic and were studied by Igel-Mann, Stol, and Preuss,[42]. This compound along with LiTl provide insight about the ability for a Group I metal to lose more than a -1 charge, even if the charge lost is only a fraction more than the -1 assumed. In this structure, potassium atoms clearly transfer charge to thallium atoms donating enough charge that thallium atoms form discreet covalently bound clusters. The formation of these clusters, found within elemental arsenic, support the conclusion

40

that potassium in donating a fractional charge over the assumed -1 charge and that this compound also follows the ZKC. This conjecture is supported by the information that was garnered in two previously analyzed structures, LiAl$_3$ and LiTl. The formation of discreet clusters were noted in LiAl$_3$, where a fractional charge transfer occurred and was found to be enough charge transfer to shift the packing and bonding found within the structure to its neighboring group; something that can be seen here if one assumes potassium donated more than -1 charge. The justification for this conjecture that potassium could donate a charge greater than a -1 resides in the structure LiTl. In LiTl, it was it was shown that lithium was donating more than a -1 charge due to thallium's lanthanide contraction, since the bonding and packing of thallium mirrored arsenic. Therefore, it seems reasonable to assume potassium atoms in KTl could be donating more than a -1 charge, making thallium a Ψ-As. Since this structure exhibits a similar packing and bonding scheme as arsenic, this structure would be behaving as predicted by the ZKC.
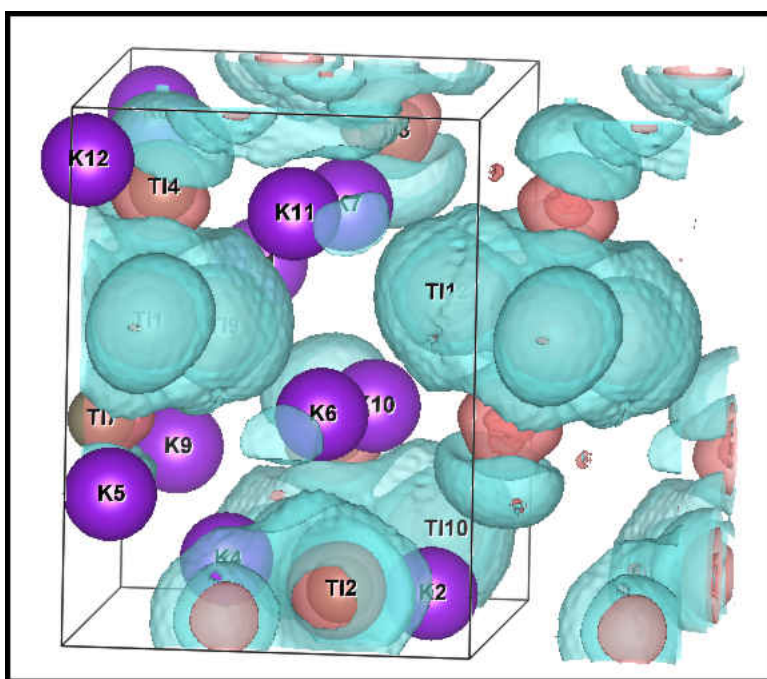
Figure 3.26: Charge Density Difference of KTl (64).

< 50% Ratio - Group I

In this section, Zintl compounds with Group I metals, being in the stoichiometric minority, will be discussed. This is because, as seen previously in LiAl$_3$, a fractional charge transfer is enough to place the Group XIII metal pseudo-atom behavior into a neighboring group. While all the structures presented below are not the same, the packing and bonding exhibited

by the Group XIII metals do conform to the elemental packing of it's Group XIV neighbor, due to the additional fractional charge transferred from the cationic metal.

Lithium Compounds

Li_2Ga_7[7]

In the case of Li_2Ga_7, each gallium would receive a -0.3 charge transfer, assuming a formal charge transfer of -1 from each lithium atom. This charge transfer is similar to that of $LiAl_3$ and in figure 3.27, one can see a loss of charge density on lithium atoms and charge density accumulation between gallium atoms as they form discreet dodecahedrons. These dodecahedrons are similar to those formed by elemental silicon[56].
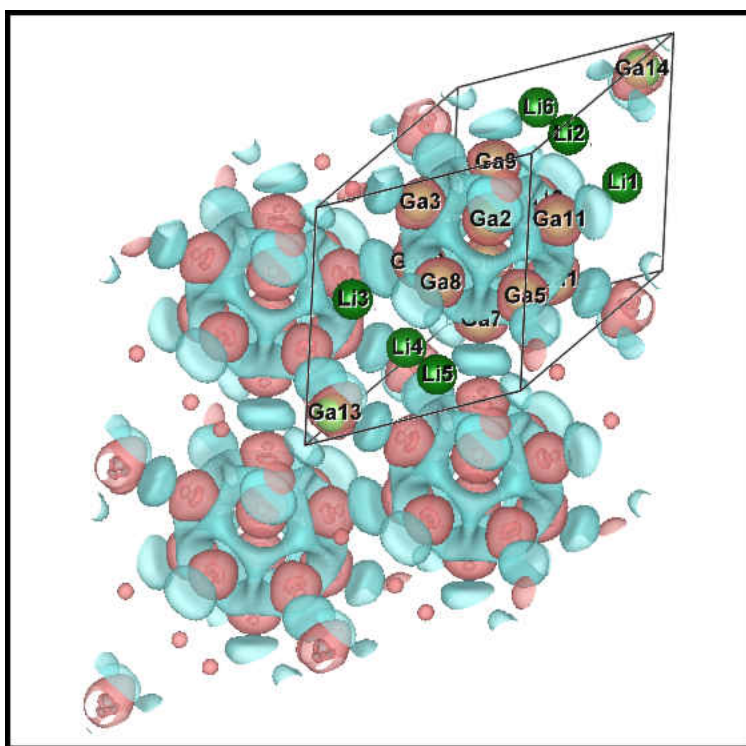
Figure 3.27: Charge Density Difference of Li_2Ga_7.

By removing where the charge density loss occurred in figure 3.28,the covalent bonding between gallium atoms can be more easily seen. This can be seen in the charge density between gallium atoms bridging the dodecahedrons (a), and gallium atoms, not part of the dodecahedron structure (b), forming covalent bonds between dodecahedrons. Since the formation of dodecahedrons can found in elemental silicon and there was charge transfer from lithium to gallium, the ZKC seems to apply to this compound as well.
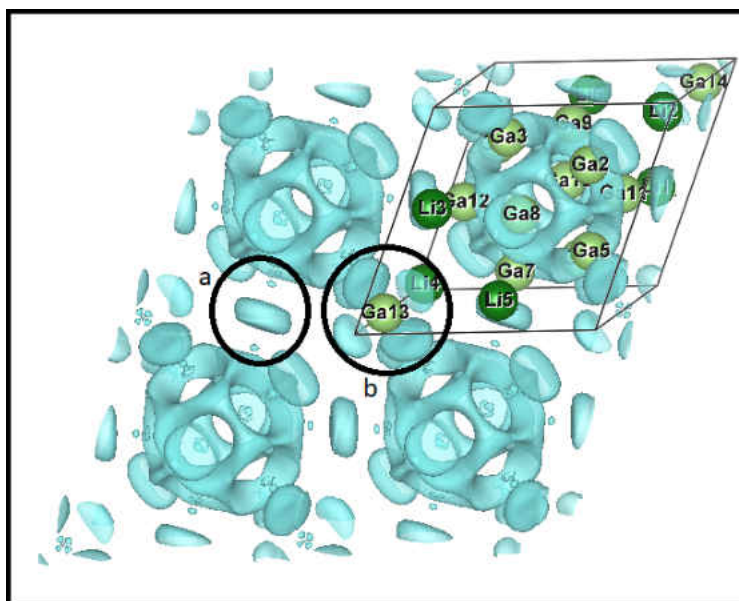
Figure 3.28: .

sodium and potassium Compounds

The compounds $NaGa_4$ and KIn_4 exhibit similar packing and bonding schemes yet still following the guidelines set by the ZKC.

$NaGa_4$[12]

In figures 3.29 and 3.30, the charge density difference maps show charge density accumulation between gallium atoms and indium atoms, which pack and bond much like elemental silicon, including the formation of the covalent bond. This formation has also been found in other Zintl Compounds such as $BaAl_4$, KGe_4, $RbGe_4$, KSn_4, and KPb_4, not found in this study, but discussed by Hoffmann & Zheng[115].

43
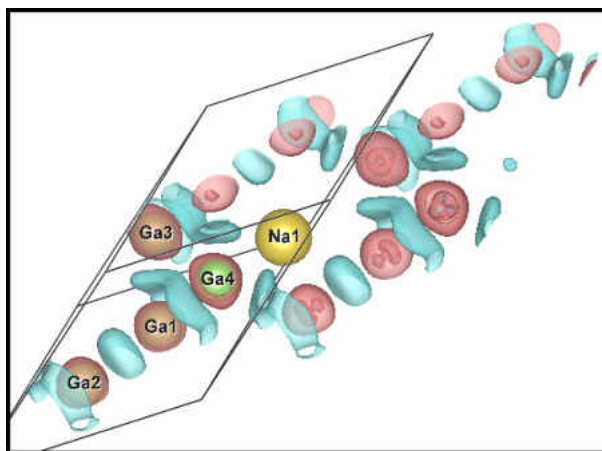
Figure 3.29: Charge Density Difference of NaGa$_4$.

KIn$_4$[13]
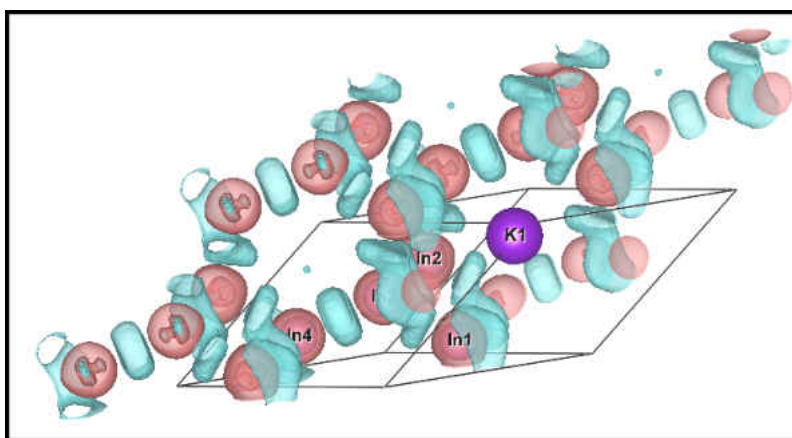
Figure 3.30: Charge Density Difference of KIn$_4$.

The following Zintl Compounds depicted, with potassium and gallium, also demonstrate packing and bonding like its Group XIV neighbor. In KGa$_3$, figure 3.31, charge density is seen to accumulate between gallium atoms while there is charge density loss on potassium atoms. Structures pack and bond similar to silicon and have matching anionic lattices to RbGa$_3$ and CsGa$_3$, which are also classified as Zintl Compounds and discussed in a paper by Belin, Ling, et al[6], once again following the ZKC.

KGa$_3$[94]
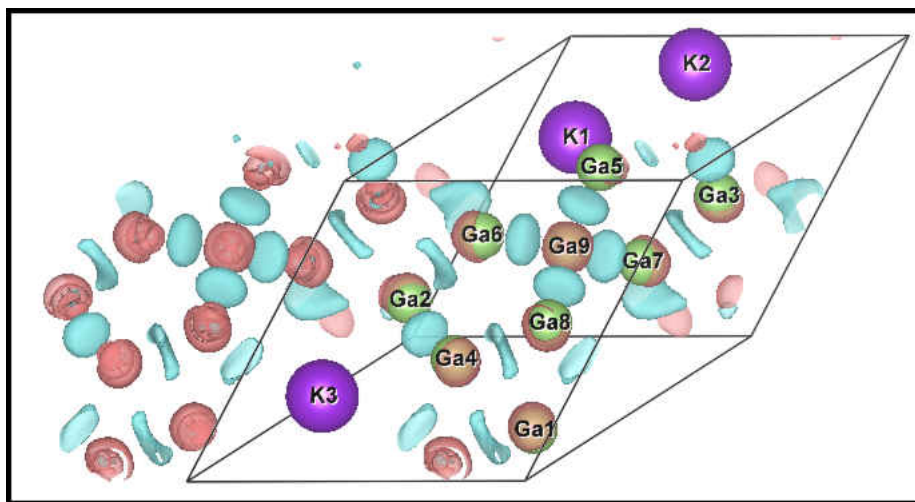
Figure 3.31: Charge Density Difference of KGa$_3$.

The following structure, packs like LiAl$_3$, in figure 3.10, and has the Group XIII metal forming cuboids similar to those found in elemental carbon.

K$_2$Ga$_3$[36]
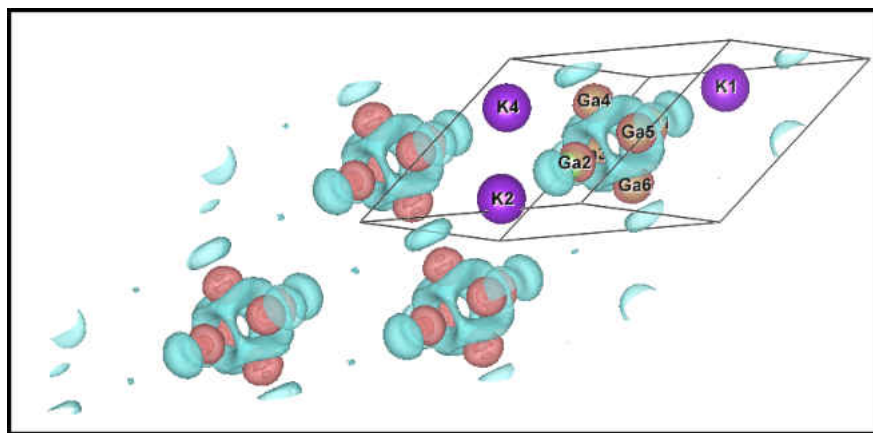
Figure 3.32: Charge Density Difference of K$_2$Ga$_3$.

The structures of Zintl Compounds composed of either sodium or potassium presented in this section, all exhibit a fractional charge transfer, where the less electronegative element transfers charge to the more electronegative element. The charge density difference maps for these structure show the anionic metal packing and bonding like the neighboring Group XIV.

This fractional charge transfer still causes structures to behave like the ZKC anticipated, giving rising support to this concept.

$> 60\%$ Ratio - Group I

Structures in this section have a greater than 60 percent stoichiometric ratio of Group I metal to the metals from Group XIII, in the Zintl Compound formed. As in Li_9Al_4, this excess in electronic charge transfer from the Group I metal has placed the Group XIII metal in an electron-rich environment and shifted the pseudo-atom behavior into groups past Group XIV.

Lithium Compounds

In the next three compounds, the ratio of lithium to the Group XIII metal is 2:1. Th assumed charge donation would be -1 donation per lithium atom, making the amount of charge donated by lithium atoms a total charge transfer of -2, placing the pseudo-atom behavior in Group XV. The bonding and packing by the anionic metal in the next three structures is akin to black phosphorus. Since the packing and bonding occurs like that of Group XV, this once again confirms the ZKC

Li_2Ga[84]
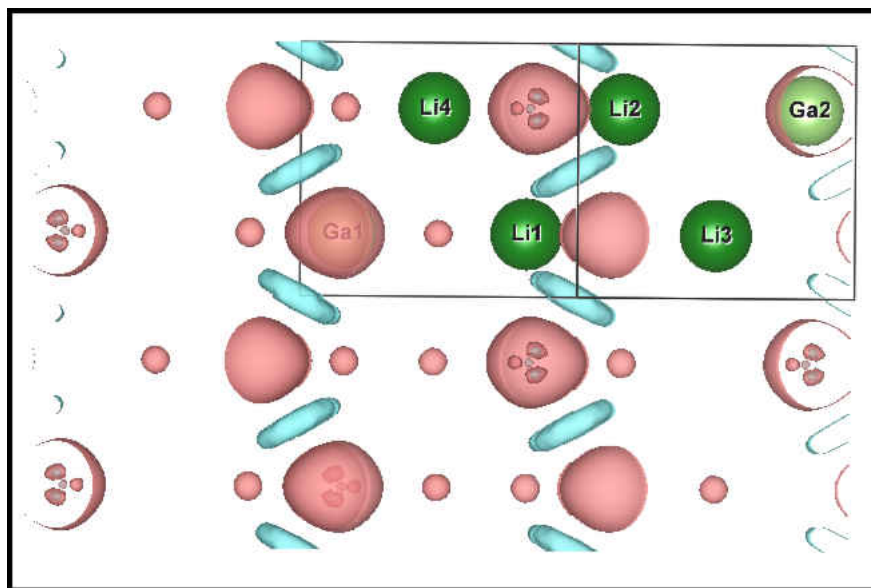
Figure 3.33: Charge Density Difference of Li_2Ga.

Li$_2$In[84]
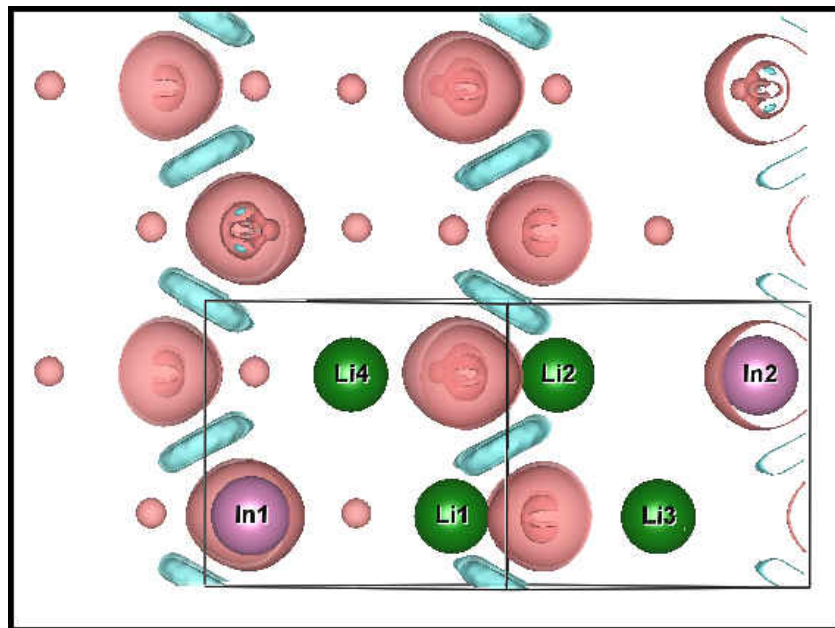
Figure 3.34: Charge Density Difference of Li$_2$In.

Li$_2$Tl[84]
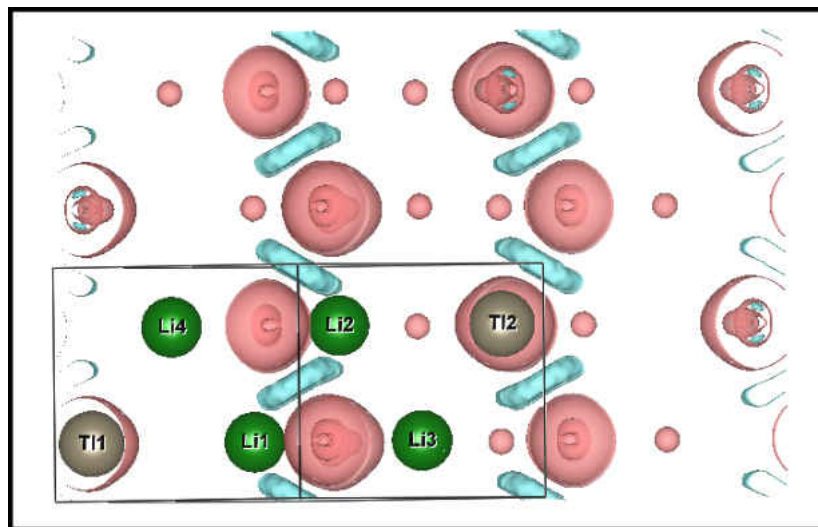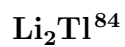
Figure 3.35: Charge Density Difference of Li$_2$Tl.

All three figures 3.33, 3.34, and 3.35, have the anionic metal bonding in zig-zag planar chains where charge density has accumulated between the Group XIII metal in creation of covalent

bonds. This packing and bonding formation is found within elemental phosphorus and once again seems to confirm the ZKC proposed behavior.

Sodium Compounds

In the next two structures Na_2In and Na_2Tl, the Zintl Compound present with a ratio of 2:1 with sodium to the Group XIII metal. It is assumed to donate a total of 2 electrons to the Group III metal. This would cause the Group XIII metal, per the ZKC, to bond like arsenic in Group XV.

Na_2In[116]
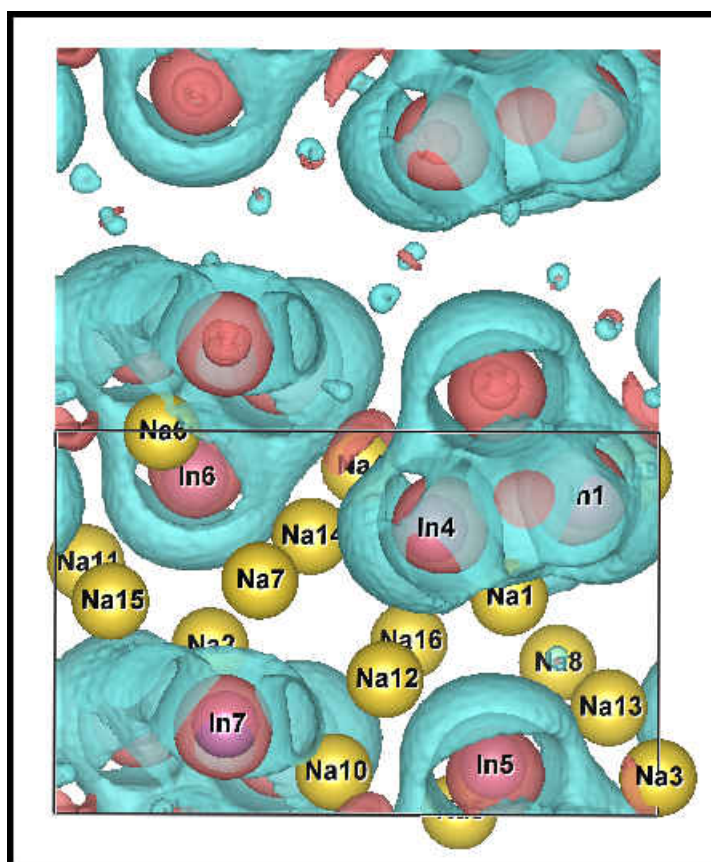
Figure 3.36: Charge Density Difference of Na_2In.

In figures 3.36 and 3.37, there is a clear charge density accumulation between and around indium and thallium atoms so that discreet tetrahedrons form which are separated by sodium ions, which have lost charge. This type of structure and bonding, found in both Na_2Tl and Na_2In, are identical to the tetrahedron formations found in elemental arsenic[62] and elemental phosphorus[79]. This behavior would once again seem to support the ZKC.

Na₂Tl[32]
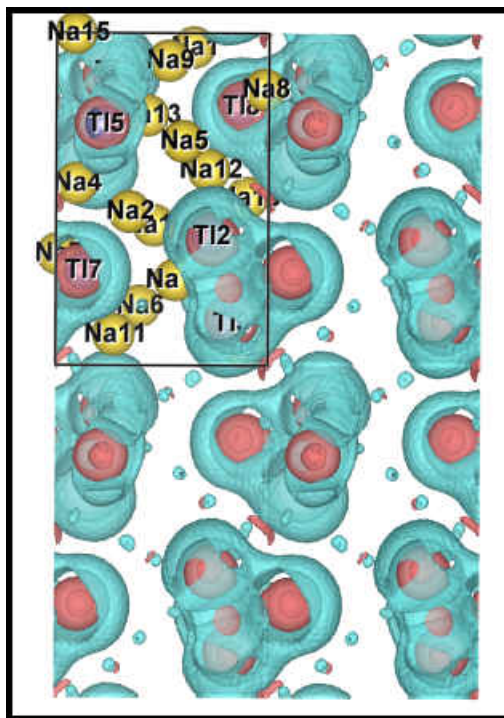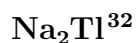
Figure 3.37: Charge Density Difference of Na$_2$Tl.

Deviation from Zintl-Klemm Concept in Group I

In Zintl Compounds formed between Group I and Group XIII, the majority follow the ZKC, as seen in the extended solids above. However, there does seem to be deviation from the ZKC when looking at more electron-rich solids. One such solid is Li$_3$Tl, found in figure 3.38 or 3.39, below. In this structure, the stoichiometric ratio is 75 percent lithium and the anionic metal seems to reach an electron acceptance cap. Lithium atoms in this extended solid seem to have donated enough charge to thallium that no bonding between thallium atoms is needed. The structure's charge density difference map shows a decidedly ionic solid since lithium atoms have lost charge and thallium atoms have gained charge density, in a spherical manner, with no charge density between thallium atoms. This can be seen in figures 3.38 and 3.39, which show thallium atoms, spherical in nature, with no charge accumulation between themselves. This structure is packed like BiF$_3$[60] which is also ionic in nature.

Li$_3$Tl[84]
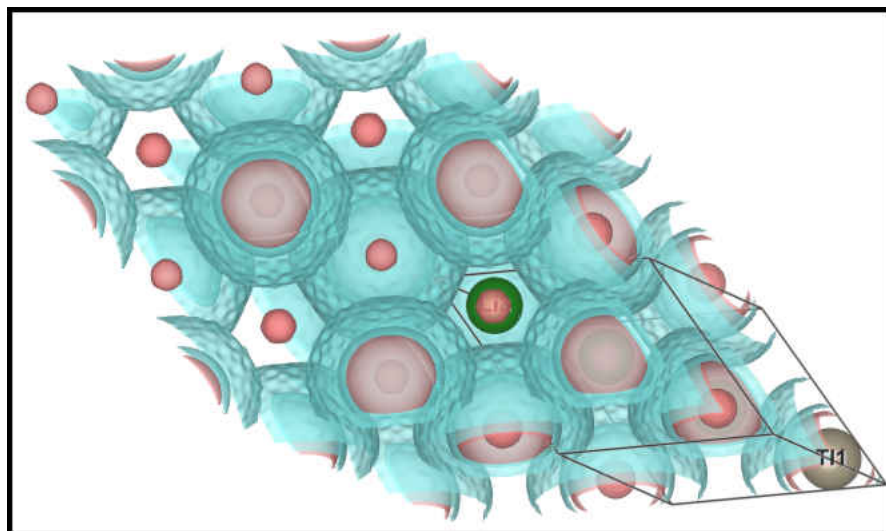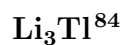
Figure 3.38: Charge Density Difference of Li$_3$Tl.
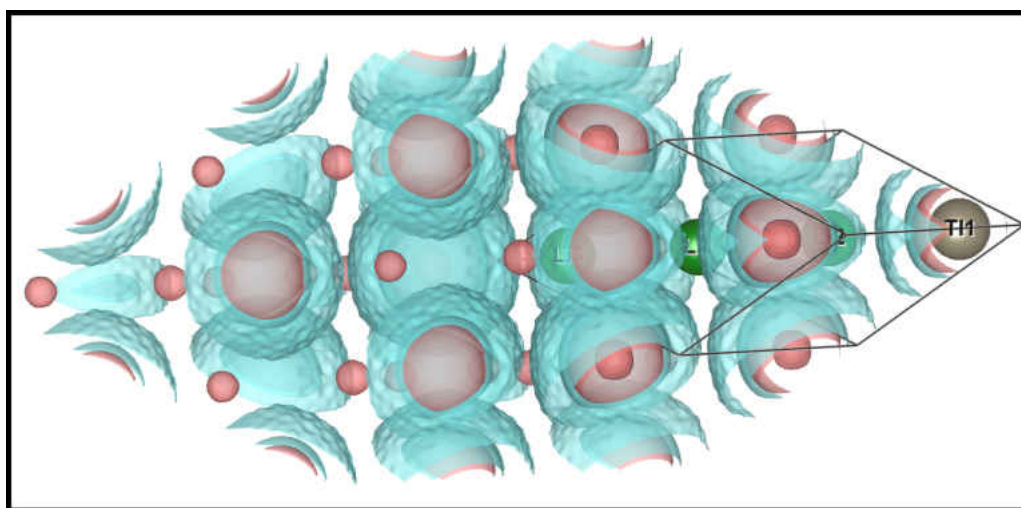
Figure 3.39: Charge Density Difference of Li$_3$Tl.

3.4   Group II Relationships

The structures assessed from Group II were those with magnesium and calcium. While many of the structures did conform to the ZKC, with charge being donated from least electronegative metal to the more electronegative metal and the more electronegative element forming bonds, there where just as many that did not follow this bonding concept. Some of the compounds displayed ionic characteristics like (Mg$_5$Ga$_2$ and Mg$_5$In$_2$), and others displayed more

metallic characteristics such as $MgIn_3$, CaTl, and $CaTl_3$. Those compounds that followed the ZKC are presented in table 3.4, and the charge density difference maps of those compounds may be found in Appendix A. While over 70 percent of the compounds (including those with metals from Group I) do follow the ZKC, a significant portion of those compounds that do not are compounds that contain a Group II metal. Therefore, it seemed pertinent to address those compounds below.

Magnesium & Calcium Following ZKC (Subset of Group II Zintl Compounds)		
MgGa	Mg_2Ga_5	Mg_2Ga
$MgGa_2$ (194)	MgIn	Mg_2In
$MgGa_2$ (55)	MgTl	Mg_5Tl_2
Mg_2Tl	$CaGa_2$	$CaGa_4$

Table 3.4: List of Zintl Compounds which follow the ZKC and will be presented in Appendix A.

Deviations from the ZKC

Within the compounds that presented unusual bonding, the majority constitute the Zintl Compounds formed from calcium. The unusual bonding behavior mechanism uncovered via the charge density difference maps of these compounds depict calcium atoms gaining charge density at the expense of the more electronegative metal, however the more electronegative metal, now deprived of electrons still form covalent bonds between themselves to stabilize within the structure. In many cases, after calcium has acquired charge, the Group XIII metal seems to be a positive ion. The formation of a calcium anion is supported by the heavily polarization of the cationic Group XIII metal towards the anionic calcium. While this phenomena cannot be explained by the ZKC, it is interesting to note that many of the bonding schemes seen by the Group XIII mirror their more electronegative neighbors. This could be caused by Group XIII metal's collective electronegativity, which would cause the charge deficient metal to more efficiently share its electrons and as such pack in structures that maximize this need. This more efficient packing and bonding scheme can usually be found in more electronegative elements such as carbon, arsenic, phosphorus, selenium, and sulfur. While these solids seem to pack like there more electronegative neighbors, there seems to be no discernible pattern as to which bonding and packing scheme the Group XIII metal

takes. Below are the charge density difference maps of seven calcium solids that display this behavior.

Unusual Calcium Behavior

The first structure presented is $CaAl_2$, which according to the ZKC would have the calcium donating a -1 charge to each aluminum atom. This would place the aluminum metal in Group XIV and bonding like a pseudo silicon or even a pseudo carbon (as seen in $LiAl_3$).

$CaAl_2$[40]
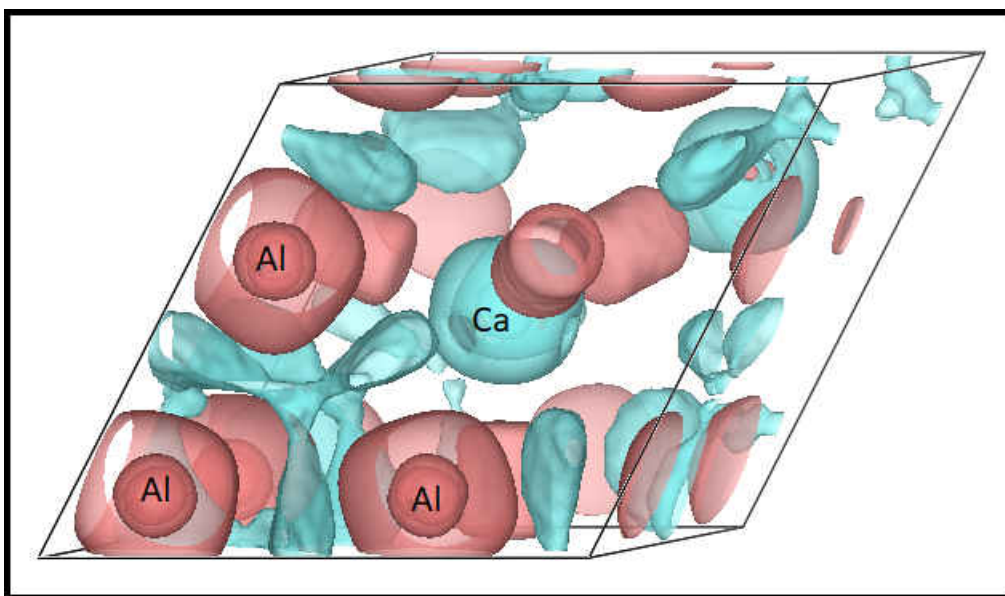
Figure 3.40: Charge Density Difference of $CaAl_2$.

While the packing and bonding displayed by aluminum in $CaAl_2$, in figure 3.40, can also be found in amorphous carbon[58], it does not exhibit the the charge transfer expected of calcium atoms, but instead calcium atoms have gained charge density at the expense of aluminum atoms. This solid, and the following solids presented in this section, demonstrate why the need to look at a solids electronic structure as well as its packing is of utmost importance. If only being guided by the packing of the aluminum atoms, one could determine this solid to behave as any other Zintl Compound, yet it is not until one peers into the electronic structure that one witnesses that the ZKC actually fails to explain the behavior presented in this solid.

CaAl₄[65]

The compound $CaAl_4$, which has two additional aluminum atoms per unit cell, in comparison to $CaAl_2$, figure 3.41, has aluminum atoms creating a lattice similar to those found in silicon, which is what one would expect of this structure if one was solely basing their examination on only the packing of aluminum atoms within the compound. However, in figure3.41, calcium atoms are gaining charge density which is not the ZKC expected behavior for this metal.
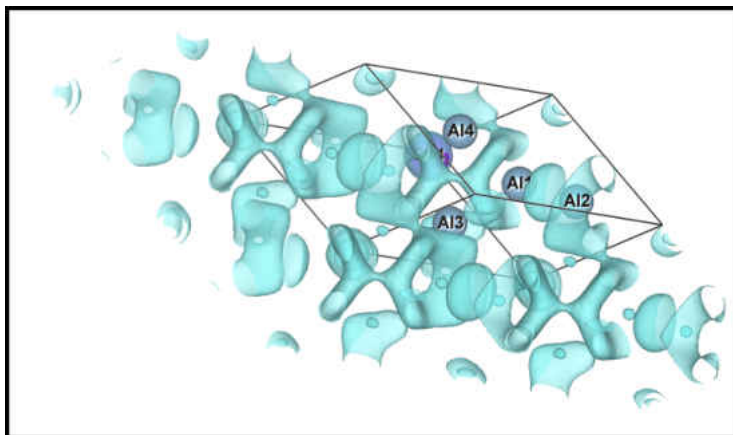
Figure 3.41: Charge Density Difference of $CaAl_4$.

CaGa[59]

In CaGa, figures 3.42 and 3.43, gallium atoms gains charge density between themselves to create Ga-Ga zig-zag chains, however, calcium atoms having gained charge density create a polarizing effect on the gallium atoms. The calcium atoms do not form bonds but stay as stable anions. This zig-zag chain was also found in a study by Harms, Wendorff, and Röhr[34].
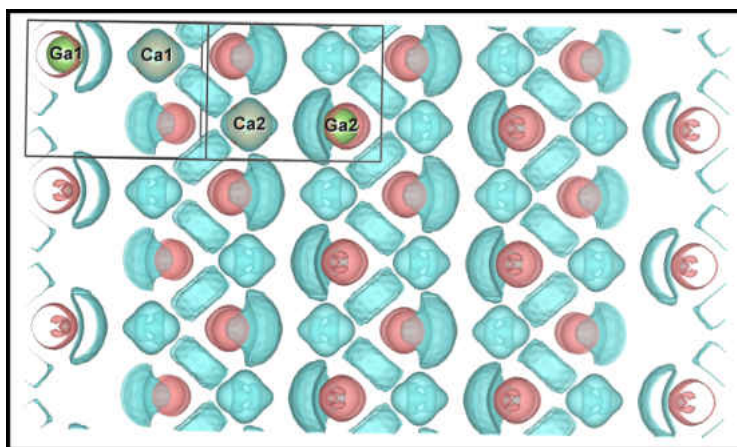
Figure 3.42: Charge Density Difference of CaGa.
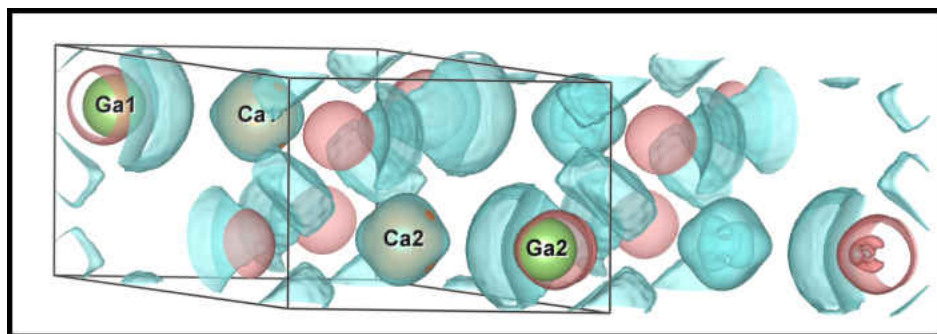
Figure 3.43: Charge Density Difference of CaGa. Magnified to make the polarization of gallium atoms towards calcium atoms more observable.

Ca_3Ga_5 [18]

In figure 3.44, there is charge density found between gallium atoms, forming covalent Ga-Ga bonds, which form kinked zig-zag chains and polarize towards calcium atoms, which have acquired charge density around themselves to form calcium anions.
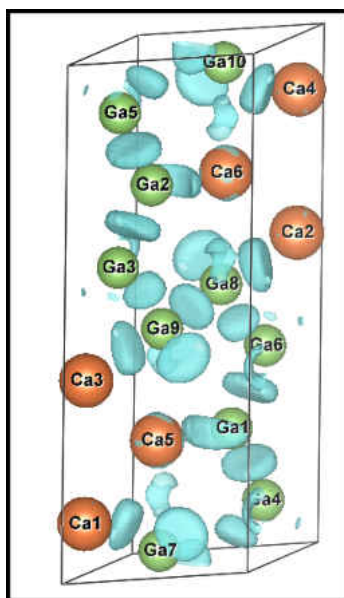
Figure 3.44: Charge Density Difference of Ca_3Ga_5.
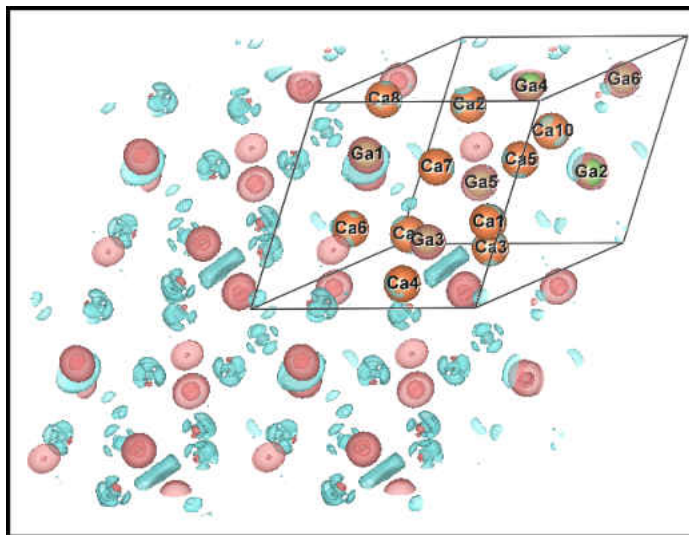
Ca$_5$Ga$_3$[14]

Figure 3.45: Charge Density Difference of Ca$_5$Ga$_3$.

In the structure of Ca$_5$Ga$_3$, figure 3.45, calcium atoms have gained charge density while gallium atoms form discreet diagallium clusters with charge density accumulation between them, similar clusters form in both elemental sulfur and elemental iodine. However, this cannot be accounted for since no charge has been donated by calcium. Instead, calcium atoms have gained charge density at the expense of gallium atoms, going directly against the proposed charge transfer mechanism in the ZKC.

CaIn[55]

In figure 3.46, (a) shows where there is charge accumulation between indium atoms, and (b) shows that calcium atoms has acquired charge density almost spherically, indicating that it is functioning as an anion. The packing and bonding seems like that found in elemental arsenic3.17, however calcium does not seem to be donating 2 electrons as expected, so while a pseudo-arsenic behavior would be expected if the charge transfer was occurring as the ZKC stated, the ZKC cannot explain the bonding of indium in this compound adequately.
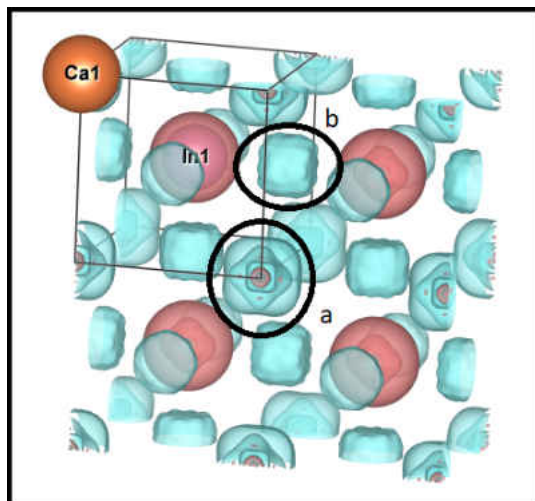
Figure 3.46: Charge Density Difference of CaIn.

CaIn$_2$[39]

While CaIn$_2$ has a space group of $P6_3/mmc$ (194) and packs just like MgGa$_2$ and CaGa$_2$, which do follow the ZKC, this solid does not follow the charge transfer method proposed by the ZKC. In this structure, the charge density is not lost from calcium atoms, but gained, even though indium atoms shows an increase of charge density between them creating covalent bonds. The forming of covalent bonds between indium atoms is irrespective of the charge density lost to calcium atoms. The lattice formed by indium packs in layers of hexagonal sheets like those found in graphite. This can be seen in figure 3.47.
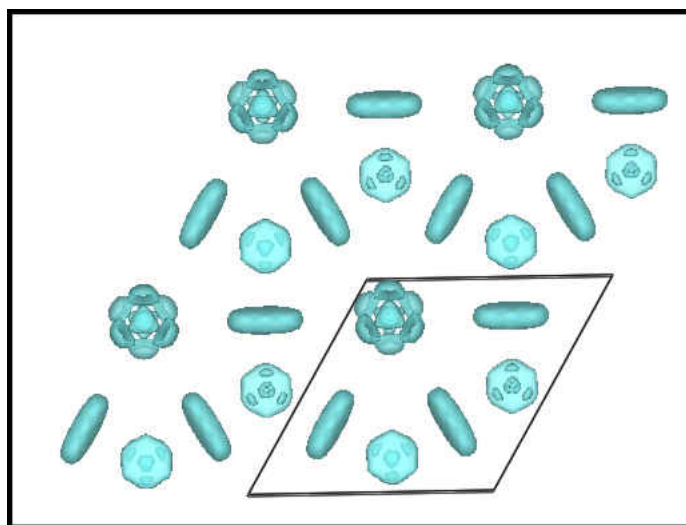
Figure 3.47: Charge Density Difference of CaIn$_2$.

Other Deviations from the ZKC

The next three compounds to be assessed, $MgAl_2$, Mg_3In, and Ca_3Tl, all display unusual bonding.

$MgAl_2$[86]

In the first compound, $MgAl_2$, one would expect that magnesium atoms donate charge to aluminum and have aluminum pack and bond like its neighboring groups, however this is not the case. This could be due to the relative closeness between aluminum and magnesium as they are neighbors themselves. While there does seem to be loss of electron density from magnesium atoms, as one would expect, there is also loss of charge density from aluminum atoms. The charge density seems to be accumulated between both magnesium atoms and aluminum atoms as seen in figure 3.48. While there is no covalent bonding seen between magnesium atoms there does appear to be covalent bonds between aluminum-aluminum and magnesium-aluminum atoms.
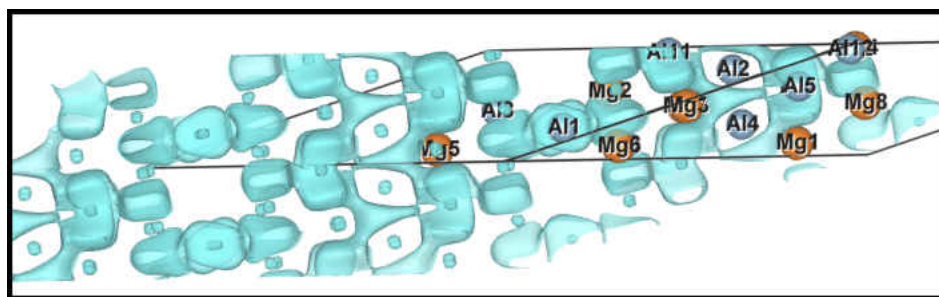
Figure 3.48: Charge Density Difference of $MgAl_2$.

In the next two structures, the Group II metal makes up 75 percent of the stoichiometric ratio with its Group XIII metal. This would suggest that in such an electron-rich environment the Group XIII, being more electronegative than Group II metals might form ionic solids much like in Li_3Tl, however that is not the case in either solid.

Mg_3In[80]

In structure Mg_3In, figure 3.49, charge density is seen to be lost by magnesium atoms in a spherical manner giving credence that they have lost charge to form cations. However, despite the accumulation of charge density between and around indium atoms (b), there is also charge accumulation between the the twelve magnesium atoms in the unit cell (a), in all probability to stabilize the positive magnesium ions within the structure.
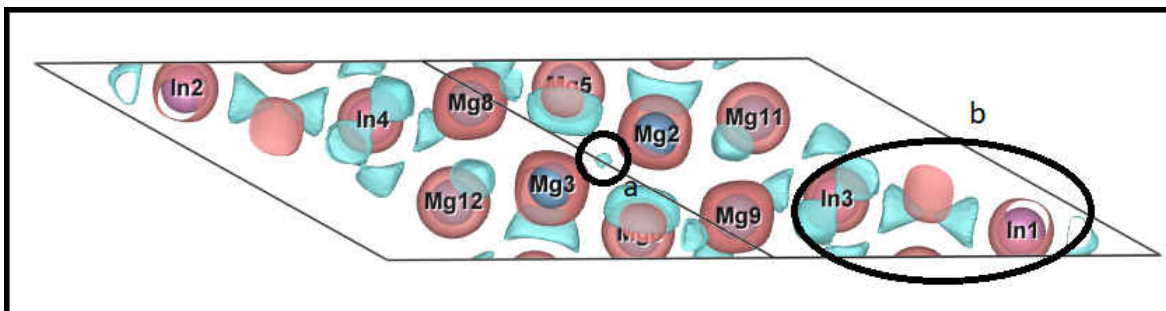
Figure 3.49: Charge Density Difference of Mg$_3$In.

Ca$_3$Tl[11]

In contrast Ca$_3$Tl, exhibits similar behavior to the other calcium compounds examined above, where calcium gains charge density while thallium loses charge density. The effect calcium has on thallium, a Group XIII metal, can be seen more clearly in figure 3.50. In this structure, calcium atoms closest to thallium atoms gain charge spherically and do not seem to interact with thallium atoms or other calcium atoms, suggesting that a cap of transfered charge has been met by these calcium atoms. However, calcium atoms between the other calcium atoms appear to not have acquired enough charge and cause thallium atoms to heavily polarize the remaining charge on thallium towards itself. Despite calcium atoms having already gained electron density, (A) charge density is still being polarized towards Ca1 despite the more electronegative aspect of thallium . (B) The placement atoms were removed for easier viewing so that the two types of calcium anions can be easily seen. The first type, like Ca2 and Ca3, are spherical in nature and are packed next to thallium atoms, seeming to have acquired the maximum charge calcium can contain, while the second type of calcium, Ca1, polarizes thallium atoms charge towards itself.
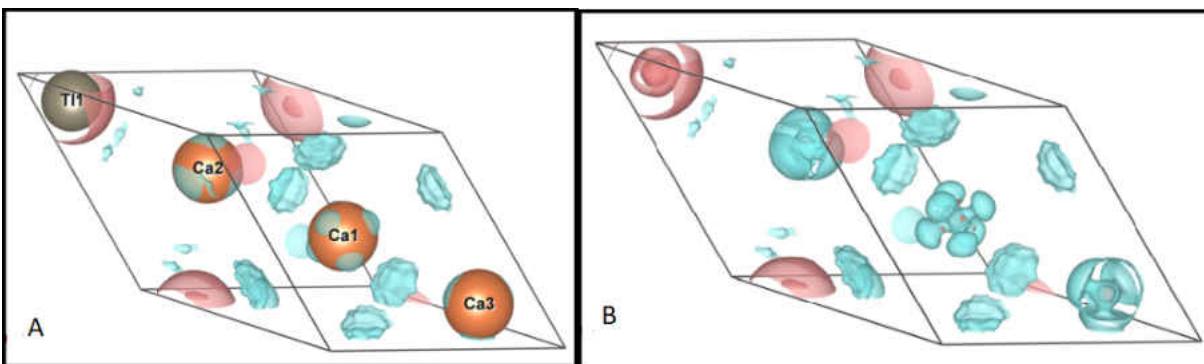
Figure 3.50: Charge Density Difference of Ca$_3$Tl.

58

3.5 Concluding Remarks

In this study, over 50 different Zintl Compounds were analyzed using various computational methods. These extended solids were then looked at in terms of the ZKC, and while some do not conform to the Zintl-Klemm Concept, most notably all the calcium compounds studied, over 70 percent of the compounds studied did follow the bonding mechanism proposed by this concept. The concept does not account for each elements unique properties, yet the ZKC still provides a suitable method of rationalizing and predicting how the bonding and packing in these intermetallics will behave. Based on a simple electron counting scheme, this scheme is able to be applied regardless of differing stoichiometric ratios found within the compounds. This study also revealed that a fractional charge transfer to the more electronegative metal can cause distortions in the bonding and packing of these intermetallics, such that when a more electronegative element acquires a fractional charge it could shift the pseudo-atom behavior in the metal into a neighboring group. This behavior was noted in $LiAl_3$ and in Li_9Al_4. In compounds like LiTl and in KTl, where the charge transfered was hypothesized to be more than the -1, the formal charge assumed for the Group I metal, the anionic metal was seen to behave like arsenic, which is in the next Group XV. These compounds allowed for new insight on the ability of the different metals to donate more than the assumed formal charge and the role the lanthanide contraction plays in that donation.

The calcium compounds, present a puzzling phenomena, and go in part against the ZKC. In part because in almost all cases the calcium compounds show calcium as the one that acquires charge instead of donating it, becoming an anion. The calcium anion does not seem to bond with either itself or other elements, but instead cause a strong polarizing effect in the other metal. The more electronegative metal, in this study Group XIII, continue to form covalent bonds with itself, despite its polarization towards calcium. The bonds and lattices formed by the Group XIII metal are similar to those found in what would have been their pseudo-atom if calcium had donated its charge. The behavior calcium exhibits could be caused by calcium's ground state electron configuration. This element has an empty 3d subenergy level and a closed 4s subenergy level. With the 3d subenergy level extremely close to the nuclei, it seems that it could be experiencing an effect similar to those found in phosphorus, sulfur, chlorine, and have an expanded octet. In addition, it also contains a closed subenergy level, which may provide an added stabilizing effect as seen in zinc and cadmium. This stabilization provided by the closed 4s subenergy level and the empty 3d energy level might allow this element to acquire charge when placed in an electron-rich environment. Although this study did not examine structures formed with elements further down Group II to determine if strontium, the element directly below calcium, also

59

presents these unique properties, studies suggest that it does behave like a traditional Zintl Compound[20,75].

Chapter 4

Theoretical Analysis of the Extended Zintl-Klemm Concepts

4.1   Model - 1

In the previous chapter, the Zintl-Klemm Concept demonstrated an ability to predict and rationalize the intermetallics first assigned under the term "Zintl Compounds" by using a simple electron counting scheme. With the success of the Zintl-Klemm concept (the concept and the compounds it consisted of), it was extended to include transition metals and late post transition metals, with the new term to encompass these solids being "Extended Zintl Compounds". This extension, the Extended Zintl-Klemm Concept Model 1 (EZKC-1 model), based on Hoffman and Papoian's work[67], was created in order to widen the volume of solids that can be rationalized and predicted. In this section, this study will be examining this extension by focusing on a subset of antimony compounds that reportedly bond and pack like sulfur in FeS_2. This change between elemental sulfur to sulfur within a compound is part of the evolution of the defined term "pseudo-atom". Since pseudo-atoms in this extension are found within similar compounds, this analysis must begin with an examination of the packing and bonding found in the extended solid the pseudo-atom derives from. The compounds that will be examined in this section are presented in the table 4.1, below.

4.1.1 FeS_2 - The Pseudo Compound

By taking advantage of the many compounds which have been synthesized and cataloged since the creation of the original ZKC, one can determine the pseudo-atom by looking at various compounds that pack similarly while also containing a nonmetal that would be isoelectronic to the more electronegative metal after it has accepted a charge transfer from

Extended Zintl Compounds
FeS$_2$ (pseudo-atom compound)
FeSb$_2$
CoSb$_2$
NiSb$_2$
CrSb$_2$ (58)
CrSb$_2$ (140) (unmentioned in Hoffman's study)
TiSb$_2$ (unmentioned in Hoffman's study)

Table 4.1: List of Extended Zintl Compounds to be analyzed in terms of The Extended Zintl-Klemm Concept (Model 1).

the transition metal donating its charge. The difficulty lies in accurately determining the charge transfered, as transition metals have multiple oxidation states, requiring knowledge of stable oxidation states in transition metals. In the antimony compounds presented below, the majority of structures are packed like FeS$_2$ and the more stable oxidation state that the transition metals share is that of +2. This donation of 2 electrons by the transition metal would mean that each antimony atom would receive a charge of -1, making antimony isoelectronic to Group XVI. This would make antimony a Ψ-S. This extension also proposed the idea of long range bonding interactions between the anionic metals, lengths that would have previously thought too long for any significant bonding to occur. In these Extended Zintl Compounds, it was hypothesized that antimony, in these structures, would be capable of having bonding interactions, which range between 2.80Åto 3.26Å. This investigation will show that these bonding ranges actually span farther than initially suggested. The first CDD map to be examined is FeS$_2$[15] which will be indicative of how the antimony atoms will be bonding in the other structures to be analyzed.

In figure 4.1, one can see that each sulfur atom has tetrahedral bonding with sulfur bonded to three iron atoms and the sulfur atom in the neighboring cell (a). The distances between S-Fe and S-S bonds range between 2.21Åand 2.25Å. There is an increased charge density accumulation between the S-Fe versus the S-S bond, but this can easily be accounted to the large difference in electronegativity between iron and sulfur. If the EZKC-1 model is correct then the bonding scheme exhibited by the sulfur in FeS$_2$ will be shared by antimony
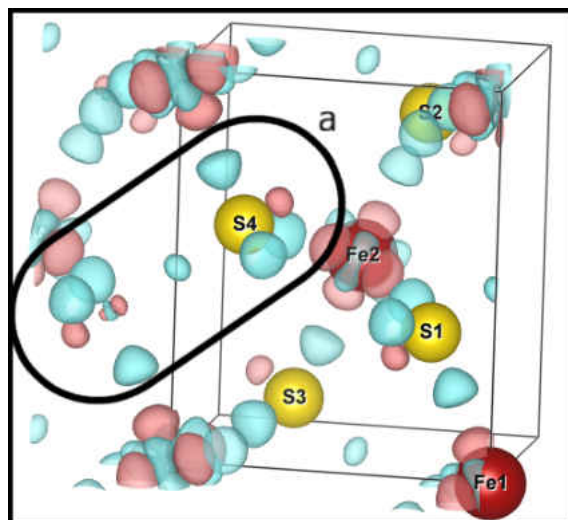
Figure 4.1: Charge Density Difference of FeS_2.

in the compounds found in table 4.1, irrespective of the longer distances found within the solids. The study proposed the possibility of antimony forming the following ions, which are traditional sulfur bonding schemes. The possible antimony anions can be seen in figure 4.2.
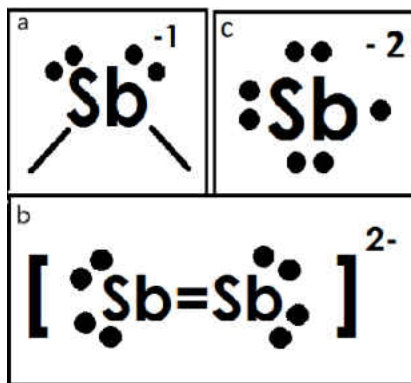
Figure 4.2: Possible Antimony Ions in the MSb_2 (where M= Fe, Co, Ni, and Cr).

4.1.2 Antimony a Pseudo-Sulfur

Figure 4.3, shows the compound $FeSb_2{}^2$, which is similar in the way it is structured to FeS_2. In this structure iron remains packed the same and instead of being surrounded by sulfur atoms, iron is surrounded by antimony atoms. Antimony atoms in $FeSb_2$ seem to bond tetrahedrally, just like sulfur atoms in figure 4.1, with antimony seeming to form the ion (a) in figure 4.2. In the ions presented in the study (and shown above) a -2 charge transfer is assumed to occur between iron to antimony, however iron has two stable oxidation states of +2 and +3. While iron does have two states and could be donating more than the assumed

-2 charge, the behavior of the antimony, like sulfur, supports this proposed bonding scheme. In the CDD map of FeSb$_2$, there seems to be a larger charge density accumulation between the Sb-Sb bond between cells than the S-S bonds seen in FeS$_2$. The larger charge density accumulation between the antimony-antimony atoms supports the claim that even at longer distances there does seem to be metal metal interactions. The distance between the Sb-Sb bond is 3.15Å, much larger than those seen in the S-S bond, in FeS$_2$, which had a bond length of 2.21Å. The behavior of antimony in this structure appears to support the new extension to the ZKC as bonding between the antimony atoms is apparent despite long distances, and the bonding in the antimony mirrors its pseudo-atom, sulfur.
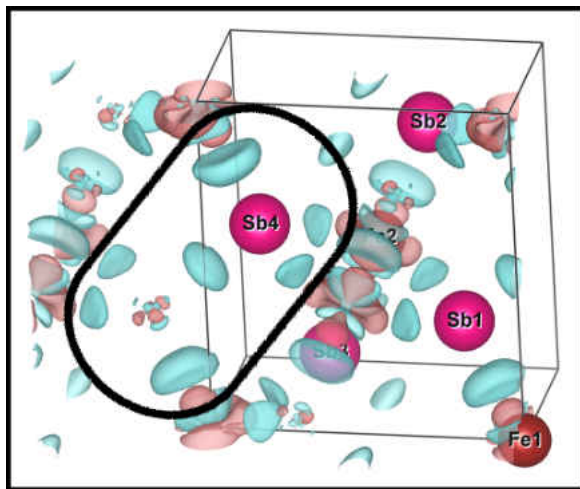
Figure 4.3: Charge Density Difference of FeSb$_2$.

The next structure, NiSb$_2$, also follows the similar bonding and packing pattern seen above. However, the importance of the next structure lies in that nickel has only one stable oxidation state of +2. By only having one stable oxidation state it confirms the charge transfer of the previous structures, supporting that antimony is behaving like its isoelectronic pseudo-atom sulfur. The structure can be seen in figure 4.4. The bond between Sb-Sb in NiSb$_2$, has a bond length of 2.88Å.
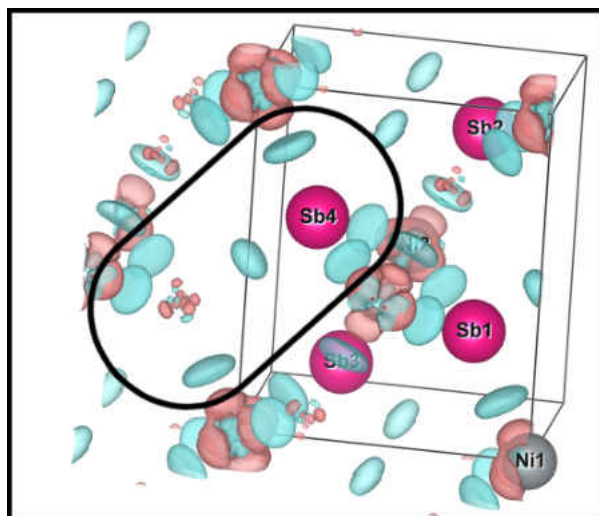
Figure 4.4: Charge Density Difference of NiSb$_2$.

The next structure to be examined is CoSb$_2$[1], which also has stable oxidation states of +2 and +3, and can be seen below in figure 4.5.
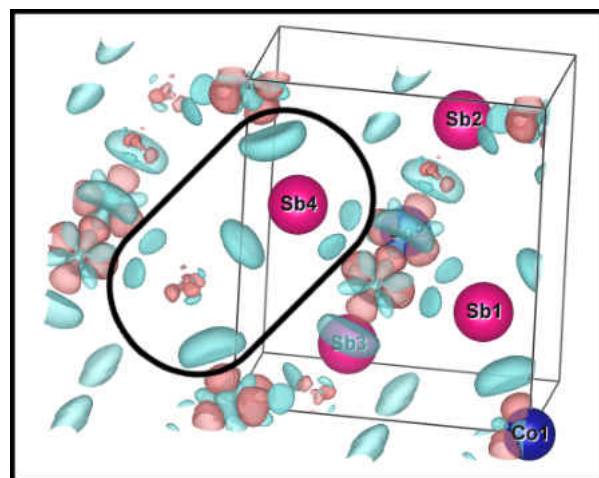
Figure 4.5: Charge Density Difference of CoSb$_2$.

This structure shows similar bonding in antimony to that of sulfur in FeS$_2$ and nickel in NiSb$_2$, confirming that cobalt is donating a -2 charge to antimony and behaving like its pseudo-atom, sulfur. The bond length between Sb-Sb is shorter than the previous structures with a length of 2.69Å. The presence of a bond can be noted since there is a large accumulation of charge density between the Sb-Sb bond. While it is uncanny that these structures should pack and seemingly bond as their pseudo-atom sulfur, they do. This is a behavior predicted by the EZKC-1 model.

65

4.1.3 Chromium a Pseudo-Chalcogen

While nickel has only one stable oxidation state of $+2$, the next structure, $CrSb_2$ containing chromium, does not. Chromium has three stable oxidation states of $+2$, $+3$, and $+6$. This compound also has two structure types, one packing exactly like the rest of the structures seen so far, with space group $Pnnm$ (58), the other having a space group of $I4/mcm$ (140). When examining the chareg density difference of $CrSb_2$ (58), it seem apparent that the multiple states of chromium made an impact on the electronic structure of this solid regardless of the similar packing scheme the structure presented.
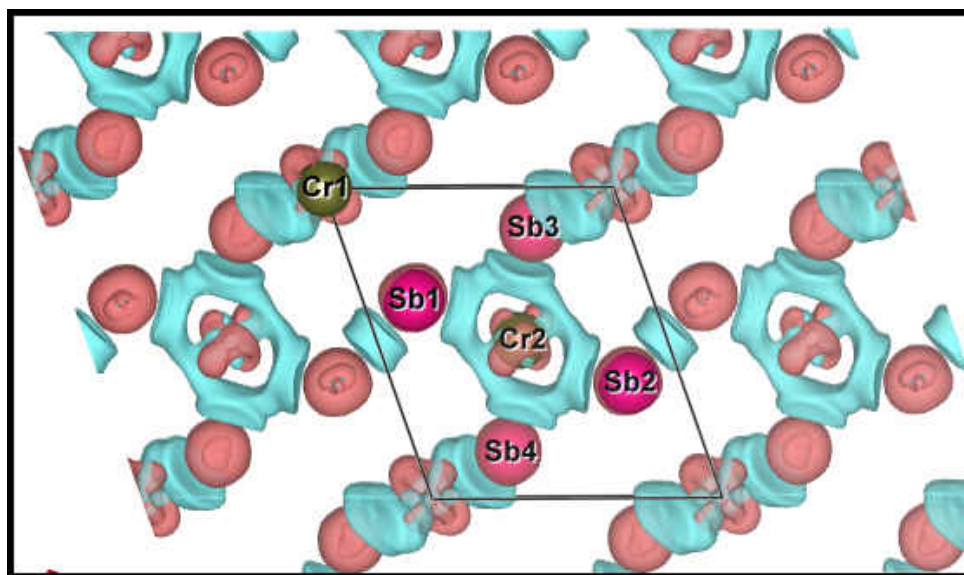
Figure 4.6: Charge Density Difference of $CrSb_2$ (58).

In figure 4.6, one can see here are two types of chromium atoms in the structure as well as two different types of antimony. The first type of chromium atoms (marked as Cr2) seem to form a square planar bond with the surrounding antimony atoms. The other chromium atoms (like Cr1) seem to form a bond linking two antimony atoms together (Sb3 and Sb4). The second type of antimony atom (like Sb1 and Sb2) have charge density accumulation between antimony atoms in the neighboring cell with bond length between Sb-Sb at 2.86Å. The question then posed was if the chromium, which has the smallest electronegativity in the series, was donating the assumed -6 or -4 charge transfer. These two possible charge transfers were arrived at due to the presence of the two different types of antimony atoms found within the structure. If the proposed ions in figure 4.2 are true then this structure could be presenting with ions (b) and (c), which would account for the two different bonding types seen in antimony. This would then give the chromium an oxidation state of $+4$. The other possible oxidation state that could be given to the chromium is $+6$. This could

be the case since the study introduced another possible antimony ion. The other possible antimony ion is Sb_2^{-4} ion, however it was implied that if it were to form it would form discreet Sb_2^{-4} clusters, a representation of the ion is presented in figure 4.7. The Sb-Sb bond with a bond length of 2.86Åcould be forming $Sb_2^{-4}$and accounting that the other antimony atoms would contain a -2 charge. This could mean that the overall oxidation of chromium might be +6.
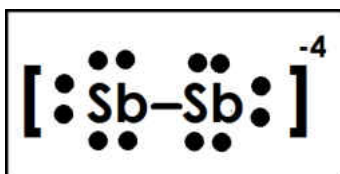
Figure 4.7: Possible Ion Formation of Sb_2^{-4}.

While +4 is notably not a stable oxidation state for chromium, looking at the chromium's oxidation states revealed that while chromium does not usually have a stable oxidation state of +4, there are only a few structures that exist where chromium does; one such structure is CrO_2[16]. If chromium is behaving as a Ψ-S, and one takes into account that sulfur is part of the Chalcogen group (and lies right below oxygen), then the possibility of having a +4 oxidation state on chromium is not unreasonable. While an oxidation state of +6 on chromium might be possible, it was postulated that the Sb_2^{-4} ion would be found as discreet clusters. Since no clusters are seen in $CrSb_2$ (58), it could lead to the conclusion that chromium is donating -4 to antimony. Still, confirmation of either Sb_2^{-2} or Sb_2^{-4} ion in the structure was a question that needed to be answered. This question could be answered by calculating the other chromium structure of $CrSb_2$, since that structure only presents with one type of antimony atom, allowing for easier identification of the oxidation state of chromium and the charge transferred to antimony. Before the charge transferred to antimony could be determined, it was necessary to discern the formation of a Sb_2^{-4}. This was accomplished with the calculation and analysis of $TiSb_2$, with space group $I4/mcm$ (140). The other stable structure of $CrSb_2$ also has the same packing structure as $TiSb_2$, with space group $I4/mcm$ (140). The $TiSb_2$ structure was studied because titanium has only one stable oxidation state, that of +4, and it could be used to determine what a Sb_2^{-4} ion could look like electronically, that is if it were to exist as postulated by Hoffman and Papoian. Looking at the $TiSb_2$ structure, figure 4.8, one can note that discrete Sb_2^{-4} ions can be seen, as predicted.
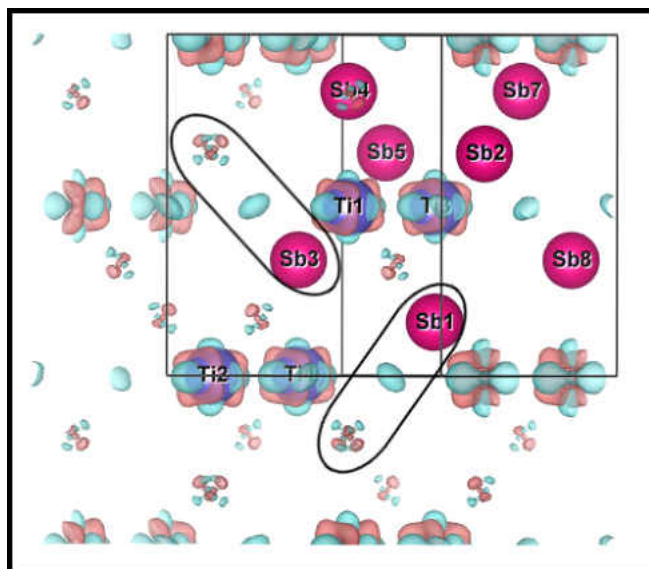
Figure 4.8: Charge Density Difference of $TiSb_2$.

The Sb_2^{-4} ion, with a bond length of 2.98Å, has been circled in the charge density difference map of $TiSb_2$. Since the same bonding scheme is not present in $CrSb_2$ (58), as no discreet clusters of antimony atoms are seen, this implies that the antimony atoms have formed the Sb_2^{-2} ion and the Sb^{-2} ion (in figure 4.2, ions (b) and (c)), for a total of a -4 charge transfer. This would then mean that the charge transfer from chromium to antimony was a -4 and not a -6 charge transfer. This is further confirmed by looking at the next structure, $CrSb_2$ (140), figure 4.9. In the $CrSb_2$ (140) CDD map, figure 4.9, one can see that antimony atoms in $CrSb_2$ (140) show the same electronic structure as antimony atoms $TiSb_2$, supporting the proposed formation of discreet Sb_2^{-4} ions.
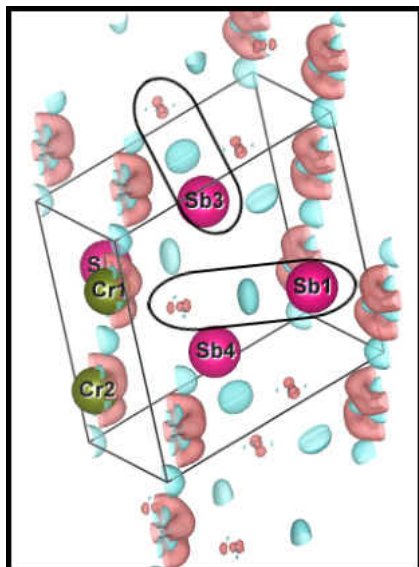
Figure 4.9: Charge Density Difference of $CrSb_2$ (140).

4.1.4 Concluding Remarks on EZKC-1 model

While the EZKC-1 model was able to predict the bonding of antimony in $FeSb_2$, $CoSb_2$, and $NiSb_2$, it was unable to predict the bonding seen in $CrSb_2$, as this concept bases the connections between structures and pseudo-atoms mainly on the physical structure (packing, lattices, and substructures) versus the electronic one. However, while it failed to predict the bonding seen within the electronic structure of $CrSb_2$ in terms of the pseudo compound, its insight led to evidence that antimony does behave like a pseudo-chalcogen in both of its structures. This was something that could not have been arrived at without the EZKC-1 model . Its proposed ions were seen in all of the structures studied, even those not mentioned ($TiSb_2$ and $CrSb_2$ (140)). Overall, the EZKC-1 model was able to rationalize and predict the behavior of these compounds by extending the ZKC to solids composed of more than just Group I/II metals with Group XIII/XIV metals. The concept was able to predict the bonding found within the systems analyzed and in the case of $CrSb_2$ (58), it was able to provide a better understanding of the bonding mechanism behind its varying electronic structure. This concept also provides a possibility of gaining more information on a solid by examining solids that show similar packing arrangements and bonding schemes. This conclusion was further supported by finding similar magnetic properties in CrS_2[93], CrO_2[78], $CrSb_2$[87], TiS_2[43], and $TiSb_2$[87]. Another important insight brought forth by the EZKC-1 model was the long range bonding interactions that exist between the anionic metals within these intermetallic compounds. These distances, found up to 3.46Å, were previously thought too far for actual bonding, however the antimony atoms showed an increase in charge density despite the long

distances, establishing that bonding interactions between metals at long distances do occur.

4.2   Model - 2

The EZKC-1 model of Hoffman and Papoian expanded the scope of solids that could be assessed by this evolving concept. With the success of the EZKC-1 model, the Extended Zintl-Klemm Concept Model 2 (EZKC-2 model) attempts to bridge the gap between these intermetallics, more specifically the Zintl Compounds, to their oxides. This extension attempts to predict and rationalize these oxides by way of the possible long range metal-metal interactions postulated by EZKC-1 model, an elaborate counting scheme, and a heavy focus on physical similarities between the Zintl Compounds and their oxides. Many of the oxides studied under the EZKC-2 model show that the distances of the more anionic metal remain similar to those of the Zintl Compounds, such that it is suggested that the original anionic lattice remains similar to the Zintl Compound and that oxygen atoms of the oxide seem stuffed into regions of high electron density within a similar anionic lattice or substructures formed from the anionic metal. The EZKC-2 model has predicted and rationalized many structures by relying heavily on the similarity that the structures being analyzed have to intermetallics with similar substructures. The theory postulates that despite the presence of oxygen, the anionic metals in an electron-rich environment maintain these metal-metal interactions. These interactions, which fall within the bonding ranges seen in the EZKC-1 model, are enough to maintain the structure's substructure. These structures can be rationalized by an electron counting scheme that presents structures of other compounds with similarities to the substructure of the compound being rationalized. In this study, we will be examining various oxides, their Zintl Compounds, and other possible substructural matches. While it would be a formidable task to provide a comprehensive study of all the structures rationalized or successfully predicted with this concept, our goal is to determine if the internal electronic structure matches the ideas posed by this concept. As with the EZKC-1 model, this exploration into the electronic structure of these oxides is done with hopes that it will lead to a better understanding of these extended solids. The oxide structures that will be examined in this section, in terms of the EZKC-2 model, can be found in table 4.2. The charge density difference maps of many other oxides can be found within Appendix B.

4.2.1   The structures of LiAlO$_2$

The EZKC-2 model attempts to link oxides with their Zintl Compound, and in the case of LiAlO$_2$ there are two stable structures available[109,38], one with space group $P4_12_12$ (92) and

Zintl Compound Oxides
LiAlO$_2$ (92)
LiAlO$_2$ (166)
CaAl$_4$O$_7$
MgAl$_2$O$_4$

Table 4.2: List of Zintl Compound Oxides to be analyzed in terms of The Extended Zintl-Klemm Concept (Model 2).

the other with space group $R-3m$ (166). These structures are the oxide to LiAl, in figure 4.10.
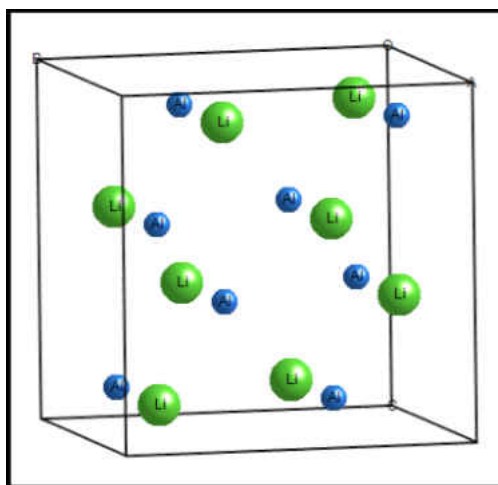
Figure 4.10: Structure of LiAl.

4.2.2 LiAl versus LiAlO$_2$ (92)

The first step is to assess the packing of aluminum atoms in a side by side comparison of the structures. In both of the structures, figure 4.11, lithium atoms have been removed and in the oxide, oxygen atoms have been removed as well. By removing all other atoms but aluminum in the structures, one can more easily verify if the packing by aluminum in the oxide is either similar or the same to the anionic lattice formed by aluminum in the Zintl Compound.

71

Al-Al Distances	
LiAl	LiAlO$_2$ (92)
2.76Å	3.12Å
4.50Å	4.06Å
5.23Å	4.94Å
	5.43Å

Table 4.3: Al-Al Distances in LiAl & LiAlO$_2$ (92).
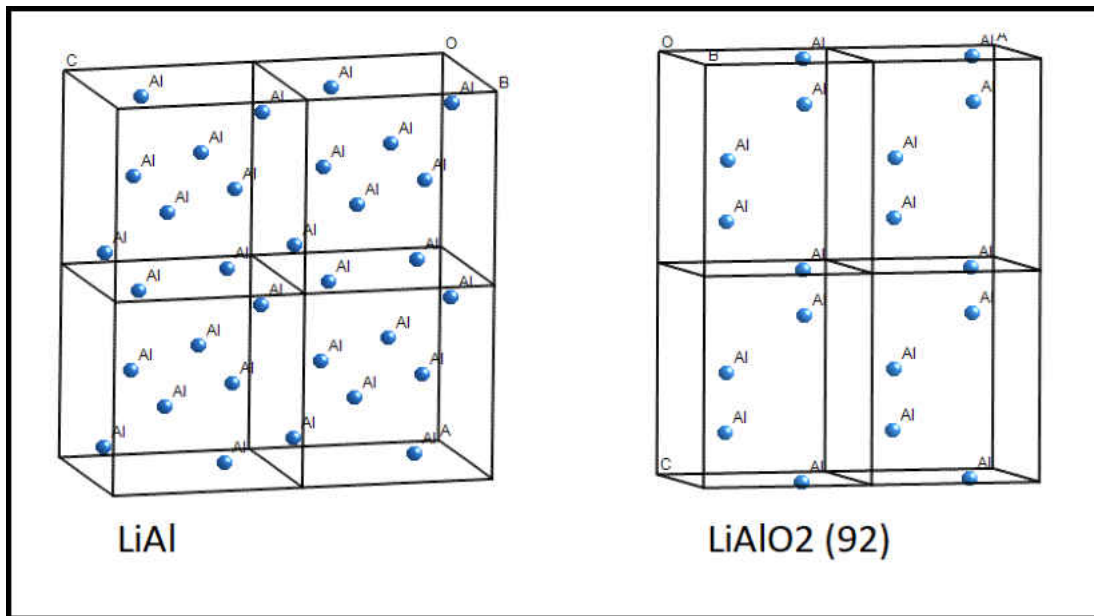
Figure 4.11: Aluminum Atoms in LiAl versus LiAlO$_2$ (92).

Looking at figure 4.11, one can see that the packing of aluminum atoms in both structures are not the same, but by expanding the unit cell of LiAlO$_2$ (92) the aluminum atoms do seem to form the familiar hexagonal shape displayed by the anionic lattice in LiAl. This hexagonal formation can be seen in figure4.12.
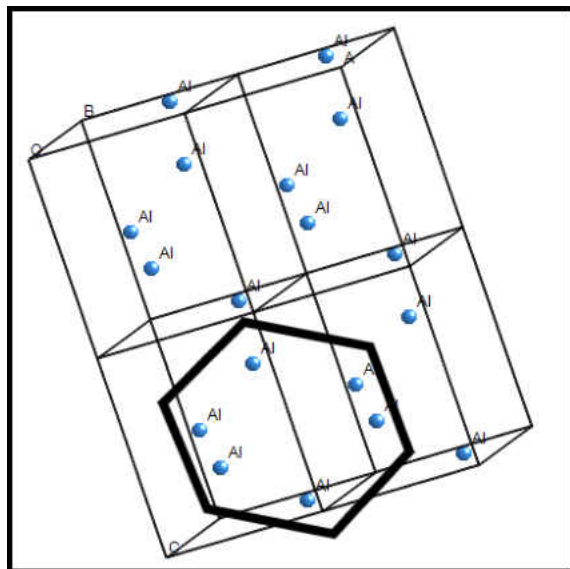
Figure 4.12: Hexagonal Packing in LiAlO$_2$ (92) by Aluminum.

While this does seem to follow the EZKC-2 model proposed packing scheme, not all aluminum atoms within LiAlO$_2$ (92) seem to be within the range of possible metal-metal bonding seen in EZKC-1 model. However, in table 4.3, and the Al-Al distances in LiAlO$_2$ (92) show that, in LiAlO$_2$ (92), there is an Al-Al distance of 3.12Å, which does fall within bonding range.

Looking at the charge density difference of LiAlO$_2$ (92), figure 4.13, one can see in (a) that aluminum atoms have lost significant charge density around itself and that oxygen atoms have gained charge density in a spherical manner indicating that aluminum atoms have become cations and oxygen anions. In (b) only charge density gain is shown in order to discover if any charge density accumulation between aluminum atoms is apparent; however, aluminum atoms seem to have contracted spherically, a common behavior in cations. Since aluminum does not have Al-Al interactions no pseudo-atom approach can be used, which eliminates any viable electron counting schemes that could be applied to this solid. Lithium atoms have also lost charge density and are obscured by the placement atoms. This structure does not seem to support the long range metal-metal distances proposed by the EZKC-2 model. This can be attributed to the highly electronegativity of oxygen, which is present within the structure.
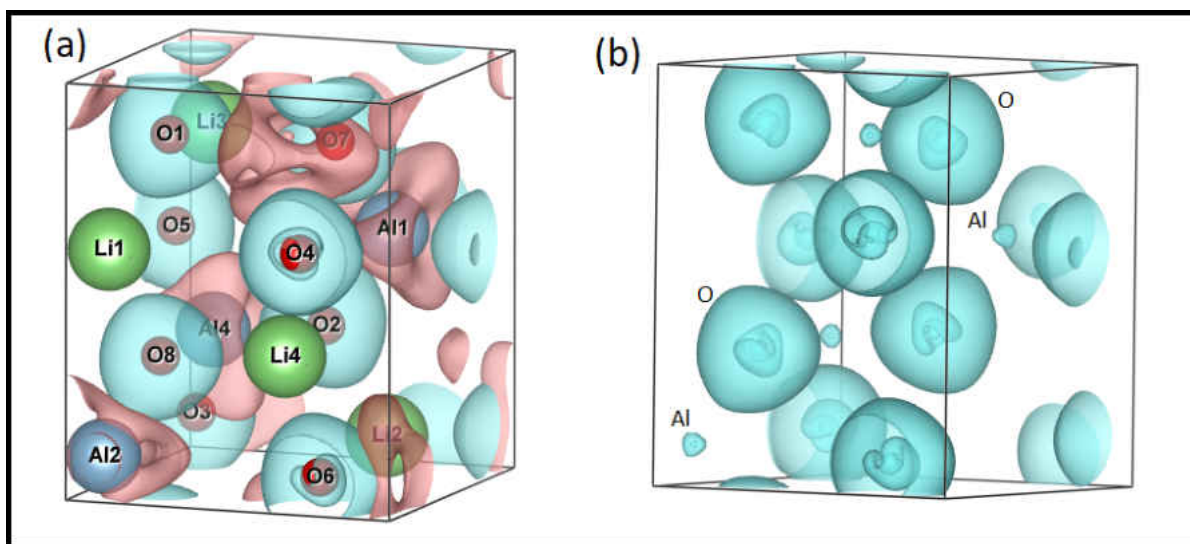
Figure 4.13: Charge Density Difference of $LiAlO_2$ (92).

However, it is important to note that in previous studies[90,8,102,44,73], it has been remarked that oxygen atoms will reside within the voids of a structure where the anionic metal has charge accumulation. This can been seen in this structure by looking at two charge density difference maps. These maps are presented in figure 4.14, where (a) is the charge density difference map of the hypothetical Compound of $LiAlO_2$ (92) by removing the oxygen atoms from the calculations of this solid. This removes the influence exerted by oxygen atoms and demonstrates that there is charge density accumulation between aluminum atoms such that aluminum atoms display a tetrahedral bonding scheme. The distance between bonding aluminum atoms is 3.12Å, as predicted by the EZKC-1 model. When looking at the charge density difference of $LiAlO_2$ (92) with oxygen atoms present, we find that oxygen atoms are now located where there Al-Al bonding interactions, creating aluminum-oxygen tetrahedrons.
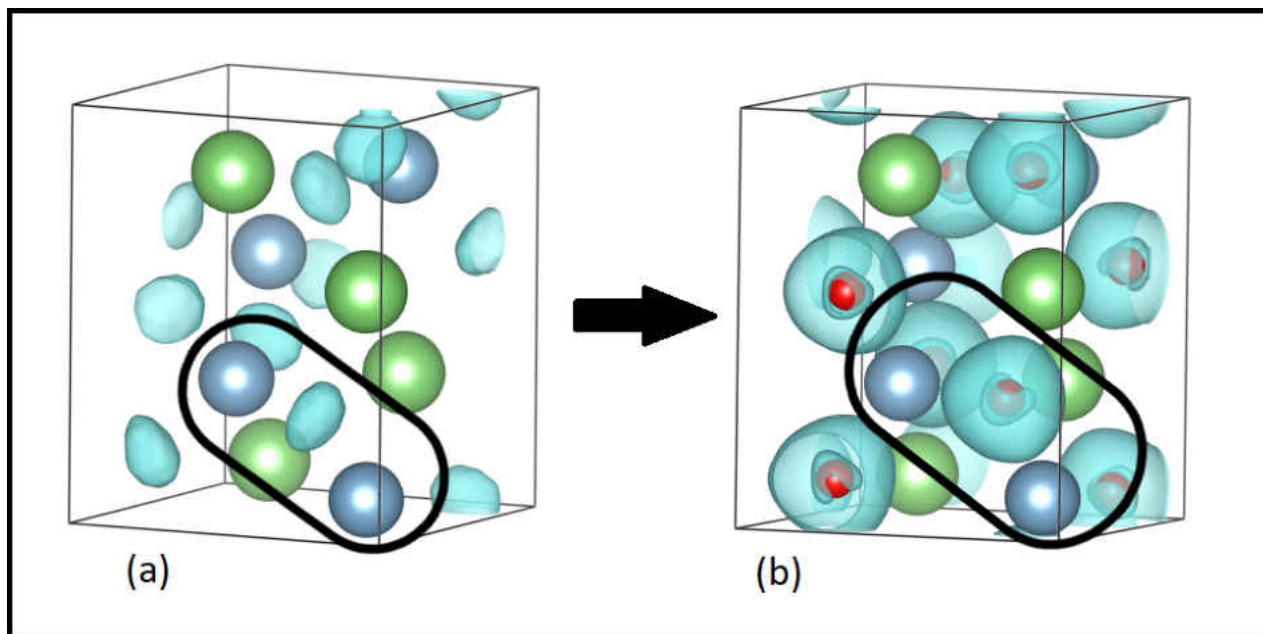
Figure 4.14: Charge Density Difference of $LiAlO_2$ (92) (minus Oxygen) and $LiAlO_2$ (92).

While the EZKC-2 model did not demonstrate the metal-metal interactions with the oxygen atoms present, it is clear that when looking at the structure without oxygen present, the sites occupied by oxygen atoms now hold metal-metal bonds. Another interesting aspect when looking at the structure was the presence of the hexagonal packing by aluminum atoms, since no electronic hexagonal bonding structure was found. Aluminum atoms within each hexagonal packing formation presented distances that ranged too far for bonding interactions, distances that are even far longer than those proposed in EZKC-1 model. This presents a puzzling behavior demonstrated by aluminum since the cause of this hexagonal packing scheme, in light that no interactions can be seen electronically, is unexplained.

4.2.3   LiAl versus $LiAlO_2$ (166)

Looking at the other structural form of the LiAl oxide, $LiAlO_2$ (166), one hopes to see metal-metal interactions within the oxide. This structural form presents distances within aluminum atoms, table 4.4, that are quite close at 2.80Åand might be close enough to present with metal-metal bonding within $LiAlO_2$ (166) despite the presence of oxygen atoms.

While the distances between aluminum atoms, in $LiAlO_2$ (166), does seem to be favorable for bonding interactions, looking at the packing of only the aluminum atoms within the structure, figure 4.15, show that the packing of aluminum in this oxide is not similar to the packing of aluminum in the Zintl Compound.

Al-Al Distances	
LiAl	LiAlO$_2$ (166)
2.76Å	2.80Å
4.50Å	5.00Å
5.23Å	Å

Table 4.4: Al-Al Distances in LiAl & LiAlO$_2$ (166).
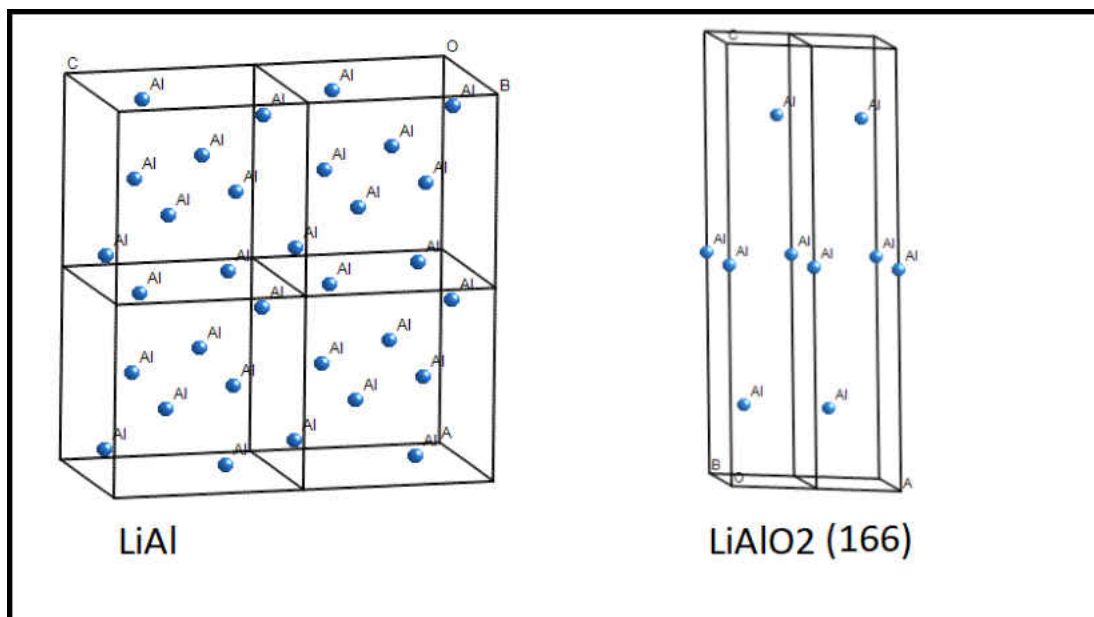
Figure 4.15: Aluminum Atoms in LiAl versus LiAlO$_2$ (166).

However, although aluminum atoms in LiAlO$_2$ (166) does not display similar packing by aluminum in the Zintl Compound, oxygen does demonstrate the same bonding behavior by oxygen in LiAlO$_2$ (92). This behavior which can be seen in figure 4.16. When looking at the charge density difference map of the hypothetical compound of LiAlO$_2$ (166) by removing the oxygen atoms (a), the area between aluminum atoms shows charge density accumulation. In the charge density difference of the LiAlO$_2$ (166) with oxygen included (the real structure) (b), one can note that the locations where there would have been accumulation of charge density between aluminum atoms now contain oxygen atoms.
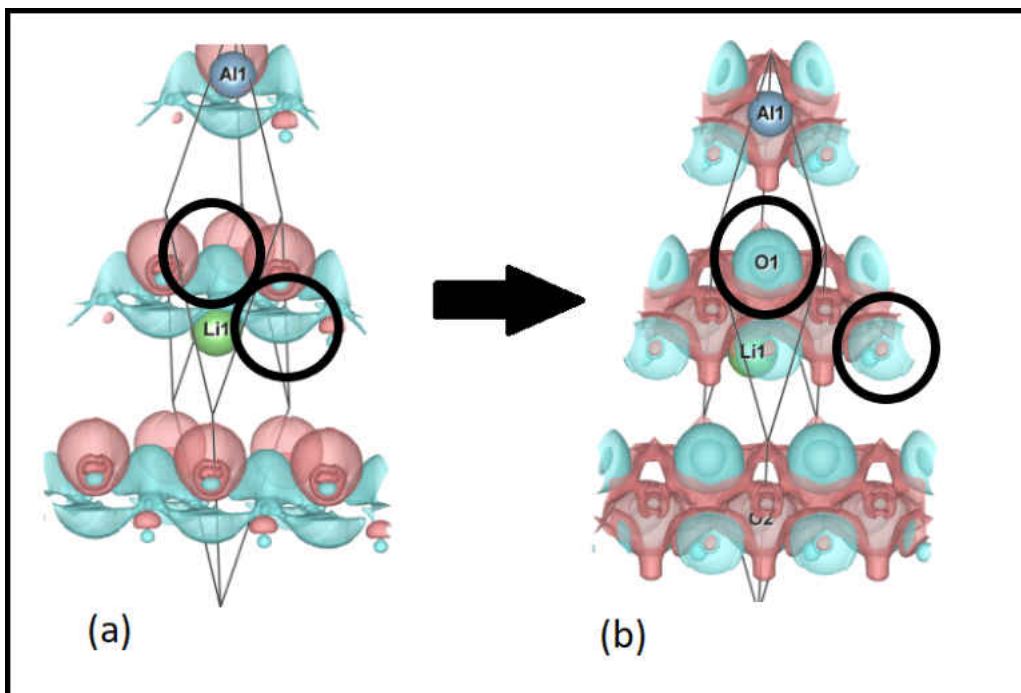
Figure 4.16: Charge Density Difference of LiAlO$_2$ (166) (minus Oxygen) and LiAlO$_2$ (166).

Taking another closer look at (b), figure 4.16, it can be seen that aluminum atoms have lost charge to become a cations, and oxygen atoms, gain charge spherically, having become anions. This is more easily depicted by removing the charge density loss (pink) and leaving only where there has been charge density gain, figure 4.17.
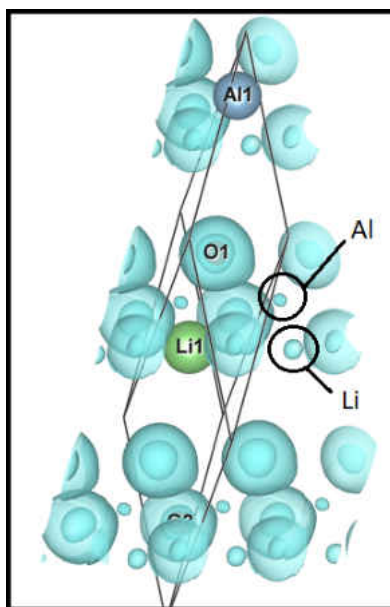
Figure 4.17: Charge Density Difference of LiAlO$_2$ (166).

Bader Charges	LiAlO$_2$ (92)	LiAlO$_2$ (166)
Lithium	+0.90	+0.90
Aluminum	+2.54	+2.00
Oxygen	-1.72	-1.45

Table 4.5: Bader Charges on LiAlO$_2$ (92) & LiAlO$_2$ (166).

The charge density difference map of LiAlO$_2$ (166), shows what could be classified as an ionic solid. There seems to be no charge density accumulation between aluminum atoms despite the small distance between atoms. Instead, all species within the compound are spherical in nature as one would expect of ions. Since no metal-metal bonding occurs, no pseudo-atom approach can be taken which means no viable electron counting schemes can be applied.

4.2.4 Bader Charges on the Structures of LiAlO$_2$

Both structural forms of LiAlO$_2$, one with space group $P4_12_12$ (92) and the other with space group $R-3m$ (166), show charge density difference maps that display ionic behavior. Since these compounds are relatively small, Bader charges were calculated and are presented below in table 4.5. The charges seem to support the information presented in the charge density difference maps of these extended solids. The charges while supporting the ionicity of this solid also support the EZKC-2 model in part. Looking on the charge of aluminum atoms in the different structures one can see that there is a fractional charge difference of -0.54 in LiAlO$_2$ (166). While there does not seem to be any metal-metal charge density accumulation between aluminum atoms, the relative closeness on distance seems to have had an effect on the amount of charge being donated by aluminum to oxygen, giving credence that while no visible bonding can be seen there might be some other interactions between aluminum that has yet to be explored.

4.2.5 The Structure of CaAl$_4$O$_7$

CaAl$_4$O$_7$

The structure CaAl$_4$O$_7$[71] is an oxide which has two possible Zintl-Klemm Compounds. It could be an oxide to: CaAl$_2$ and CaAl$_4$, both of which can be seen in chapter 3. These structures present a range of Al-Al distances, table 4.6, which include distances where Al-Al

Al-Al Distances		
CaAl$_4$O$_7$	CaAl$_2$	CaAl$_4$
2.91-5.90Å	2.84-5.68Å	2.61-5.10Å

Table 4.6: Al-Al Distances in CaAl$_4$O$_7$ & CaAl$_2$ & CaAl$_4$.

bonding interactions can occur.

However, looking at the structures of these three solids, where only aluminum atoms are shown, seems to provide little correlation between the anionic lattices seen in the Zintl Compounds and their oxide, unlike the structural similarity seen in LiAl and LiAlO$_2$ (92). The images of the three calcium-aluminum solids can be seen in figure 4.18.

Looking at the images side by side, with oxygen removed from oxide, one can see that while the Zintl Compounds exhibit the hexagonal packing exhibited by Group XIV, aluminum in CaAl$_4$O$_7$ does not seem to pack in accordance to the EZKC-2 model, therefore seemingly difficult to rationalize or predict the structure. Interestingly enough, the same phenomena seen above can be seen in CaAl$_4$O$_7$. When calculating the charge density of the hypothetical CaAl$_4$O$_7$ by removing oxygen from the structure, there is definite ZKC behavior occurring as covalent bonds form between the anionic metal to form an anionic lattice. However, as soon as oxygen is introduced back into the crystal structure, the location of the bonds between aluminum atoms is replaced by oxygen atoms. This can be seen in the charge density difference of both CaAl$_4$O$_7$ minus oxygen and CaAl$_4$O$_7$ in figure 4.19.
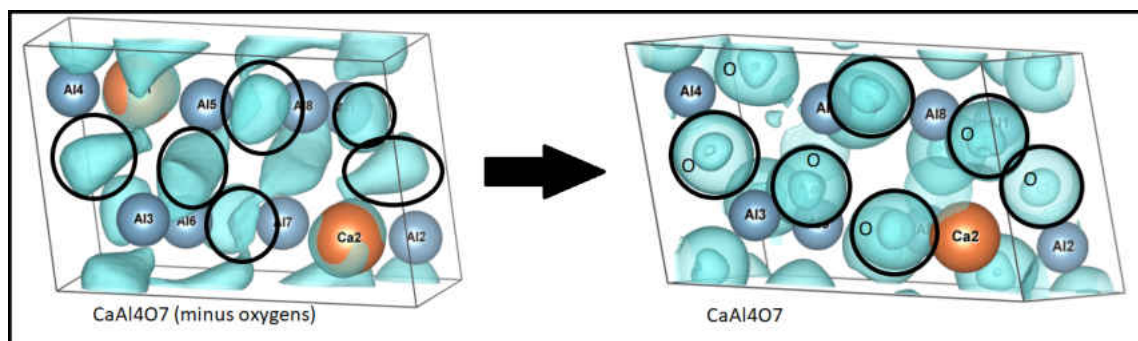
Figure 4.19: Charge Density Difference of CaAl$_4$O$_7$ (minus Oxygen) and CaAl$_4$O$_7$.

Although this structure does not show Al-Al interactions in the oxide, despite aluminum atoms being within bonding distance, this structure does present similar calcium behavior present in the majority of calcium Zintl Compounds. While the lack of Al-Al bonding, and the application of the pseudo-atom approach could not be applied in the oxide, this could be
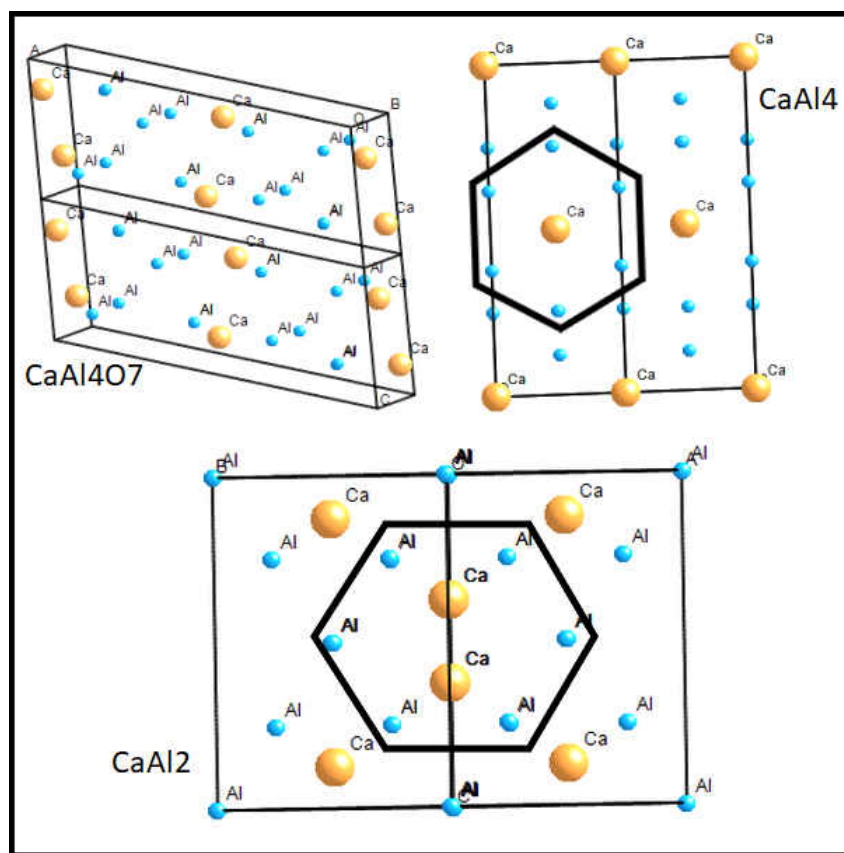
Figure 4.18: Aluminum Atoms in $CaAl_4O_7$ versus $CaAl_2$ & $CaAl_4$.

Bader Charges	CaAl$_4$O$_7$
Calcium	-2.0
Aluminum	+2.6
Oxygen	-1.2

Table 4.7: Bader Charges on CaAl$_4$O$_7$.

due to the large electronegativity in oxygen. However, the increase in charge density around calcium can not be explained. In the Zintl Compounds, calcium acquired charge density at the expense of a more electronegative metal, while the cationic metal still forming covalent bonding similar to the elements in neighboring groups. Looking at figure 4.20, one can see that aluminum atoms has lost charge density. Removing the calcium placement atom for the calcium atom circled, one can see that calcium atoms has gained charge density and has become polarized towards the spherical oxygen ions.
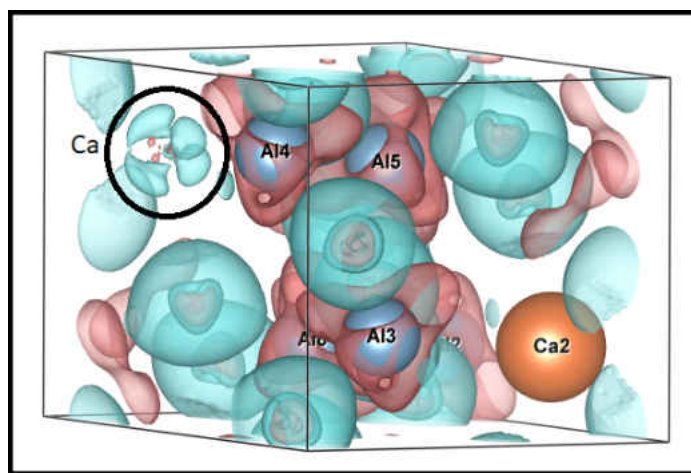
Figure 4.20: Charge Density Difference of CaAl$_4$O$_7$.

The importance of this structure, although it failed to be predicted or rationalized by the EZKC-2 model, does support that the location of the oxygen atoms and charge transferred to oxygen could be due to the more electronegative metal's lattice and voids, where charge density seems to accumulate. This structure, like the others presented in this section, seem to display a charge density difference map that shows spherical gain and loss of charge density making all the species in the solid ions. To verify the ionicity of the structure, the Bader charges were calculated and presented in table 4.7.

These charges seem to verify the strange behavior seen on the charge density difference

concerning calcium. It is interesting to note that while oxygen has gained charge it has gained less charge than the less electronegative metal calcium. These results were corroborated by two different computational programs, in order to avoid calculation bias. Though there does not seem to be complete agreement with these Zintl Compounds and their oxides as the EZKC-2 model suggests, there does seem to be a subtle effect between that the metals within these compounds poses to oxygen.

4.2.6 The Structure of $MgAl_2O_4$

The structure, $MgAl_2O_4$[5], presented in a study[73] by Santamaria-Perez and Vegas, in like of the ZKC. In the study it was justified that instead of looking at the Zintl Compound $MgAl_2$ as a possible guide for the packing of $MgAl_2O_4$, one must look at the $MgAl_2$ subarray within $MgAl_2O_4$ as $CaAl_2$. This was justified by claiming that the $MgAl_2$ subarray within $MgAl_2O_4$ must be considered as a high pressure phase which packs like $CaAl_2$.

Looking the structures of both $CaAl_2$ and $MgAl_2O_4$ (minus all oxygen atoms), figure 4.21, one can clearly see the packing of the magnesium and aluminum is nearly identical to the packing found within the real Zintl Coupound, $CaAl_2$.

Zintl Compound: CaAl2   MgAl2O4 (minus Oxygen atoms)
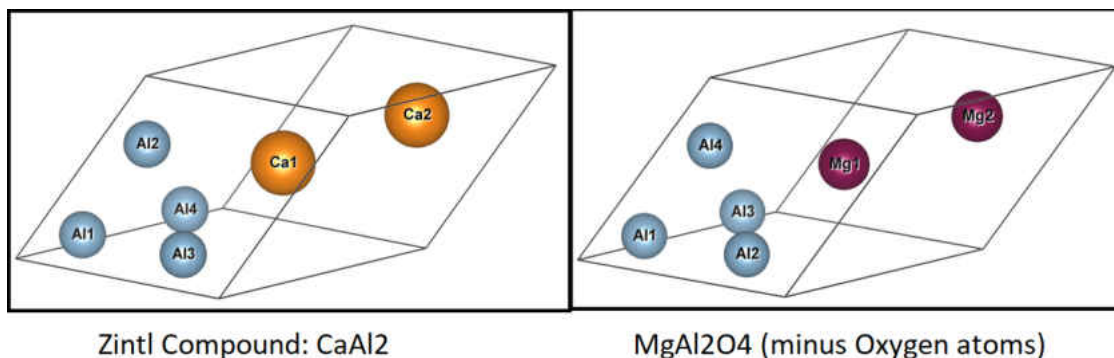
Figure 4.21: Structure of $CaAl_2$ and $MgAl_2O_4$ (minus oxygen atoms).

However, looking at the charge density difference of both the real Zintl Compound and the hypothetical $MgAl_2$ and comparing the charge density in both structures one can see similarities in the way aluminum atoms bond together to form tetrahedrons. Yet, that is where similarities end. While one might consider $MgAl_2$ similar in packing to $CaAl_2$, the bonding behavior and the mechanism behind it must be radically different. In figure 4.22, one can see that magnesium atoms have lost charge, as expected in a Zintl Compound, and charge density has accumulated between aluminum atoms. However, the real Zintl Compound,$CaAl_2$, can be seen as deviating from the ZKC and has calcium atoms acquiring charge from aluminum atoms, however, despite calcium atoms having acquired charge and

becoming anions, aluminum atoms still form covalent bonds with each other. This can be explained since in both structures the Al-Al metal distance is about 2.8Å. A distance close enough to create covalent bonds between aluminum atoms.
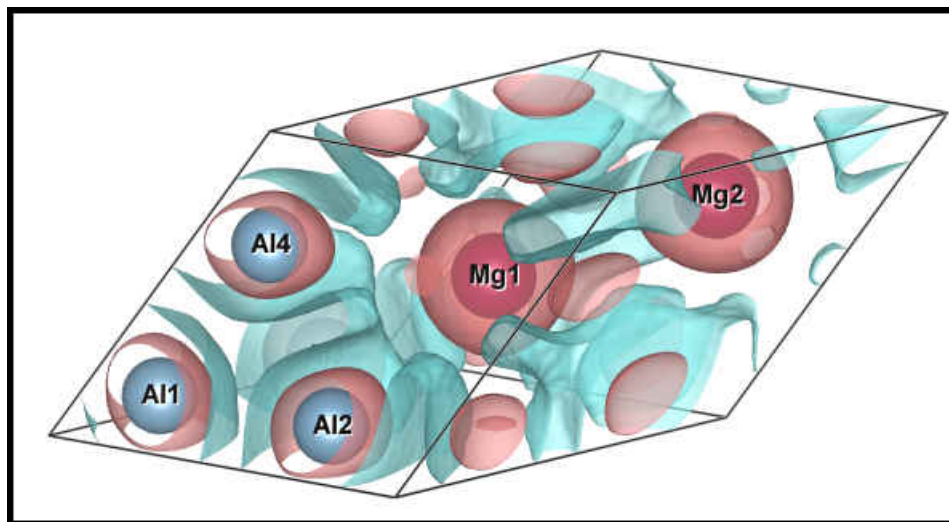
Figure 4.22: Charge Density Difference of Hypothetical $MgAl_2$.
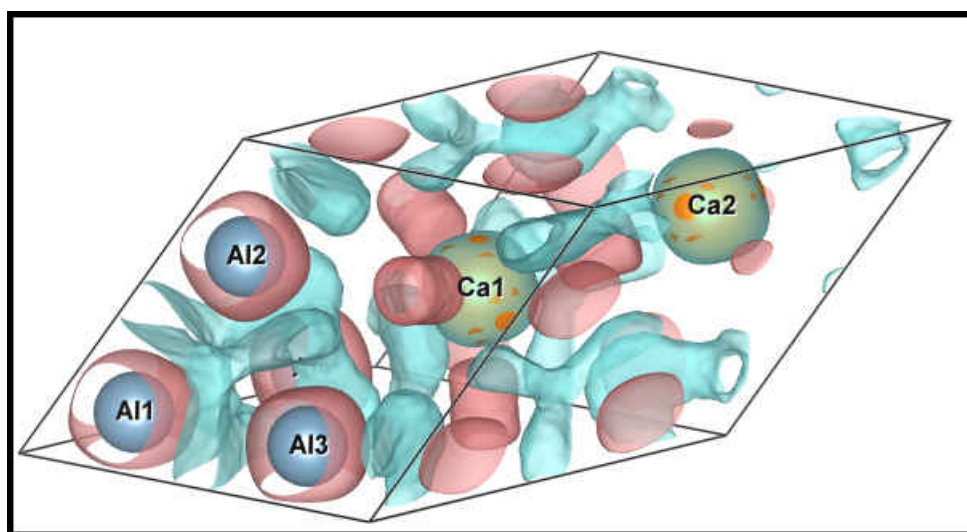
Figure 4.23: Charge Density Difference of $CaAl_2$.

In this case, the EZKC-2 model was able to find a Zintl Compound that mirrored the packing within the oxide. While the EZKC-2 model seemed to bypass the actual $MgAl_2$ Zintl Compounds, it would be remiss if this study failed to look at charge density difference of $MgAl_2$, to see if any similarities can be seen. This Zintl Compound, figure 4.24 does not seem to match in the packing of the actual $MgAl_2O_4$.
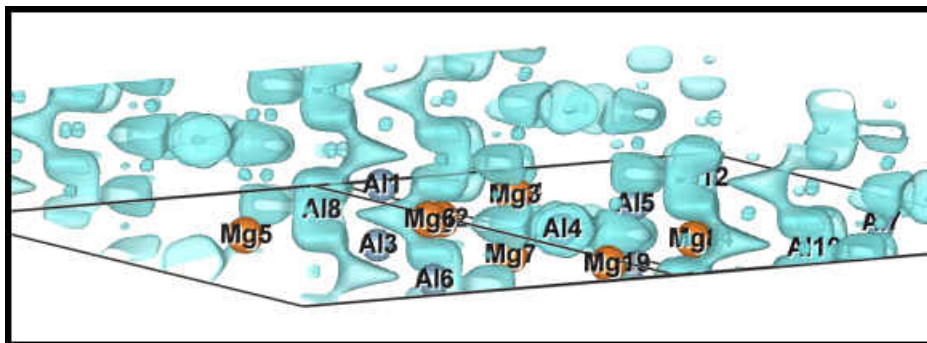
Figure 4.24: Charge Density Difference of MgAl$_2$.

Interestingly, if not looking at the actual MgAl$_2$, but at the structure calculated without oxygen atoms, figure 4.25, one can see that oxygen atoms once again seem located where there was charge accumulation between the aluminum atoms in the hypothetical MgAl$_2$ structure.
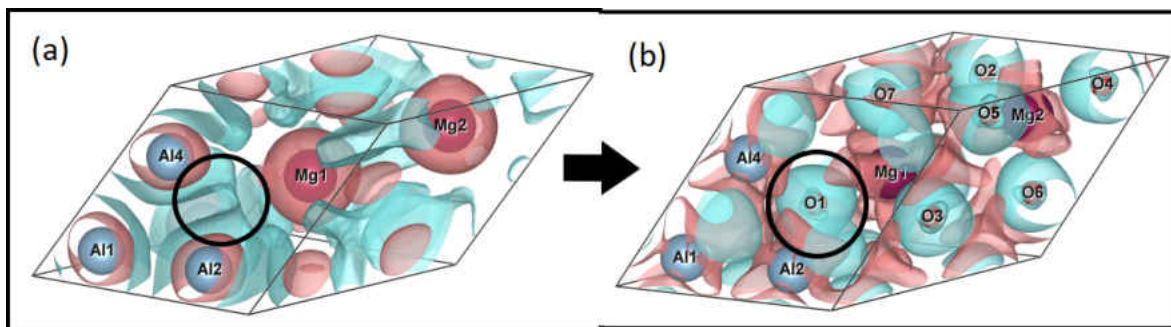
Figure 4.25: Charge Difference Density of MgAl$_2$O$_4$ (minus oxygen atoms) and MgAl$_2$O$_4$.

Taking a closer look at the charge density difference of MgAl$_2$O$_4$, figure 4.26, where only the charge density gain is shown once can see that no metal-metal interactions can be seen. As with the previous structures, the chemical species within the solid all seem to have lost or gained chart density spherically, which is consistent with the formation of ions.

Bader Charges	MgAl$_2$O$_4$
Magnesium	+1.3
Aluminum	+2.7
Oxygen	-1.7

Table 4.8: Bader Charges on MgAl$_2$O$_4$.
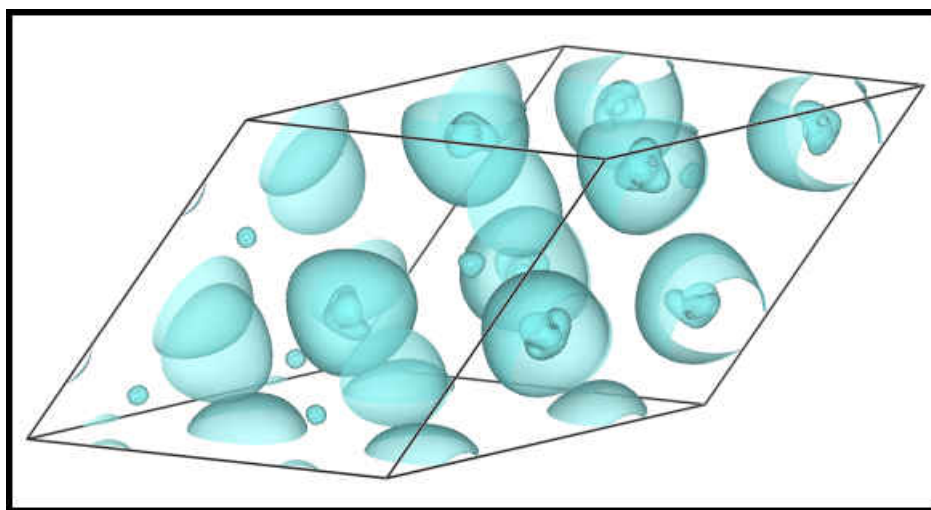
Figure 4.26: Charge Difference Density of MgAl$_2$O$_4$.

In order to verify ionicity, Bader charges were calculated and can be seen in figure 4.8. Even though it seems that the Zintl Compound that was used as a guide was CaAl$_2$, the charge density difference maps were quite different. These charges calculated for MgAl$_2$O$_4$ support the charge density difference maps MgAl$_2$O$_4$.

4.2.7 Concluding Remarks on EZKC-2 Model

In this section four oxides were assessed based on the EZKC-2 model and were compared to both the matching Zintl Compound and their hypothetical Zintl Compound solid. In the 4 cases that were examined only LiAlO$_2$ (92) showed the packing of aluminum atoms to be similar to the lattice formed within the matching Zintl Compound. However, the distances between the aluminum atoms were too far to form the proposed bonding. In fact, when examining the charge density difference of all the oxides (and those in Appendix B), no metal-metal interactions were seen irrespective of distance, hence no counting scheme or pseudo-atom approach could be applied to any of the solids. In most solids, the chemical

species within the oxides seems to gain or lose charge density spherically, indicating the formation of ions, making the structure ionic in nature. To verify and quantify the charge transfered in these solids, since the solids were relatively small in size, the Bader charge calculations were applied to the charge density. Most solids appeared to have charges that indicated charge transfer close to the formal charges assumed. When examining these solids in terms of the charge density difference of their hypothetic Zintl Compound, an interesting pattern emerged. Without oxygen in the compound, the ZKC seemed to hold true and the more anionic metal acquired charge density between atoms. Not only did these anionic metal gain charge between them, but in the case of $CaAl_4O_7$, a very electron-rich environment, there seemed to be charge density accumulation in the voids between atoms despite long distances, once again confirming the EZKC-1 model bonding length theory. However, it was posed that if oxygen were to be added to these hypothetical Zintl Compounds the oxygens would be "stuffed" within the electron-rich voids. This conjecture proved to be seen in all structures analyzed. The oxygen atoms seemed to insert themselves where the charge density accumulation increased between anionic metals within the structure. Overall, this EZKC-2 model was not able to adequately rationalize or predict the structure and bonding within these extended solids.

Chapter 5

Methods

Extended solids are still a largely unexplored area in theoretical chemistry. While the synthesis of solid materials has boomed, the properties of these extended systems have neither been classified nor explained at the pace in which they are being synthesized. In the past, extended systems have been too complex to be modeled effectively with quantum chemistry software. However, in recent years increasing computer power and the creation of accurate density functionals has made it possible to analyze these systems. In this work, three ab initio programs, all using density functional theory to calculate the charge density of a specific class of solids known as Zintl compounds and their oxides, are compared. By comparing the results, we can determine whether or not these fundamentally different approaches effectively model the same charge densities and properties of extended systems. In addition, the comparison with the computational program VASP allows us insight into the role of core electrons in the charge density distribution, energy, and properties of these materials. In order to be able to analyze the charge density we will be comparing the methods qualitatively by using difference charge density maps and the Laplacian of the electron density. We also obtain a more quantitative comparison between computational chemistry programs by analyzing the charges resulting from the integration over gradient trajectory bound volumes of the charge density as described by Bader's "Atoms in Molecules"[4] theory described in chapter two.

The programs in this investigation of Zintl Compounds and their oxides includes FLAIR[92], an all-electron Full-potential Linearized Augmented Plane Wave (FLAPW) program that uses muffin tin approximations for the core electrons[108] and has been used to successfully model Zintl Compounds in a study by Evers[25] among others. In other studies by Wang and Miller[106,105] VASP was used to model these solids. The program VASP[47] also uses plain wave basis sets, but approximates the core electron density with pseudo-potentials – therefore using only using the valence electrons when calculating the electron density. CRYSTAL14[23] is

an all-electron molecular orbital computational program, using atomic basis sets to model the atoms in the crystal and calculate the wave functions to obtain the charge density. The basis sets utilized in the calculations of these solids were gaussian basis sets of triple-zeta valence with polarization[69] for solid-state calculations. Both FLAIR and CRYSTAL14 take advantage of a crystal's symmetry to arrive at convergence, making the calculations more efficient by requiring fewer operations to compute both the charge density and the total energy. VASP's efficiency stems from the pseudo-potentials used to model a frozen core. In the calculation of these solids, the pseudo-potentials used were those recommended by VASP when running calculations on solids and when running versions of VASP.5.X. In order to keep the calculations consistent and therefore comparable, the structures of the solids were attained from experimental data published, and were kept consistent throughout the three programs. In all structures, the grid size used for the charge density maps was also kept the same at over 10^6 fine mesh grid points. The Brillouine zone was at 8 x 8 x 8 in all three programs. The DFT exchange and correlation functionals used in both FLAIR and VASP were the generalized gradient approximation[70] (PBE-GGA). In CRYSTAL14 the exchange and correlation functionals used were a hybrid generalized gradient approximation (PBE-GGA) with 25% (1/4) of HF exchange functional presented in Adamo and Barone[3]. The global hybrid (GH) functional generalized form, where A is the constant fraction of the HF exchange is:

$$E_{xc}^{GH} = (1 - A) * E_x^{DFA} + A * E_x^{HF} + E_c^{DFA} \tag{5.0.1}$$

Once the calculations on the extended solid converged and the charge density was produced, the charge density was processed by a charge density utility program written by Professor Bennett. This charge density utility (CDU), able to perform various functions, applied the Bader Charge Analysis Program[35] to the selected charge density in order to provide charges on the chemical species within the extended solid. In the case of VASP, the CHGCAR file only contains the charge density of the valence electrons. This was corrected by setting LAECHG=.TRUE. in the INCAR file. This creates two additional files: AEC-CAR0, where the core charge density is written, and AECCAR2, where the valence charge density is written. These two files are then added to create a complete charge density file for the solid calculated by VASP. This summation is included as a script file when one acquires the Bader Charge Analysis Program[35]. Once the complete charge density was computed it could be processed like the other charge densities attained from the other two programs. The CDU program was also used to calculate the Laplacian on the charge density files, and lastly it was able to create the charge density difference maps by subtracting the initial atomic charge densities from the converged crystal's charge density. These charge difference

densities were created with only FLAIR and Crystal as VASP was unable to provide initial atomic charge densities. Once all the charge density difference maps and the Laplacian of the charge densities were created these cube files were then visualized by the program VESTA[50].

However, both CRYSTAL14 and VASP exhibited limitations when applied in this investigation. While CRYSTAL14 can use pseudo-potentials to reach convergence on many solids, when running all electron calculations, it failed to converge on solids containing elements greater than atomic number 20 (calcium). While VASP able to converge on all solids calculated, it could not produce the initial atomic charge density maps which are needed to create the charge difference density maps. Additionally, while the charge density can be assessed by applying the Laplacian, it would require exponentially larger grid sizes, so the electronic structure of these solids can be clearly seen. Since larger grid sizes would make the calculation of these charge densities time consuming, the calculation of these solids becomes impractical. Since VASP can only be assessed via the Laplacian, it would require exponentially larger grid sizes making it an impractical choice. Yet, the electronic structures of these solids needed to be compared in order to determine the veracity of the information acquired when analyzing the bonding within these structures. Therefore, the electronic structures of the extended solids that will be compared contain only lithium, aluminum, and oxygen, as these solids where small enough that CRYSTAL14 was able to converge on these solids efficiently. The grid size used when calculating these aluminum Zintl Compounds provided a Laplacian that displayed the electronic structure of these solids clearly.

5.1   Comparison of Methods

The aluminum Zintl Compounds compared with all three programs can be found in table 5.1. The first step in comparing these solids was calculating the Bader Charge, since the concepts in this investigation all proposed charge transfer occurring between the metal species. The Bader Charges, seen in figure 5.1, do reveal the charge transfer proposed within the Zintl-Klemm concept, but not in the Extended Zintl-Klemm Concept Model-2, and while the comparisons of the Laplacian and charge density on all solids demonstrated the same conclusion that all three programs provided equivalent information, the Laplacian and charge density of the highlighted compounds will be shown below. The color scheme used in the charge density difference maps is as follows: blue signifies positive charge density, indicating where charge density has been gained (where it has migrated to); while pink signifies negative charge density, where there has been a loss of charge density (where it has migrated from).

Zintl Compounds	Oxides
LiAl	$LiAlO_2$ (92)
$LiAl_3$	$LiAlO_2$ (166)
Li_3Al_2	$LiAl_5O_8$
Li_9Al_4	$NaAlO_2$ (33)
$MgAl_2$	$NaAlO_2$ (92)
$CaAl_2$	K_3AlO_3
$CaAl_4$	$BeAl_2O_4$
	$MgAl_2O_4$
	$CaAl_4O_7$

Table 5.1: List of Lithium-Aluminum Zintl Compounds and their Oxides, where the number in parenthesis signifies the space group this structure belongs in.

5.1.1 Bader Charges

The Bader charges of all the compounds in table 5.1 can be seen in figure 5.1. The concepts analyzed within this study posit that charge transfer occurs and gives rise to metal-metal interactions. The charge transfer occurs such that the least electronegative metal donates charge to the more electronegative metal, forming an anionic lattice. In the oxides, the Extended Zintl-Klemm Concept Model-2 still proposes that the more electronegative metal would still attain enough charge, despite oxygen, in order to form metal-metal bonding interactions. The charges presented in figure 5.1 are the charges acquired from the charge densities of all three programs after applying the Bader Charge Analysis program. In all but one case, $CaAl_4O_7$, the trend the charges exhibit seem to coincide. When looking at the charges in the Zintl Compounds, the charges seem to confirm the charge transfer proposed to the more electronegative metal, with the exception of $CaAl_2$, as calcium is the less electronegative metal and should contain a positive charge. In the Zintl Compound $MgAl_2$, CRYSTAL14 had difficulty modeling this solid and in converging (converging after 39 iterations). This is probably due to the closeness between aluminum and magnesium, as they are atomic neighbors. This can be noted in the large difference in the charges presented for this solid even though the charge still maintained the similar positive/negative trend.

Zintl Compound Oxides			
LiAlO2-92	Li	Al	O
Crystal	0.9	2.7	-1.8
Flair	0.9	2.5	-1.7
Vasp	0.9	2.4	-1.7
LiAlO2-166	Li	Al	O
Crystal	1.0	2.2	-1.6
Flair	0.9	2.0	-1.5
Vasp	0.9	2.5	-1.7
LiAl5O8	Li	Al	O
Crystal	1.0	1.9	-1.3
Flair	1.0	1.9	-1.3
Vasp	0.8	2.7	-1.8
NaAlO2-33	Na	Al	O
Crystal	0.9	2.7	-1.8
Flair	0.8	2.6	-1.7
Vasp	0.8	2.6	-1.7
NaAlO2-92	Na	Al	O
Crystal	0.8	2.6	-1.7
Flair	0.8	2.5	-1.6
Vasp	0.8	2.4	-1.6
K3AlO3	K	Al	O
Crystal	0.8	2.7	-1.7
Flair	0.7	2.6	-1.6
Vasp	0.5	2.7	-1.4
BeAl2O4	Be	Al	O
Crystal	1.8	2.9	-1.9
Flair	1.7	2.7	-1.8
Vasp	1.7	2.3	-1.6
MgAl2O4	Mg	Al	O
Crystal	1.4	2.8	-1.8
Flair	1.3	2.7	-1.7
Vasp	1.3	2.6	-1.6
CaAl4O7	Ca	Al	O
Crystal	-1.7	2.3	-1.3
Flair	-2.0	2.6	-1.2
Vasp	1.9	2.6	-1.7

Binary Zintl Compounds		
Li9Al4	Li	Al
Crystal	0.9	-2.0
Flair	0.9	-2.0
Vasp	0.8	-1.8
Li3Al2	Li	Al
Crystal	0.8	-1.2
Flair	0.8	-1.2
Vasp	0.8	-1.3
LiAl	Li	Al
Crystal	0.8	-0.8
Flair	0.8	-0.8
Vasp	0.8	0.8
LiAl3	Li	Al
Crystal	0.9	-0.3
Flair	0.9	-0.3
Vasp	0.9	-0.3
MgAl2	Mg	Al
Crystal	0.7	-0.4
Flair	1.4	-0.9
Vasp	1.5	-1.0
CaAl2	Ca	Al
Crystal	-0.5	0.3
Flair	-1.0	0.5
Vasp	-0.6	0.3
CaAl4	Ca	Al
Crystal	1.3	-0.3
Flair	1.2	-0.3
Vasp	1.5	-0.4

Figure 5.1: Bader Charges of Aluminum Zintl Compounds, where blue indicates an anion and pink a cation.

The charges on the oxides seem to be as expected, with the metals donating charge and oxygen acquiring it, with the only exception being the charges on $CaAl_4O_7$, which deviate
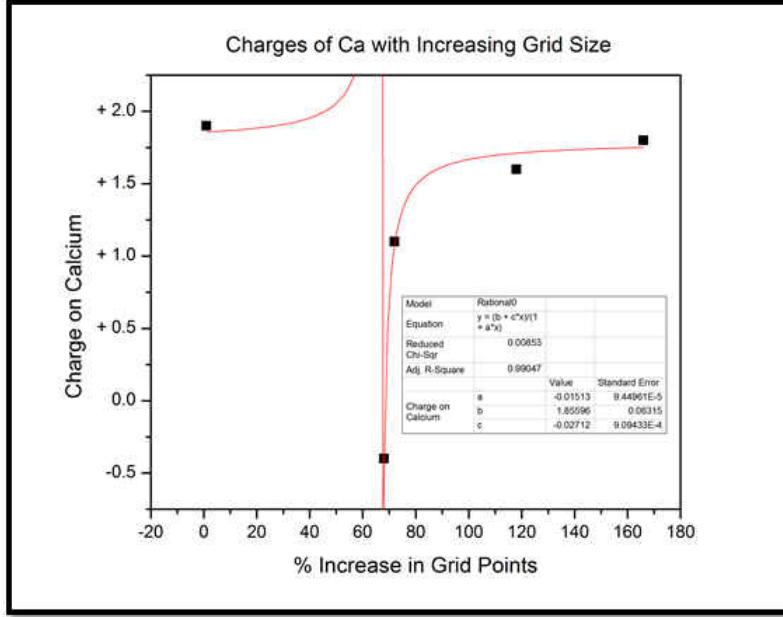
Figure 5.2: Bader Charges on Calcium in $CaAl_4O_7$ with increasing Grid Sizes in VASP.

from the expected behavior since calcium is usually a cation. It is interesting to note that despite the inconsistency in charge agreement on the charges of $CaAl_4O_7$, the only other deviation in charge also is an extended solid that contains calcium. With VASP's charges being the only charges that presented this behavior, a behavior that would have been assumed since calcium ions are usually considered a $+2$, two questions needed to be answered. If this effect on calcium was due to its core electrons, which could be a possibility since VASP assumes a frozen core, or if this was a grid size error. While the the Bader charges can not divulge any core electron behavior, the calculation for $CaAl_4O_7$ was subsequently run in VASP with the only variation being exponentially bigger grid sizes. In figure 5.2, the charges on calcium seems to oscillate, with a negative charge on calcium after an 68% increase on the 10^6 fine mesh grid originally used. This could be due to the addition of the frozen core electrons to the valence, but as $CaAl_4O_7$ is also the largest (electrons/unit cell) extended solid in this aluminum series, this could also indicate that Bader Charges are grid sensitive. The sensitivity to grid size in both VASP and in the Bader Charge Analysis programs indicate that, when examining these solids, the Laplacian (which is grid sensitive) and the Bader Charges can only be used in smaller extended solids, if maintaining a fine mesh grid of around 10^6 or greater.

In the following sections, the highlighted solids in table 5.1 will be compared. The Li-Al-O solids were chosen since they behave as expected, as seen in chapter 3, while the Ca-Al-O solids were chosen since the behavior of calcium in these compounds display unusual

behavior. The comparison of these solids is made to dispel any doubt about computational bias present and verify that the unexpected behavior is not a computational error.

5.1.2 LiAl

The first structure to be compared will be LiAl. In figure 5.3, the electrons are marked and lie between aluminum atoms, indicating a covalent bond. In the figure: (a) represents the Laplacian calculated from the charge density from CRYSTAL14, (b) represents the Laplacian calculated from the charge density from FLAIR, and (c) represents the Laplacian calculated from the charge density from VASP. While there are minor differences, the overall picture indicates that the same information can be attained from all three varying calculational methods.
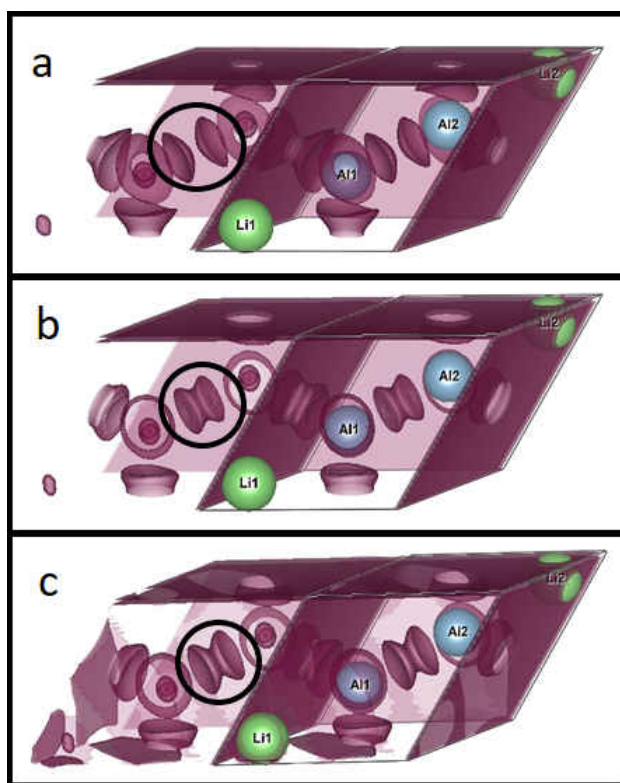

Figure 5.3: Laplacian Maps of LiAl from (a) CRYSTAL14, (b) Flair, and (c) VASP.

Looking at the charge density difference of LiAl, from both CRYSTAL14 (a) and FLAIR (b), figure 5.4, one can see that the CDD maps remain consistent but also mirror the information seen with the Laplacian.
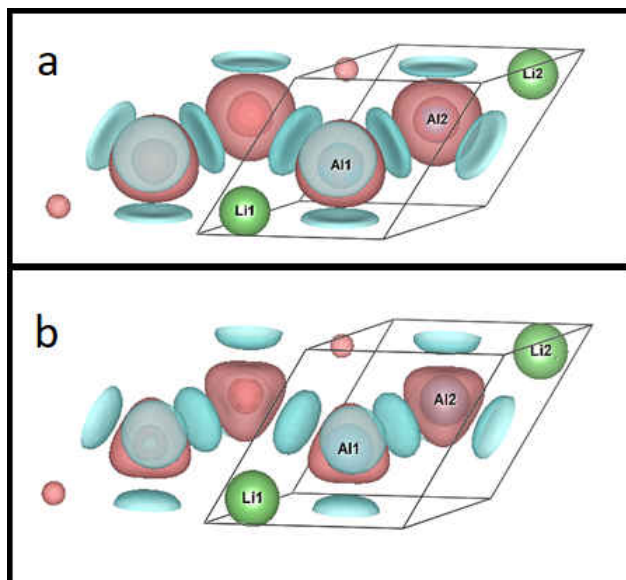
Figure 5.4: Charge Density Difference Maps of LiAl from (a) CRYSTAL14 and (b) Flair.

5.1.3 LiAl$_3$

In the next structure LiAl$_3$, lithium is in the minority, stoichiometrically, and would be donating a fractional charge. This behavior was of interest, since the effects of a fractional charge transfer seemed to have a significant effect on the anionic metal and needed to be verified. In figure 5.5: (a) represents the Laplacian calculated from the charge density from CRYSTAL14, (b) represents the Laplacian calculated from the charge density from FLAIR, and (c) represents the Laplacian calculated from the charge density from VASP. While there are minor differences, the overall picture indicates that the same information can be attained from all three varying calculational methods.
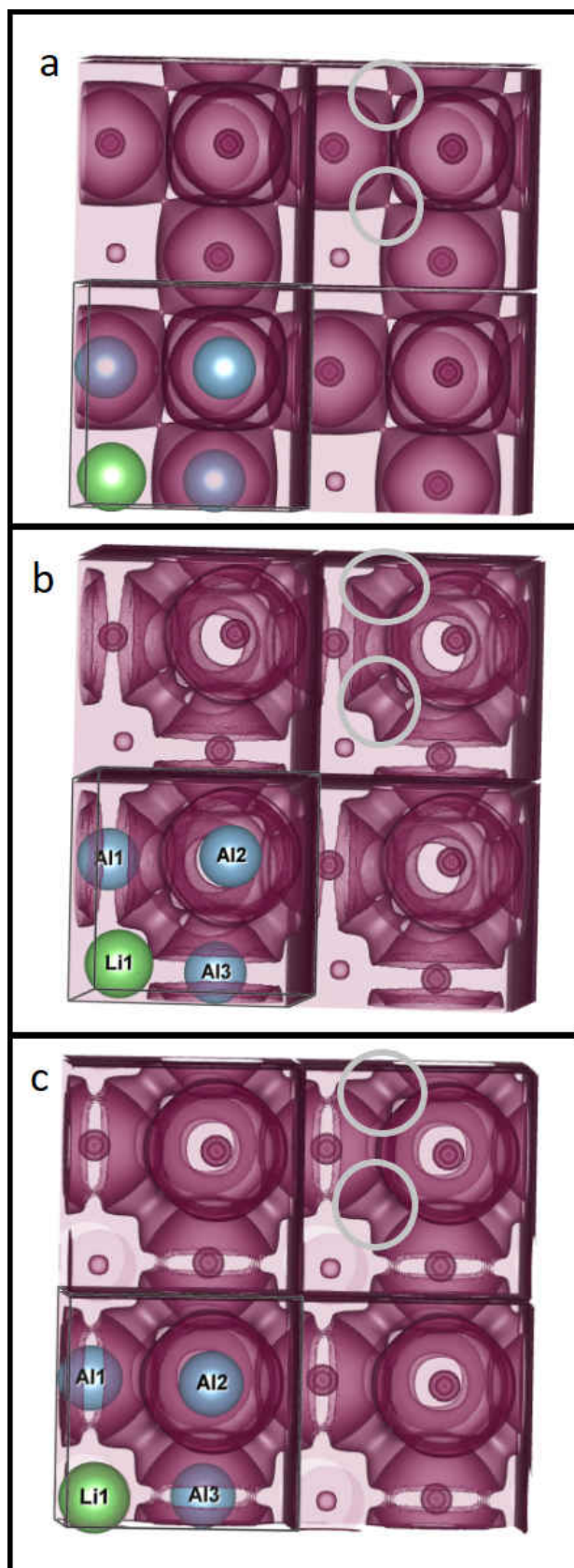
Figure 5.5: Laplacian Maps of LiAl$_3$ from (a) CRYSTAL14, (b) Flair, and (c) VASP.

Looking at the charge density difference of LiAl$_3$, from both CRYSTAL14 (a) and FLAIR (b), in figure 5.6 one can see that the CDD maps remain consistent despite minor differences, and also mirror the information seen with the Laplacian.
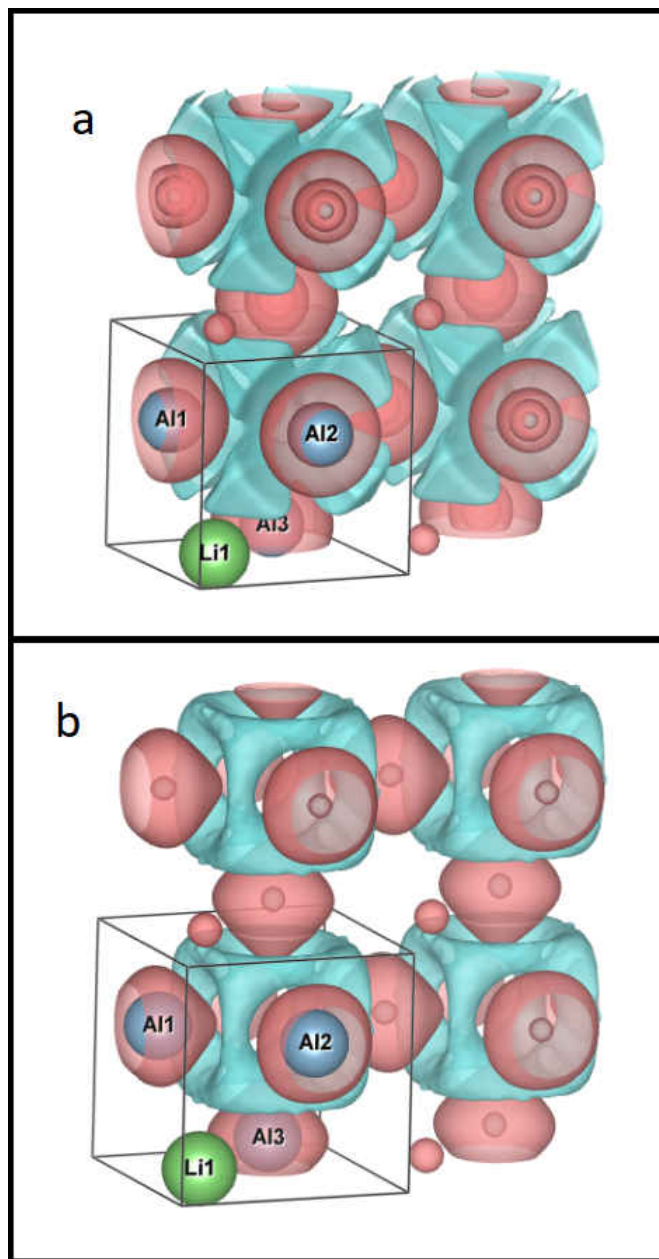

Figure 5.6: Charge Density Difference Maps of LiAl$_3$ from (a) CRYSTAL14 and (b) Flair.

5.1.4 LiAlO$_2$ (92)

The Zintl Compounds above displayed the bonding expected by the Zintl-Klemm Concept. The next structure, LiAlO$_2$ (92), has been postulated to contain metal-metal bonding seen

by aluminum atoms by the Extended Zintl-Klemm Model - 2. In figure 5.7, the Laplacian of $LiAlO_2$ (92) can be seen where (a) represents the Laplacian calculated from the charge density from CRYSTAL14, (b) represents the Laplacian calculated from the charge density from FLAIR, and (c) represents the Laplacian calculated from the charge density from VASP. In all of the Laplacians calculated, almost no difference can be seen. There is also no electron accumulation between aluminum atoms but the electrons are gathered spherically around all species in the compound, indicating that all the species within the compound have become ions.
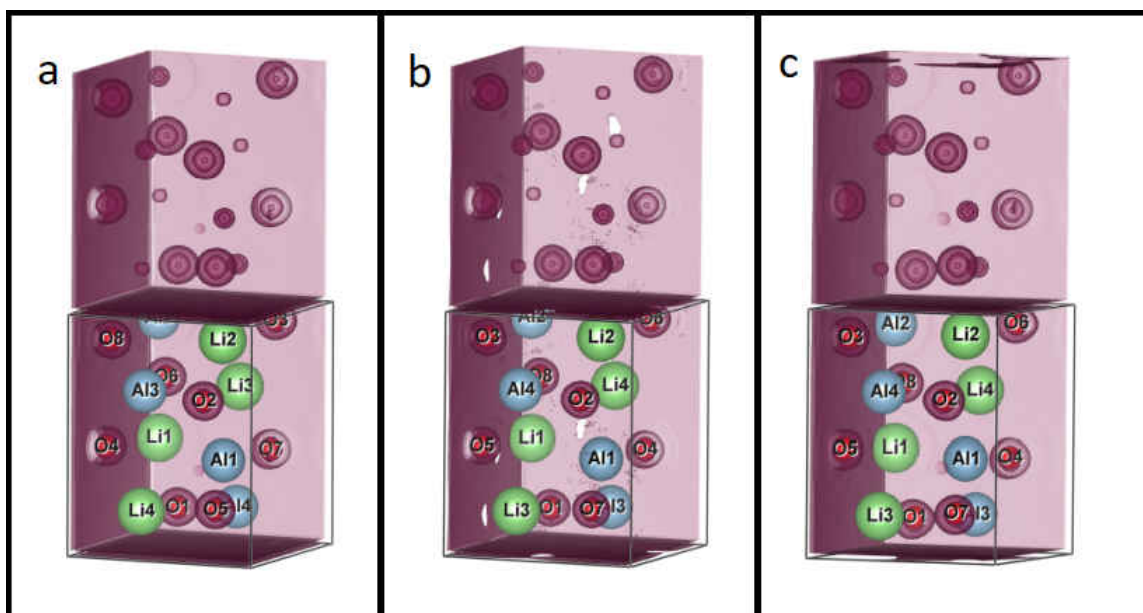

Figure 5.7: Laplacian Maps of $LiAlO_2$ (92) from (a) CRYSTAL14, (b) Flair, and (c) VASP.

Looking at the charge density difference of $LiAlO_2$ (92), from both CRYSTAL14 (a) and FLAIR (b), in figure 5.8 one can see that the CDD maps remain consistent despite minor differences, and also mirror the information seen with the Laplacian. The oxygen atoms have gained charge density spherically and aluminum and lithium atoms have lost charge density, indicating what could be classified as an ionic solid.
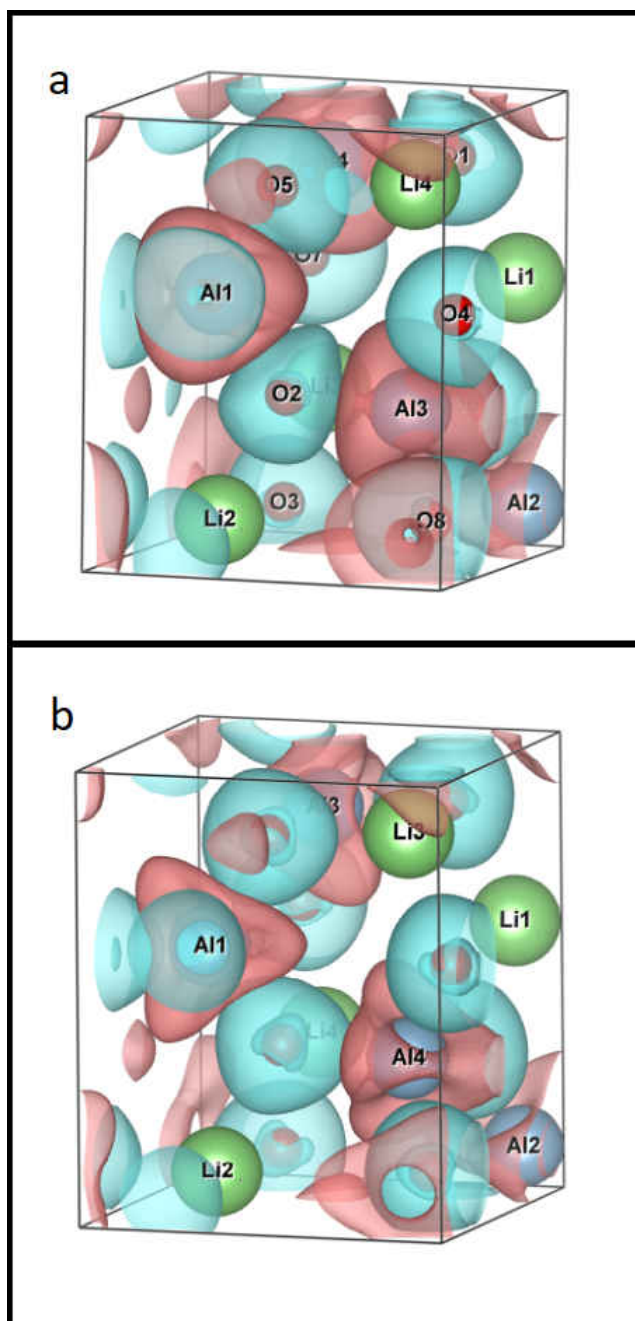
Figure 5.8: Charge Density Difference Maps of LiAlO$_2$ (92) from (a) CRYSTAL14 and (b) Flair.

5.1.5   CaAl$_2$

The solid CaAl$_2$ was chosen since the Bader Charges on the calcium ion indicated that it seemed to be acquiring charge, unusual and unexpected behavior for calcium. By looking at the Laplacian and Charge Density Difference Maps, the internal electronic structure can be

examined to see if this behavior is also seen. In figure 5.9, the Laplacian of all three programs where (a) represents the Laplacian calculated from the charge density from CRYSTAL14, (b) represents the Laplacian calculated from the charge density from FLAIR, and (c) represents the Laplacian calculated from the charge density from VASP, can be seen. In these figures the same information is present, with the gray circle indicating an accumulation of electrons between aluminum atoms and the black circle showing the calcium atom expanding with an increase of charge spherically around itself, as one would expect when in the formation of an anion.
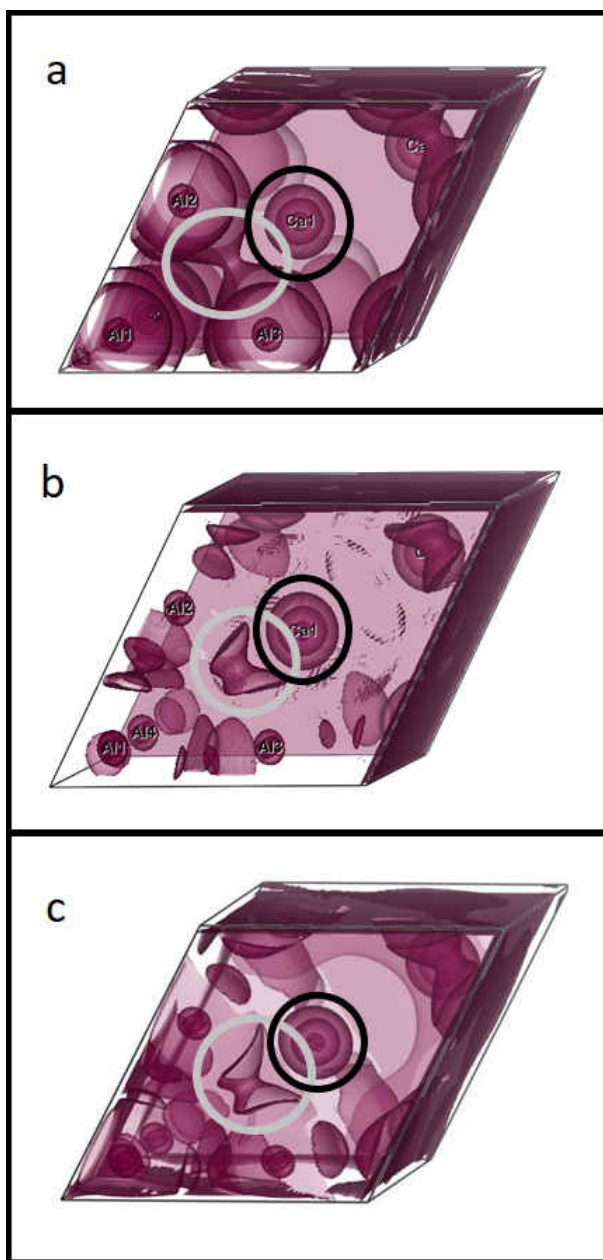

Figure 5.9: Laplacian Maps of $CaAl_2$ from (a) CRYSTAL14, (b) Flair, and (c) VASP.

Looking at the charge density difference of $CaAl_2$ for both CRYSTAL14 (a) and FLAIR (b), in figure 5.10 one can see that there is charge density accumulation (blue) around the calcium atom and between the aluminum atoms, corroborating the information gathered from the Laplacian of this solid. This also supports the charges given by the Bader Charge Analysis.
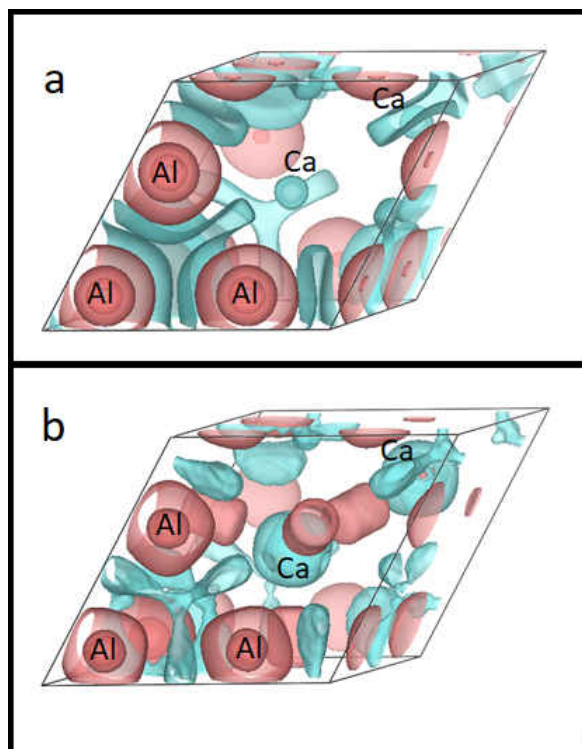

Figure 5.10: Charge Density Difference Maps of $CaAl_2$ from (a) CRYSTAL14 and (b) Flair.

5.1.6 $CaAl_4O_7$

The oxide $CaAl_4O_7$ was chosen since the Bader Charges on this solid indicated a strange behavior with the calcium ion in this structure. The charges of both FLAIR and CRYSTAL14 indicate that calcium seems to be acquiring charge, becoming an anion, while VASP had fluctuating charges depending on grid size, leaving the ionic behavior of calcium in question . By looking at the Laplacian and Charge Density Difference Maps, the internal electronic structure can be examined to see if calcium seems to be gaining or losing charge. In figure 5.11, the Laplacian of all three programs where (a) represents the Laplacian calculated from the charge density from CRYSTAL14, (b) represents the Laplacian calculated from the charge density from FLAIR, and (c) represents the Laplacian calculated from the charge density from VASP, can be seen. As expected, all species within this solid seem to show no electronic accumulation between species but spherically around themselves, as one would expect of ionic behavior. When calculating the Laplacian, with all three programs' charge

densities, the information seen is nearly identical. The calcium ion is circled in black while the aluminum ion is circled in green. This was done to highlight the contraction of the aluminum, the expected behavior of a cation, while the calcium ion seems to be expanded out, much like the oxygen, an anion.
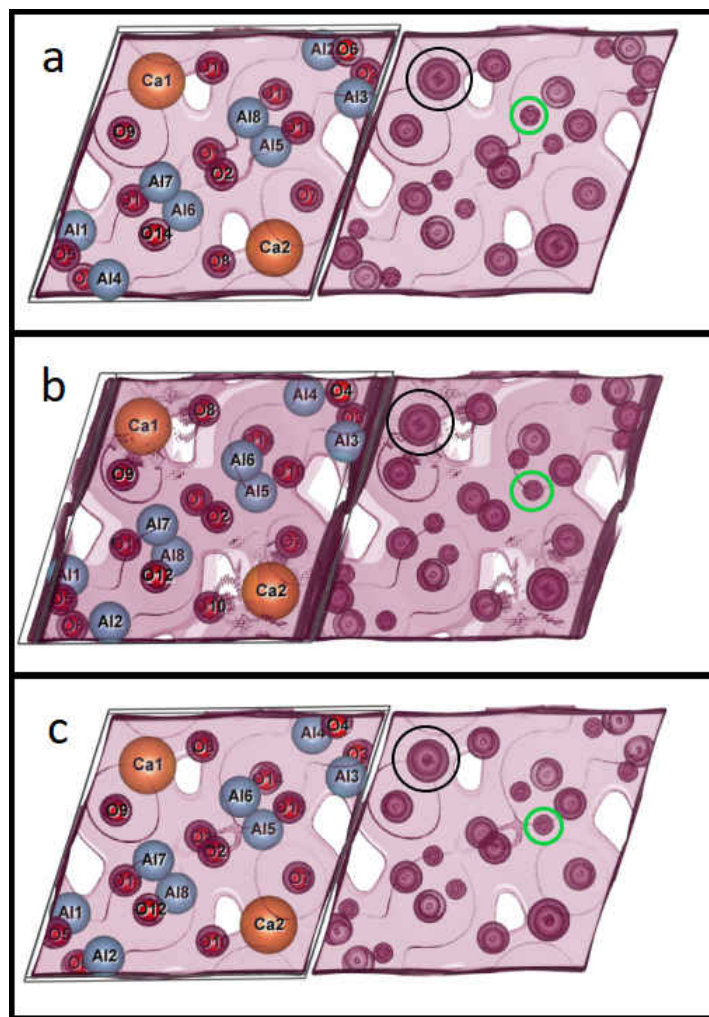

Figure 5.11: Laplacian Maps of $CaAl_4O_7$ from (a) CRYSTAL14, (b) Flair, and (c) VASP.

In figure 5.12, the charge density difference for both CRYSTAL14 (a) and FLAIR (b) can be seen. The calcium ion has been circled and both show an increase of charge density, with the charge density polarized towards the positive aluminum cations. The aluminum atoms have lost charge density around themselves, which confirms the contraction seen in the Laplacian of each charge density for $CaAl_4O_7$. The oxygen ions, much like the calcium ions, have gained charge density. The more visible expansion of the oxygen anion versus the calcium anion could be due to the relative size differences between oxygen and calcium.
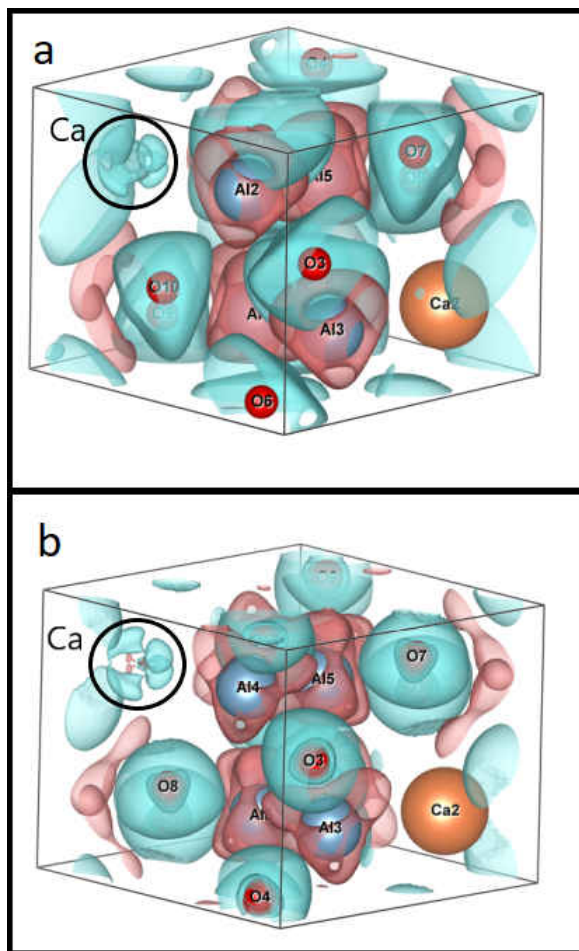
101

Figure 5.12: Charge Density Difference Maps of $CaAl_4O_7$ from (a) CRYSTAL14 and (b) Flair.

Concluding Remarks

In conclusion, while not all the programs' charge densities could be analyzed with the same methods, it does appear that all three programs provide equitable information dependent on the methods of analysis. In terms of being able to perform the calculations, several problems arose. The first was with CRYSTAL14; while seemingly to provide similar information to that of VASP and FLAIR with smaller atoms, this program is basis set dependent and proved that as the atoms got larger it was increasingly difficult to model the system correctly in term of the basis sets. This was seen when calculating $MgAl_2$ and any lattice with an element above atomic number 20. The problem stemmed from linear dependence and failure to converge. VASP, though able to perform calculations at faster speeds due to the pseudo potentials, seems to suffer by being grid size dependent. Even though VASP was able to converge on larger extended solids, the information that could be acquired from the charge density failed

to give us enough information to truly assess the bonding character found within each solid. While the Bader charges do provide clues as to what is happening with the crystal, it can not visualize where the charge density is gathering; it is grid size dependent and as such grid size must be enlarged to get more reliable charge trends. In the calculation of $CaAl_4O_7$ the largest in the aluminum series already proved to have a problem with grid size as the charged seems to oscillate, as if trapped in a local minimum. This crystal, unfortunately, is not the largest extended solid being analyzed and with increasing size the grid must then be increased as well, limiting the usefulness of VASP's efficiency, which came at the cost of losing the subtleties that might have been seen by the roles the core electrons play in the bonding of these crystals. The only two methods that could provide that information is the Laplacian of the charge density and the charge difference maps, however, both could not be performed on VASP. The Laplacian of the charge density is also grid dependent, as such very large systems cannot be calculated to get any reasonable information from it. The inability to calculate the charge difference maps from VASP occurs because of the method used to calculate the charge density of the atoms before interacting with the other species in the solid. While this might not be a hindrance to many, due to the nature of this analysis this was not feasible on these compounds. FLAIR proved to be a robust program that was able to provide the needed measures for analysis. Overall, while both VASP and CRYSTAL14 do suffer from some limitations, the information that was acquired for smaller systems was largely consistent from all three methods.

Chapter 6

Conclusions

The goal of this investigation was to perform a series of theoretical analyses and assess the ability that the Zintl-Klemm Concept, Extended Zintl-Klemm Concept - Model 1, and the Extended Zintl-Klemm Concept - Model 2 have in predicting and rationalizing the extended solids that fall under each concepts' purview. Each concept attempts to rationalize and predict the physical structure of a solid by utilizing an electron counting scheme and a pseudo-atom approach. In order to fully explore these concepts, charge density maps were acquired using multiple quantum modeling software packages, so one could peer into the electronic structure of these solids. These calculations were performed since the electronic structure of these solids should logically mirror the rationalizations and predictive measures used to rationalize and predict the external structure of these solids. If the approaches used by these concepts are mirrored in the electronic structure of these solids, it would provide better insight into the mechanism that elements employ when forming bonds. This would allow for better prediction of the physical structure of yet to be synthesized compounds, as well as possible properties these solids could exhibit.

In this study, over 85 structures were calculated and analyzed using various computational methods. The method chosen to investigate the electronic structure of these solids was systematically examining the difference in the charge density between the atoms before and after the formation of bonds – the charge difference density. The charge densities were calculated with CRYSTAL14, VASP and FLAIR, though ultimately the program FLAIR was chosen. FLAIR proved to be the more robust and better equipped program when performing these charge density difference maps. This was due to difficulties associated with CRYSTAL14 and VASP when attempting to perform the needed calculations to create the difference electron density maps. CRYSTAL14 was able to provide the charge densities in both the converged state and the initial atomic state, however this could only be accomplished with solids that contained smaller atoms. CRYSTAL14 is a program which is basis

set dependent and proved that as the atoms got larger it was increasing difficult to model the system correctly in term of the basis sets. This was seen when calculating any solid with an element above the atomic number of twenty(20), with the problem stemming from linear dependence and failure to converge. Although VASP had no trouble converging on any of the solids and was able to perform calculations at faster speeds, due to the pseudo potentials and frozen core assumptions the program makes during its calculations, it was hindered by its inability to create initial atomic charge densities that would allow the subtleties between metal-metal bonding to be seen. This program, tauted for being efficient, loses its efficiency when increasing the grid size of the charge density maps it can provide. This increase in grid size was required when attempting to calculate the Laplacian from the charge densities, since the Laplacian seemed to show the same information as the charge density difference maps. As the atoms and the solids got bigger the time needed for the calculations become too long to be practical. This was not a problem for either CRYSTAL14 or FLAIR, as both of these programs can compute the needed charge densities and utilize the crystal's symmetry to arrive at convergence quickly. While the Laplacian of the charge densities, provided by all three programs, displayed the same information as the charge difference densities, calculating the Laplacian was not a consistently viable method. While the Laplacian does provide the location of the electrons, it is also very sensitive to grid size, making the calculations impractical due to the lengthy calculation time needed for bigger solids since they would require bigger grids. Although both VASP and CRYSTAL14 have some limitations, the information that was acquired by both programs, when calculating the smaller systems, seemed consistent with FLAIR. This suggests that no calculation bias was present within the study and that with enough time and better basis sets for the larger atoms one could use any program to look at the electronic structure of a solid.

Once the computational method was chosen, the first concept to be examined was the Zintl-Klemm Concept. This concept proved to be quite successful in both predicting and rationalizing the extended solids that fell under its purview. The Zintl-Klemm Concept, which consisted of a simple electron counting scheme, was able to successfully explain over 70 percent of the Zintl Compounds studied. While the concept does not account for each element's unique properties, its rationalizations for the physical structure was mirrored in its electronic structure, giving credence to hypothesized pseudo-atom behavior the concept used as a predictive measure. The concept also proved an effective method despite the varying stoichiometric ratios found within the Zintl Compounds, such that $LiGa$ and Li_3Ga_2 behaved as predicted, both physically and electronically. In studying the compounds that contained various ratios, it was revealed that a fractional charge transfer to the more electronegative metal was enough to cause distortions in the bonding and packing of these intermetallics,

such that when a more electronegative element acquires a fractional charge it would shift its pseudo-atom behavior to a nonmetal in a neighboring group. This shift of pseudo-atom with a fractional charge transfer was especially noted in LiTl and in KTl, two compounds that were thought to not adhere to the Zintl-Klemm Concept. When the concept was applied to both compounds, the anionic metal was seen to behave like arsenic, which belongs to Group XV and confirming that a fractional charge, from both lithium and potassium, must have been donated. This means that the assumed -1 charge that is traditionally donated must have been greater than in the case of the Group I metals. This could be caused by the lanthanide contraction found within thallium.

While the Zintl-Klemm Concept was able to predict and rationalize the bulk of the Zintl Compounds, the majority of the unexplained Zintl Compounds displayed a puzzling phenomena. This surprising behavior was uncovered within the Zintl Compounds containing calcium. The behavior exhibited by calcium goes partially against the Zintl-Klemm Concept. In almost all compounds studied that contained calcium, calcium, despite being less electronegative than the Group XIII metal, acquired electronic charge instead of donating it. This made the Group II metal an anion (which is certainly unexpected) and the Group XIII metal a cation. The calcium anion exhibited this behavior in some of its structures such that it did not seem to form bonds with either itself or other elements. Instead, it caused a strong polarizing effect in the other metal, or in the event that calcium had not acquired enough charge, calcium would be polarized towards the Group XIII metal. This charge transfer goes directly against the Zintl-Klemm Concept, however even though the more electronegative metal donated charge, it continued to form covalent bonds between itself despite its loss of charge or its polarization towards calcium. Yet, the continued bonding of the Group XIII metal with covalent bonds is as expected within the Zintl-Klemm Concept. The bonds and lattices formed by the Group XIII metal are similar to those found in what would have been their pseudo-atom, if calcium had donated its charge following the donation scheme presented in the Zintl-Klemm Concept. This unusual electronic behavior highlights the necessity of looking at the electronic structure of a solid in order to better understand the bonding occurring within a structure. The only possible explanation for calcium's ability to accept electronic charge could be caused by calcium's ground state electron configuration. This element has an empty 3d subenergy level and a closed 4s subenergy level. Since the 3d subenergy level lies very close to the nuclei, it seems that it could be experiencing an effect similar to those found in phosphorus, sulfur, and chlorine, which have an expanded octet. In addition, it also contains a closed subenergy level, which may provide an added stabilizing effect as seen in zinc and cadmium. This stabilization provided by the closed 4s subenergy level and the empty 3d energy level might allow this element to acquire charge when placed

in an electron-rich environment.

Since the Zintl-Klemm Concept proved to be capable of predicting and rationalizing the bulk of Zintl Compounds examined, it was the next logical step to perform a similar analysis on the Zintl-Klemm Concept's extensions. In the theoretical analysis of the Extended Zintl-Klemm Concept - Model 1, a series of antimony compounds were evaluated in terms of this concept's modified pseudo-atom approach. The modifications made to the pseudo-atom approach by the Extended Zintl-Klemm Concept - Model 1 was successful. In the series of antimony intermetallics studied, all but one of the solids studied had the electronegative metal mirroring the behavior of its pseudo atom. This extension of the Zintl-Klemm was able to rationalize and predict the electronic structure of these compounds by way of its pseudo-atom, and with the success of this concept, allowed for the extension of the Zintl Compounds to be composed of more than just Group I/II metals with Group XIII/XIV metals. This extension of the intermetallics that could now be rationalized and even predicted with some certainty now includes transition metals and heavy post transition metals. The concept was able to predict the bonding found within the systems analyzed and in the case of $CrSb_2$ (58), it was able to provide a better understanding of the bonding mechanism behind its varying electronic structure. The insights about the bonding and potential physical properties of $CrSb_2$ (58) could not have been acquired without the use of the Extended Zintl-Klemm Concept - Model 1. Another important revelation brought forth by the Extended Zintl-Klemm Concept - Model 1 was the long range covalent bonding interactions that exist between the anionic metals within these intermetallic compounds. These distances, found to be up to 3.46Å, were previously thought too far for actual bonding, however the antimony atoms showed an increase in charge density between each other despite the long distances, establishing that bonding interactions between metals at long distances do occur.

With the success of the Extended Zintl-Klemm Concept - Model 1, the Extended Zintl-Klemm Concept - Model 2 attempts to bridge the gap between the Zintl Compounds to their oxides. This model attempts to rationalize the solids by indicating that the long range metal-metal interactions postulated by the EZKC-1 model would be present despite the presence of oxygen atoms in the solid. This seemed to be supported by the physical similarities between the anionic lattice present in the Zintl Compounds and similar packing arrangements these metals maintained in their oxides. However, while the packing was similar in some of the oxides, the distances of the metal atoms were too far, even with the farther distances seen in Model 1, to contain metal-metal bonding. Examining the oxides of the Zintl Compounds via the charge density difference maps, it was determined that, while in some solids the anionic metal in the Zintl Compounds did pack like those in the oxides, there were no metal-metal interactions found, even between the metals that were within bonding distances. In all

oxides studied, the oxygen atoms and the metal atoms had gained or lost charge spherically, indicating that no covalent bonding was occurring in these solids, since the atoms had become ions. As no metal-metal interactions were witnessed, even at the longer distances seen when analyzing the Extended Zintl-Klemm Concept - Model 1, no pseudo-atom behavior could be posited, making an electron counting scheme futile. In previous studies, it was rationalized that if oxygen was introduced to an intermetallic the oxygen atoms would locate themselves where metal-metal bonding occurs or within electron-rich voids. This behavior was seen when taking an oxide and running the calculations without oxygen in order to acquire a hypothetical Zintl Compound. When comparing the hypothetical Zintl Compound with the actual oxide, the oxygen atoms were found "stuffed" where metal-metal bonding occurred or within the electron-rich voids present within the structure. While this provides insight on the behavior of oxygen in the presence of these intermetallics, this does not seem to help predict structures as the known structure of the oxide was used to determine this behavior, not the Zintl Compound associated with the oxide. In the case where a Zintl Compound was chosen as a possible precursor to the the oxide, the electronic structure failed to demonstrate the behavior predicted. This leads to the conclusion that the Extended Zintl-Klemm Concept - Model 2 could not adequately rationalize or predict the structure and bonding seen within these extended solids.

6.1   Future Investigations

During the course of this investigation, an unexpected electronic behavior was witnessed within the calcium Zintl Compounds. While this study did not examine structures formed with elements further down Group II to determine if strontium or the following Group II metals would exhibit similar behavior, it would be of interest to examine if the behavior presented by calcium also exists in the other Group II metals. If this electronic behavior is seen, it could bring forth a better understanding about the stabilizing effects that a closed s-subenergy level plays in electron donation within extended solids. When examining $CaAl_4O_7$, which contains the highly electronegative element oxygen, charge density was still seen accumulating around calcium atoms. This behavior in calcium, which is unexplored, needs to be better understood since calcium is an essential element for life on earth and the most abundant of the Group II metals. This metal is found within many minerals and water sources and when in solution this element displays a charge of $+2$, which is what one would expect in chemistry containing a calcium, yet not the cationic behavior found within the extended solids in this study. The behavior exhibited by calcium in these intermetallics poses the possibility of creating stronger metal alloys, though they may be possibly easier to

oxidize. In all the solids where calcium acquired charge at the expense of Group XIII metal, these Group XIII metals formed covalent bonds that mirrored their more electronegative nonmetals. The covalent bonds formed by the Group XIII metal could reinforce the strength the metal alloy could exhibit. The synthesis and subsequent testing of metal alloys containing calcium would seem to merit exploration. In terms of the Extended Zintl-Klemm Concept - Model 2, it would be pertinent to continue to further explore possible rationales that could explain the similarity in packing seen within the physical structure of the oxide to their Zintl Compounds but not in the electronic one. While the physical structure of a solid is important, understanding the underlying electronic mechanism for the formation of these oxides still needs to be understood, especially as the Zintl Compounds transition into oxides.

Bibliography

1. N Kh Abrikosov and LI Petrova. System co-sb-te. *INORGANIC MATERIALS*, 14(3):346–351, 1978.

2. N Kh Abrikosov and LI Petrova. The polythermal cross-section fesb2-fete2 of the fe-sb-te system. *INORGANIC MATERIALS*, 25(8):1087–1090, 1989.

3. Carlo Adamo and Vincenzo Barone. Toward reliable density functional methods without adjustable parameters: The pbe0 model. *The Journal of chemical physics*, 110(13):6158–6170, 1999.

4. Richard FW Bader. *Atoms in molecules*. Wiley Online Library, 1990.

5. R Basso, S Carbonin, and A Della Giusta. Cation and vacancy distribution in a synthetic defect spinel. *Zeitschrift für Kristallographie-Crystalline Materials*, 194(1-4):111–120, 1991.

6. Claude Belin and Rong Guo Ling. The intermetallic phases of gallium and alkali metals. interpretation of the structures according to wade's electron-counting methods. *Journal of Solid State Chemistry*, 48(1):40–48, 1983.

7. Claude Belin and Monique Tillard-Charbonnel. Frameworks of clusters in alkali metal-gallium phases: Structure, bonding and properties. *Progress in solid state chemistry*, 22(2):59–109, 1993.

8. DJM Bevan, Raymond L Martin, and Angel Vegas. Rationalization of the substructures derived from the three fluorite-related [li6 (mvli) n4] polymorphs: An analysis in terms of the "bärnighausen trees" and of the "extended zintl–klemm concept". In *Inorganic 3D Structures*, pages 93–131. Springer, 2011.

9. A Bon, C Gleitzer, A Courtois, and J Protas. Synthese et structure cristalline d'un nouvel aluminate de potassium. *Comptes Rendus Hebdomadaires des Seances de l'Academie des Sciences, Serie C, Sciences Chimiques*, 278:785–788, 1974.

10. G Breitling and H Richter. Structure of amorphous arsenic and selenium according to the intensity curves. *Materials Research Bulletin*, 4(1):19–32, 1969.

11. G Bruzzone. Sui sistemi binari sr- tl, ba- tl e ca- tl. *Annali di Chimica, Rome*, 56:1306–1319, 1966.

12. G Bruzzone. The d13 structure type in intermetallic compounds. *Acta Crystallographica Section B: Structural Crystallography and Crystal Chemistry*, 25(6):1206–1207, 1969.

13. G Bruzzone. The d13 structure type in intermetallic compounds. *Acta Crystallographica Section B: Structural Crystallography and Crystal Chemistry*, 25(6):1206–1207, 1969.

14. G Bruzzone, E Franceschi, and F Merlo. M5x3 intermediate phases formed by ca, sr and ba. *Journal of the Less Common Metals*, 60(1):59–63, 1978.

15. T Chattopadhyay and HG Von Schnering. High pressure x-ray diffraction study on p-fes2, m-fes2 and mns2 to 340 kbar: a possible high spin-low spin transition in mns2. *Journal of Physics and Chemistry of Solids*, 46(1):113–116, 1985.

16. Wo H Cloud, DS Schreiber, and KR Babcock. X-ray and magnetic studies of cro2 single crystals. *Journal of Applied Physics*, 33(3):1193–1194, 1962.

17. John D Corbett. Polyatomic zintl anions of the post-transition elements. *Chemical Reviews*, 85(5):383–397, 1985.

18. Gerhard Cordier, Herbert Schäfer, and Michael Stelter. Elektronenmangelverbindungen des galliums zur kenntnis von ca3ga5. *Zeitschrift für anorganische und allgemeine Chemie*, 539(8):33–38, 1986.

19. JW Davenport, RE Watson, and M Weinert. Linear augmented-slater-type-orbital method for electronic-structure calculations. iii. structural and cohesive energies of the 5d elements lu–au. *Physical Review B*, 32(8):4883, 1985.

20. AA Demkov, H Seo, X Zhang, and J Ramdani. Using zintl-klemm intermetallics in oxide-semiconductor heteroepitaxy. *Applied Physics Letters*, 100(7):071602, 2012.

21. Zhenchao Dong and John D Corbett. Synthesis, structure, and bonding of the novel cluster compound ktl with isolated tl66-ions. *Journal of the American Chemical Society*, 115(24):11299–11303, 1993.

22. Roberto Dovesi, Roberto Orlando, Alessandro Erba, Claudio M Zicovich-Wilson, Bartolomeo Civalleri, Silvia Casassa, Lorenzo Maschio, Matteo Ferrabone, Marco De La Pierre, Philippe D'Arco, et al. Crystal14: A program for the ab initio investigation of crystalline solids. *International Journal of Quantum Chemistry*, 114(19):1287–1317, 2014.

23. Dovesi, R.; Orlando, R.; Erba, A.; Zicovich-Wilson, C. M.; Civalleri, B.; Casassa, S.; Maschio, L.; Ferrabone, M.; De La Pierre, M.; D'Arco, P.; Noel, Y.; Causa, M.; Rerat, M.; Kirtman, B. Crystal14, 2016-02-23. http://www.crystal.unito.it/index.php.

24. M Ellner, T Gödecke, G Duddek, and B Predel. Strukturelle und konstitutionelle untersuchungen im galliumreichen teil des systems magnesium-gallium. *Zeitschrift für anorganische und allgemeine Chemie*, 463(1):170–178, 1980.

25. Jürgen Evers. High pressure investigations on aibiii zintl compounds (ai= li to cs; biii= al to tl) up to 30 gpa. In *Zintl Phases*, pages 57–96. Springer, 2011.

26. Jürgen Evers and Gilbert Oehlinger. After more than 60 years, a new natl type zintl phase: Ktl at high pressure. *Inorganic chemistry*, 39(4):628–629, 2000.

27. LM Foster, GV Chandrashekhar, JE Scardefield, and RB Bradford. Phase diagram of the system na2o· ga2o3-ga2o3 and its relation to the system na2o· al2o3-al2o3. *Journal of the American Ceramic Society*, 63(9-10):509–512, 1980.

28. K Frank and K Schubert. Kristallstruktur von mg2ga und mg2tl. *Journal of the Less Common Metals*, 20(3):215–221, 1970.

29. VR GENRIKHSON and VG BOGUNOV. Spinel crystals mgga2-xinxo4 grown from solutions in the melt of the system mgo-ga2o3-in2o3-bao-b2o3. *INORGANIC MATERIALS*, 25(12):1727–1729, 1989.

30. H Glaum, S Voigt, and R Hoppe. Zwei vertreter des α-lifeo2 typs: Lilno2 und α-liybo2 (1, 2). *Zeitschrift für anorganische und allgemeine Chemie*, 598(1):129–138, 1991.

31. Arnold M Guloy. Polar intermetallics and zintl phases along the zintl border. *Inorganic Chemistry in Focus III*, pages 157–171, 2006.

32. DA Hansen and JF Smith. Structure and bonding model for na2tl. *Acta Crystallographica*, 22(6):836–845, 1967.

33. DA Hansen and JF Smith. The structure of li9al4. *Acta Crystallographica Section B: Structural Crystallography and Crystal Chemistry*, 24(7):913–918, 1968.

34. Wiebke Harms, Marco Wendorff, and Caroline Röhr. Structure and bonding of ternary gallides caga 1- x (si/sn/al/in) x with the crb type and related structures. *Journal of Alloys and Compounds*, 469(1):89–101, 2009.

35. Henkelman group at The University of Texas in Austin. Bader charge analysis, 2017-01-11. http://theory.cm.utexas.edu/svn/repo.

36. Robert W Henning and John D Corbett. Formation of isolated nickel-centered gallium clusters in na10ga10ni and a 2-d network of gallium octahedra in k2ga3. *Inorganic Chemistry*, 38(17):3883–3888, 1999.

37. K Hiraga, M Koiwa, and M Hirabayashi. Constitution of the indium-rich portion of the indium-magnesium system. *Journal of the Less Common Metals*, 15(2):109–119, 1968.

38. R Hoppe. Ternaäre oxide der alkalimetalle. In *Bulletin de la Société Chimique de France*, number 4, page 1115. EDITIONS SCIENTIFIQUES MEDICALES ELSEVIER 23 RUE LINOIS, 75724 PARIS CEDEX 15, FRANCE, 1965.

39. A Iandelli. Mx2-verbindungen der erdalkali-und seltenen erdmetalle mit gallium, indium und thallium. *Zeitschrift für anorganische und allgemeine Chemie*, 330(3-4):221–232, 1964.

40. A Iandelli. Crystallographic studies of the systems ma1 2-mga 2 (m= yb, ca, eu, sr). *Journal of the Less Common Metals*, 135(2):195–198, 1987.

41. Andrea Ienco, Roald Hoffmann, and Garegin Papoian. Electron-rich bonding and the importance of s, p mixing as one moves across a period: A lesson from the lisn system. *Journal of the American Chemical Society*, 123(10):2317–2325, 2001.

42. G Igel-Mann, H Stoll, and H Preuss. Structure and ionization potentials of clusters containing heavy elements: I. homonuclear group v clusters up to hexamers. *Molecular physics*, 80(2):325–339, 1993.

43. M Inoue, HP Hughes, and AD Yoffe. The electronic and magnetic properties of the 3d transition metal intercalates of tis2. *Advances in Physics*, 38(5):565–604, 1989.

44. R Isea, A Vegas, and A Ramos-Gallardo. Distribution of the mm distances in the oxides of the group 13 elements and their spinels and delafossites. *Acta Crystallographica Section B: Structural Science*, 54(1):35–40, 1998.

45. G-E Jang, IM Curelaru, and MP Hentschel. Growth and characterization of large single crystals of li ga zintl intermetallic compound. *Solid State Ionics*, 42(1-2):41–46, 1990.

46. William B Jensen. A quantitative van arkel diagram. *Journal of chemical education*, 72(5):395, 1995.

47. Jürgen Hafner, Georg Kresse, Doris Vogtenhuber, Martijn Marsman. Vasp, 2013-09-18. https://www.vasp.at/.

48. Susan M. Kauzlarich. Zintl compounds. In R. Bruce King, editor, *Encyclopedia of inorganic chemistry*. Wiley, New York, 2005.

49. Noboru Kimizuka and Takahiko Mohri. Structural classification ofrao3 (mo) n compounds (r= sc, in, y, or lanthanides; a= fe (iii), ga, cr, or al; m= divalent cation; n= 1–11). *Journal of Solid State Chemistry*, 78(1):98–107, 1989.

50. Koichi Momma & Fujio Izumi. Vesta, 2014-08-20. http://jp-minerals.org/vesta/en/.

51. LM Kovba, LN Lykova, and TA Kalinina. Physicochemical investigation of certain alkaline earth element gallates and indates. *Russian Journal of Inorganic Chemistry*, 25(3):397–399, 1980.

52. Georg Kresse and J Furthmüller. Vienna ab-initio simulation package (vasp). *Institut für Materialphysik, Vienna*, 2004.

53. K Kuriyama and N Masaki. The crystal structure of lial. *Acta Crystallographica Section B: Structural Crystallography and Crystal Chemistry*, 31(6):1793–1793, 1975.

54. Gilbert N Lewis. The atom and the molecule. *Journal of the American Chemical Society*, 38(4):762–785, 1916.

55. JD Marcoll, PC Schmidt, and Alarich Weiss. X-ray investigations of the intermetallic phases cacd1-x tlx and caln1-x tlx and knight shift measurements of 205tl-and 113cd-nmr in the system cacd1-x tlx. *Zeitschrift für Naturforschung A*, 29(3):473–476, 1974.

56. TP Martin and H Schaber. Mass spectra of si, ge, and sn clusters. *The Journal of chemical physics*, 83(2):855–858, 1985.

57. NN Matyushenko et al. C ci16 (229) im-3m–f.

58. DR McKenzie. Tetrahedral bonding in amorphous carbon. *Reports on Progress in Physics*, 59(12):1611, 1996.

59. F Merlo and ML Fornasini. The pseudobinary systems srag1- xznx, cacu1- xgax and cacu1- xgex and their use for testing structural maps. *Journal of the Less Common Metals*, 119(1):45–61, 1986.

60. Judit Molnár, Mária Kolonits, and Magdolna Hargittai. Molecular structure of sbf3 and bif3: an electron diffraction study. *Journal of molecular structure*, 413:441–446, 1997.

61. Koichi Momma and Fujio Izumi. An integrated three-dimensional visualization system vesta using wxwidgets. *Commision Crystallogr. Comput., IUCr Newslett*, (7):106–119, 2006.

62. DG Montague, MR Chowdhury, JC Dore, and J Reed. A rism analysis of structural data for tetrahedral molecular systems. *Molecular Physics*, 50(1):1–23, 1983.

63. Melanie Jean Moses. *Synthesis and Characterization of Binary Clusters to Controllable Binary Nanoparticles" The New Role of Zintl Anions"*. PhD thesis, 2004.

64. Reinhard Nesper. The zintl-klemm concept–a historical survey. *Zeitschrift für anorganische und allgemeine Chemie*, 640(14):2639–2648, 2014.

65. H Nowotny, E Wormnes, and A Mohrnheim. Investigation on the al–ca, mg–ca, and mg–zr systems. *Z. Metallkd*, 32:39–42, 1940.

66. Garegin Papoian and Roald Hoffmann. Building up complexity from strips and sheets: The electronic structure of the la12mn2sb30alloy. *Journal of Solid State Chemistry*, 139(1):8–21, 1998.

67. Garegin A Papoian and Roald Hoffmann. Hypervalent bonding in one, two, and three dimensions: extending the zintl–klemm concept to nonclassical electron-rich networks. *Angewandte Chemie International Edition*, 39(14):2408–2448, 2000.

68. H Pauly, Al Weiss, and H Witte. Phasenbreite und valenzelektronenkonzentration (vek) in den ternären kubischen zintlphasen vom natl-typ. *Z. Metallkd*, 59:554–558, 1968.

69. Michael F Peintinger, Daniel Vilela Oliveira, and Thomas Bredow. Consistent gaussian basis sets of triple-zeta valence with polarization quality for solid-state calculations. *Journal of Computational Chemistry*, 34(6):451–459, 2013.

70. John P Perdew, Kieron Burke, and Matthias Ernzerhof. Generalized gradient approximation made simple. *Physical review letters*, 77(18):3865, 1996.

71. VI Ponomarev, DM Kheiker, and NV Belov. Crystal structure of calcium dialuminate, ca2. *SOVIET PHYSICS CRYSTALLOGRAPHY, USSR*, 15(6):995–+, 1971.

72. M RABADANOV and AP Dudka. Comparative structural study of al2beo4 and al2beo4: Cr3+ (0.3 at.% cr) crystals. *Inorganic materials*, 33(1):48–51, 1997.

73. David Santamaria-Perez and Angel Vegas. The zintl–klemm concept applied to cations in oxides. i. the structures of ternary aluminates. *Acta Crystallographica Section B: Structural Science*, 59(3):305–323, 2003.

74. S Scharner et al. Structural features: Close-packed o layers in c stacking; part of fe in tetrahedral, li and remaining fe in octahedral voids. single feo. *CR Hebd. Seances Acad. Sci*, 256:5324–5326, 1963.

75. Lukas Schlipf, Alexander Slepko, Agham B Posadas, Heidi Seinige, Ajit Dhamdhere, Maxim Tsoi, David J Smith, and Alexander A Demkov. Epitaxial zintl aluminide sral 4 grown on a laalo 3 substrate. *Physical Review B*, 88(4):045314, 2013.

76. PC Schmidt, W Baden, N Weiden, and A Weiss. The intermetallic system nahg1–xtlx. x-ray investigations and measurements of the knight shift of na, hg, and tl. *physica status solidi (a)*, 92(1):205–212, 1985.

77. K Schubert, F Gauzzi, and K Frank. Kristallstruktur einiger mg-b-3-phasen. *ZEITSCHRIFT FUR METALLKUNDE*, 54(7):422–429, 1963.

78. Karlheinz Schwarz. Cro2 predicted as a half-metallic ferromagnet. *Journal of Physics F: Metal Physics*, 16(9):L211, 1986.

79. G Seifert and RO Jones. Geometric and electronic structure of clusters. *Zeitschrift für Physik D Atoms, Molecules and Clusters*, 20(1):77–80, 1991.

80. CR Shastry and S Bhan. An x-ray investigation of ordering in ternary mg 75 at.%– cd–in alloys. Technical report, Banaras Hindu Univ.(India). Dept. of Metallurgical Engineering, 1975.

81. GORDON S Smith, KF Mucker, Q Johnson, and DH Wood. The crystal structure of ga2mg. *Acta Crystallographica Section B: Structural Crystallography and Crystal Chemistry*, 25(3):549–553, 1969.

82. GS Smith, Q Johnson, and DN Wood. Crystal structure of ga5mg2. *Acta Crystallographica Section B: Structural Crystallography and Crystal Chemistry*, 25(3):554–557, 1969.

83. M Springborg and RO Jones. Sulfur and selenium helices: structure and electronic properties. *The Journal of Chemical Physics*, 88(4):2652–2658, 1988.

84. J Stöhr, W Müller, and H Schäfer. Structural principles of lithium-group-iii-compounds. *Stud. Inorg. Chem*, 3:753–756, 1983.

85. Daniel F Styer. The geometrical significance of the laplacian. *American Journal of Physics*, 83(12):992–997, 2015.

86. Challapalli Suryanarayana, Shailendra K Tiwari, and Tanjore R Anantharaman. A new metastable phase in the aluminium-magnesium system. *Zeitschrift fur Metallkunde*, 69:155, 1978.

87. Hirotsugu Takizawa, Kyota Uheda, and Tadashi Endo. A new ferromagnetic polymorph of crsb 2 synthesized under high pressure. *Journal of alloys and compounds*, 287(1):145–149, 1999.

88. W Tang, E Sanville, and G Henkelman. A grid-based bader analysis algorithm without lattice bias. *Journal of Physics: Condensed Matter*, 21(8):084204, 2009.

89. Karl-Friedrich Tebbe, Hans Georg Schnering, Barbara Rüter, and Gisela Rabeneck. Li3al2, eine neue phase im system li/al/li3al2, a new phase in the system li/al. *Zeitschrift für Naturforschung B*, 28(9-10):600–605, 1973.

90. Raymond G Teller, Larry J Krause, and Robert C Haushalter. Zintl anions from the extraction of zintl phases with non-amine solvents: isolation of (me4n) 4sn9,[k (hmpa) 2] 4sn9, and k4snte4 and structural characterization of (bu4n) 2mx (m= te, x= 5; m= se, x= 6; m= s, x= 6). *Inorganic Chemistry*, 22(12):1809–1812, 1983.

91. J Théry, R COLLONGUES, AM LEJUS, and D BRIANCON. Sur la structure et les propriétes des aluminates alcalins. *Bulletin de la societé chimique de France*, (5):973, 1961.

92. University of Wisconsin-Milwaukee (Weinert), Oregon State University (Schneider), the University of Vienna (Podloucky), and the Technical University of Vienna (Redinger). *flair*, 2015-09-06. https://people.uwm.edu/weinert/flair/.

93. AV Ushakov, DA Kukusta, AN Yaresko, and DI Khomskii. Magnetism of layered chromium sulfides m crs 2 (m= li, na, k, ag, and au): A first-principles study. *Physical Review B*, 87(1):014418, 2013.

94. JHN Van Vucht. On the crystal structures of some compounds of gallium with potassium, rubidium and caesium. *Journal of the Less Common Metals*, 108(1):163–175, 1985.

95. A Vegas, J Mejía-López, AH Romero, M Kiwi, D Santamaría-Pérez, and VG Baonza. Structural similarities between ti metal and titanium oxides: implications on the high-pressure behavior of oxygen in metallic matrices. *Solid state sciences*, 6(8):809–814, 2004.

96. Angel Vegas. Feli [po4]: Dissection of a crystal structure. In *Inorganic 3D Structures*, pages 67–91. Springer, 2011.

97. Angel Vegas. On the charge transfer between conventional cations: the structures of ternary oxides and chalcogenides of alkali metals. *Acta Crystallographica Section B: Structural Science*, 68(4):364–377, 2012.

98. Angel Vegas. The structures of cac and ca2cin the light of the extended zintl–klemm concept. *Structural Chemistry*, 27(6):1635–1639, 2016.

99. Angel Vegas and Valentin Garcia-Baonza. Pseudoatoms and preferred skeletons in crystals. *Acta Crystallographica Section B: Structural Science*, 63(3):339–345, 2007.

100. Angel Vegas and Martin Jansen. Structural relationships between cations and alloys; an equivalence between oxidation and pressure. *Acta Crystallographica Section B: Structural Science*, 58(1):38–51, 2002.

101. Angel Vegas, Raymond L Martin, and DJM Bevan. Compounds with astuffed'anti-bixbyite-type structure, analysed in terms of the zintl–klemm and coordination-defect concepts. *Acta Crystallographica Section B: Structural Science*, 65(1):11–21, 2009.

102. Angel Vegas, David Santamaría-Pérez, Miriam Marqués, Manuel Flórez, Valentín García Baonza, and J Manuel Recio. Anions in metallic matrices model: application to the aluminium crystal chemistry. *Acta Crystallographica Section B: Structural Science*, 62(2):220–227, 2006.

103. G Wagner and R Hoppe. Neue synthesewege zu metalloxiden: Na3tlo2 aus natl und na2o2. *Journal of the Less Common Metals*, 120(2):225–237, 1986.

104. G Wagner and R Hoppe. Oxydation intermetallischer phasen: Na5ino4 aus naln und na2o2. *Zeitschrift für anorganische und allgemeine Chemie*, 549(6):15–25, 1987.

105. Fei Wang and Gordon J Miller. Revisiting the zintl–klemm concept: A2aubi (a= li or na). *European Journal of Inorganic Chemistry*, 2011(26):3989–3998, 2011.

106. Fei Wang and Gordon J Miller. Revisiting the zintl–klemm concept: Alkali metal trielides. *Inorganic chemistry*, 50(16):7625–7636, 2011.

107. Fei Wang, Ulrich Wedig, Dasari LVK Prasad, and Martin Jansen. Deciphering the chemical bonding in anionic thallium clusters. *Journal of the American Chemical Society*, 134(48):19884–19894, 2012.

108. M Weinert, G Schneider, Raimund Podloucky, and Josef Redinger. Flapw: applications and implementations. *Journal of Physics: Condensed Matter*, 21(8):084201, 2009.

109. Winnie Wong-Ng, Howard F McMurdie, Boris Paretzkin, Camden R Hubbard, Alan L Dragoo, and James M Stewart. Standard x-ray diffraction powder patterns of fifteen ceramic phases. *Powder Diffraction*, 2(2):106–117, 1987.

110. Tsuyoshi Yoshi-Yama, Katsuhiko Hasebe, and Michi-hiko Mannami. Al$_3$li superlattice in al-4.5 wt.% li alloy. *Journal of the Physical Society of Japan*, 25(3):908, 1968.

111. AA Zakharov and IS Shaplygin. Synthesis and study of properties of alkali metal gallates and indates. *Zhurnal Neorganicheskoj Khimii*, 28(1):107–111, 1983.

112. AA Zakharov and IS Shaplygin. Synthesis and study of properties of alkali metal gallates and indates. *Zhurnal Neorganicheskoj Khimii*, 28(1):107–111, 1983.

113. Shaplygin I.S. Zakharov A.A. *Russian Journal of Inorganic Chemistry*, (28):59–61, 1983.

114. Hui Zhang, Shunli Shang, James E Saal, Arkapol Saengdeejing, Yi Wang, Long-Qing Chen, and Zi-Kui Liu. Enthalpies of formation of magnesium compounds from first-principles calculations. *Intermetallics*, 17(11):878–885, 2009.

115. Chong Zheng and Roald Hoffmann. An unusual electron count and electron-deficient multi-center bonding in one class of intermetallics: the baal4, caal2zn2, cemg2si2 and fcc al structures. *Zeitschrift für Naturforschung B*, 41(3):292–320, 1986.

116. E Zintl and S Neumayr. On the crystal structure of nain and the deformation of atoms in alloys. *Z. Phys. Chem. B*, 20:272–275, 1933.

Appendices

Appendix A

Difference Charge Densities of Zintl Compounds

A.1 Magnesium Compounds with Group XIII (Al, Ga, In, & Tl)

A.1.1 Gallium

MgGa[77]
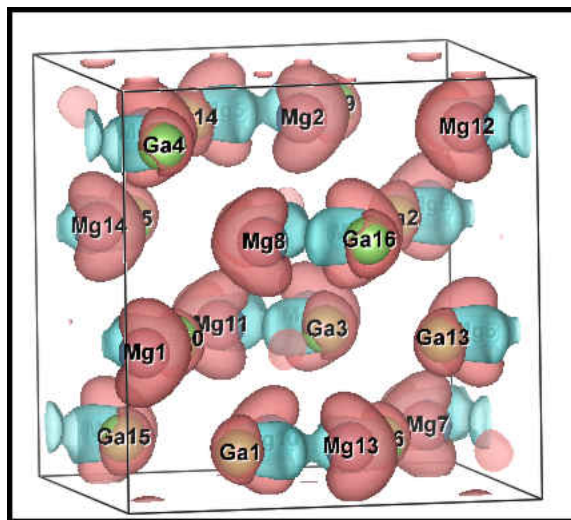
Figure A.1: Charge density is lost from the magnesium atoms, while the gallium atoms gain charge density between them to form digallium clusters, similar to those found in elemental arsenic, phosphorus, and Nitrogen.
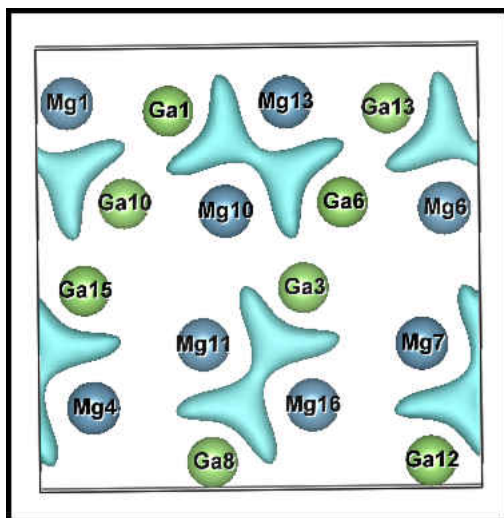
Figure A.2: Charge density is lost from the magnesium atoms, while the gallium atoms gain charge density between them to form digallium clusters, similar to those found in elemental arsenic, phosphorus, and Nitrogen. In this figure, only the charge density accumulation is seen for better clarity.
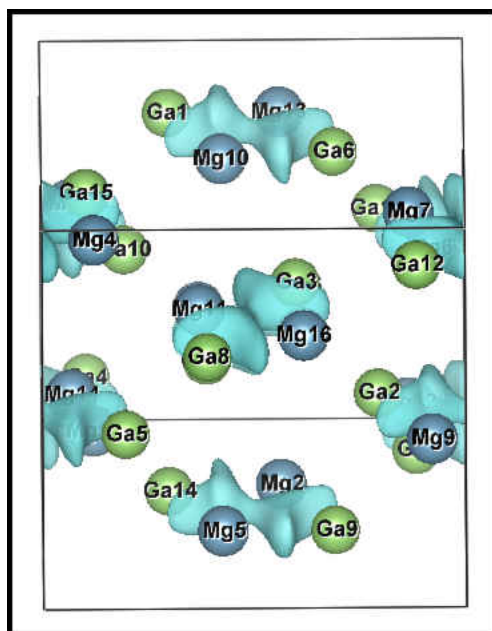
Figure A.3: In this figure one can see that these digallium clusters are discreet units and staggered in layers.

MgGa$_2$-1[81]
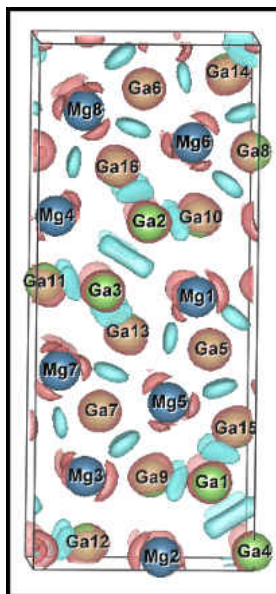
Figure A.4: The structure has a space group of oP24 (55). Charge density is lost from the magnesium atoms, while the gallium atoms gain charge density between them.
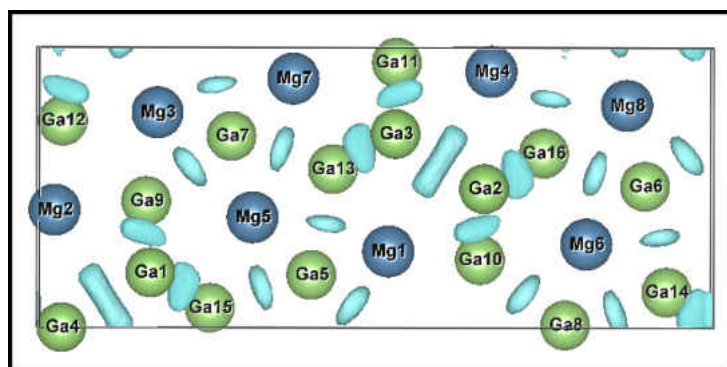
Figure A.5: The structure has a space group of oP24 (55). The gallium atoms gain charge density between them to form an anionic lattice similar to that of elemental silicon. This structure is stable at room temperature.[114]

MgGa$_2$-2[24]
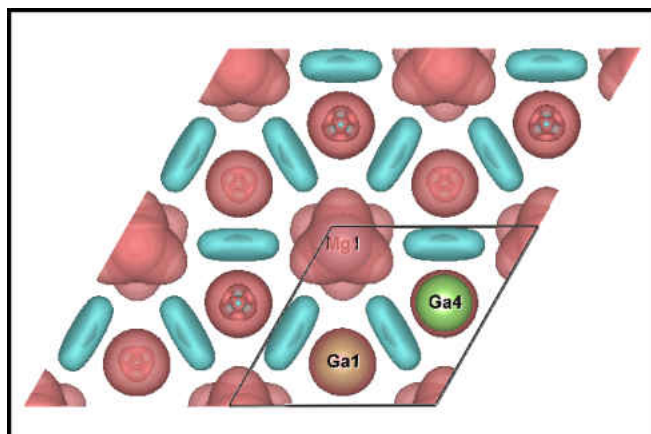
Figure A.6: The structure has a space group of $P6_3/mmc$ (194). Charge density is lost from the magnesium atoms, while the gallium atoms gain charge density between them. The gallium atoms' anionic lattice form layers of hexagonal sheets like those found in graphite.
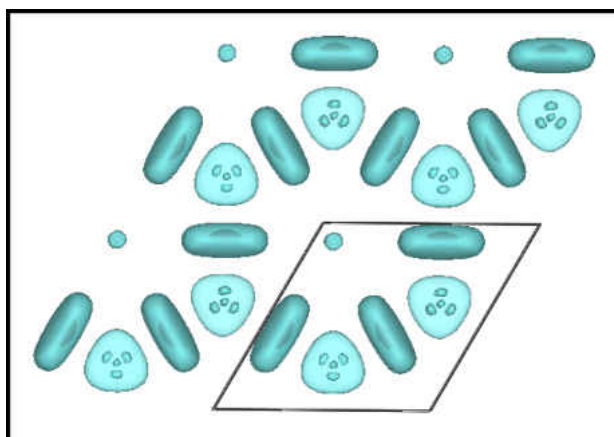
Figure A.7: The structure has a space group of $P6_3/mmc$ (194).The gallium atoms' anionic lattice forms layers of hexagonal sheets like those found in graphite. For ease of viewing, this is a top view of where the accumulation of charge density is found (between the gallium atoms).

Mg$_2$Ga[28]
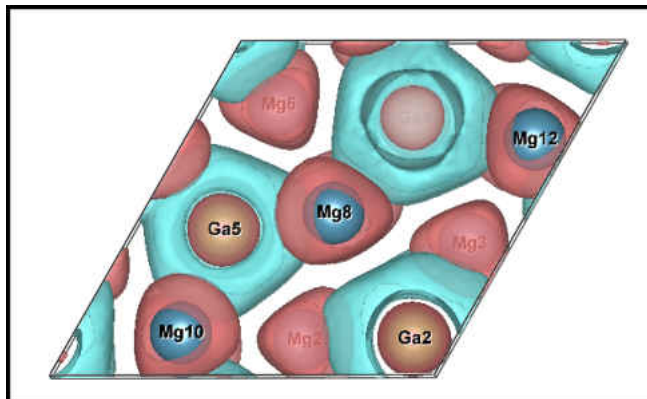
Figure A.8: Charge density is from the magnesium atoms while accumulating around and between the gallium atoms. These pack similar to that of elemental Iodine.
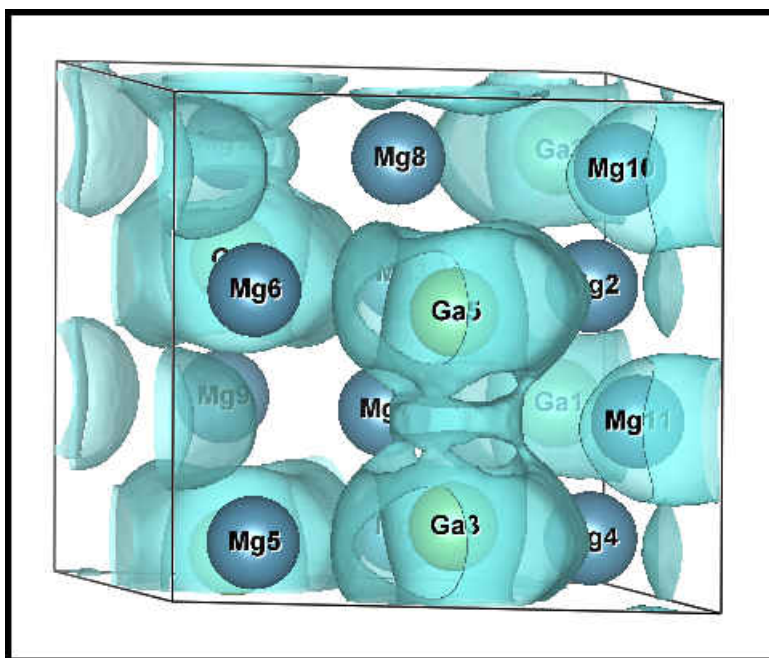
Figure A.9: The gallium atoms can be seen to form discreet clusters of digallium separated from each other by magnesium ions, forming disconnected digallium channels within the structure.

Mg₂Ga₅[82]
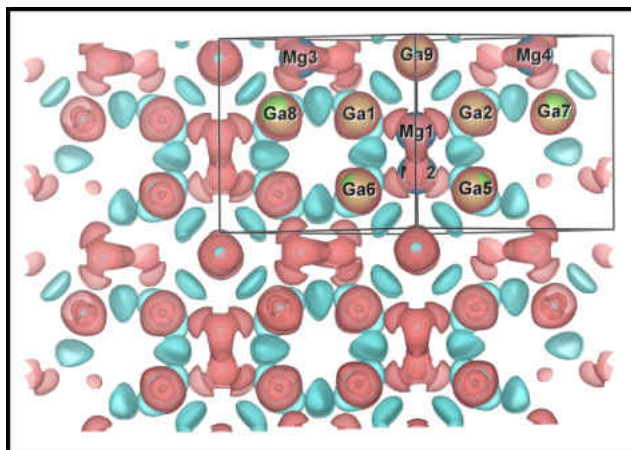
Figure A.10: Charge density is from the magnesium atoms while accumulating between the gallium atoms.
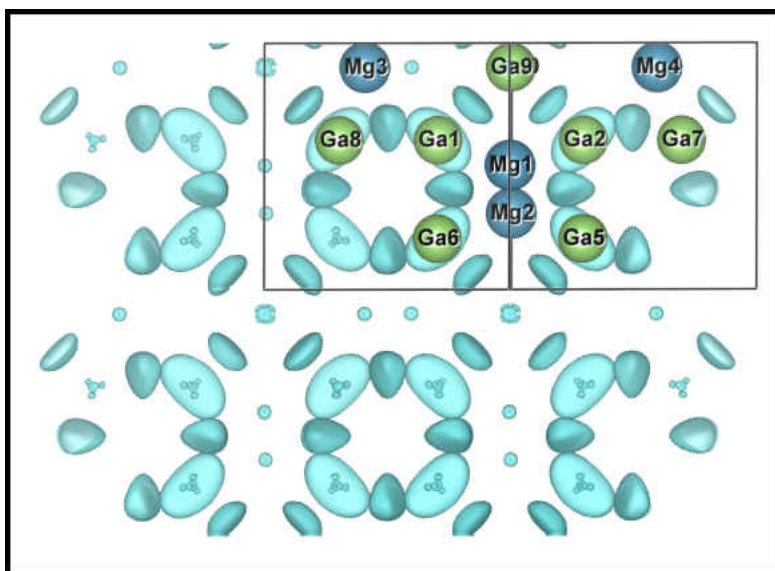
Figure A.11: In this figure, only the charge density accumulation is shown to assist the reader to more easily discern the anionic lattice formed by the gallium atoms.

A.1.2 Indium

MgIn[37]
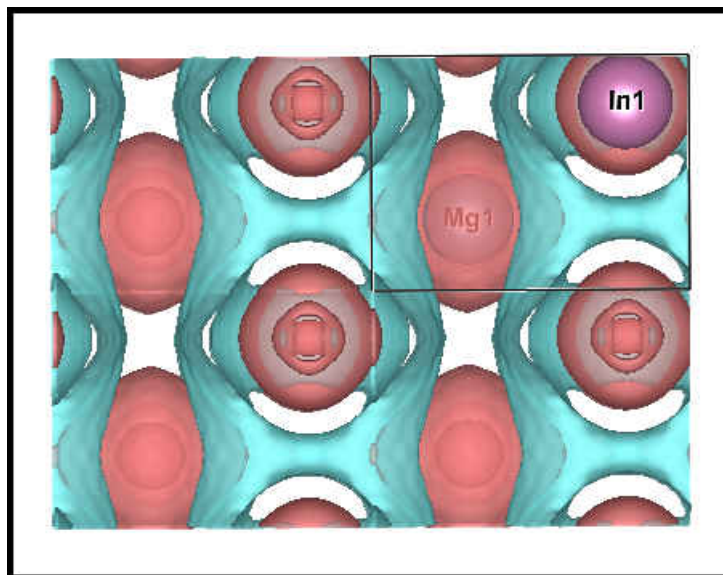
Figure A.12: Charge density is lost from the magnesium atoms while accumulating between and around the indium ions to form chains.
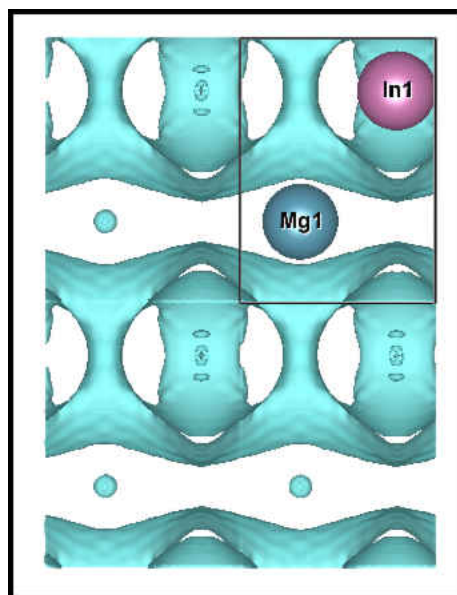
Figure A.13: Removing charge density loss and leaving only where the charge density has migrated reveals the anionic chains formed by the indium atoms.

Mg₂In[77]
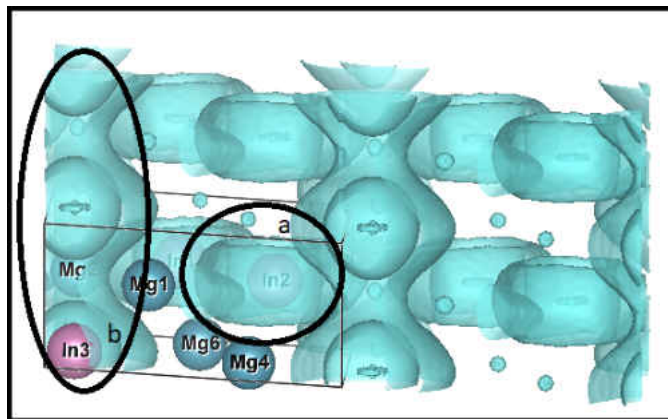
Figure A.14: Removing charge density loss and leaving only where the charge density has migrated to more clearly visualizes the bonding between the two types of indium ions. (a) Single indium ions (like In2) , separated by magnesium ions, show an increase of charge density. (b) Likewise, the second type of indium ion found by the corners (In3) have charge density built between Ga-Ga bonds to form linear chains.
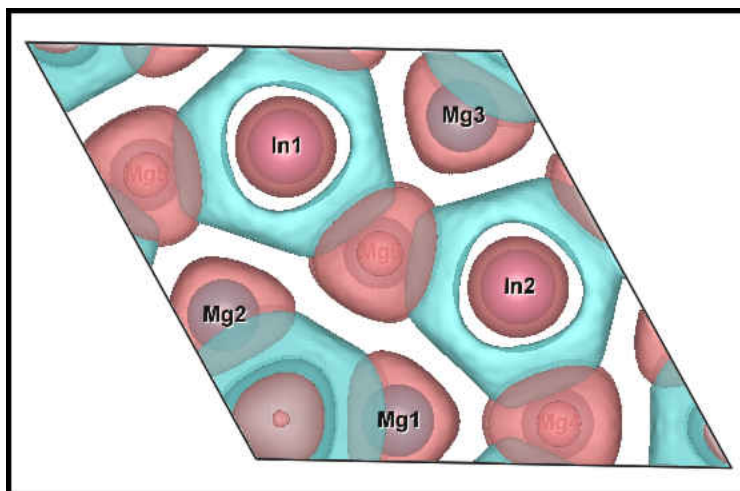
Figure A.15: Charge density is lost from the magnesium atoms, while accumulating between and around the indium ions to form both chains and channels within the structure.

A.1.3 Thallium

Mg₂Tl²⁸
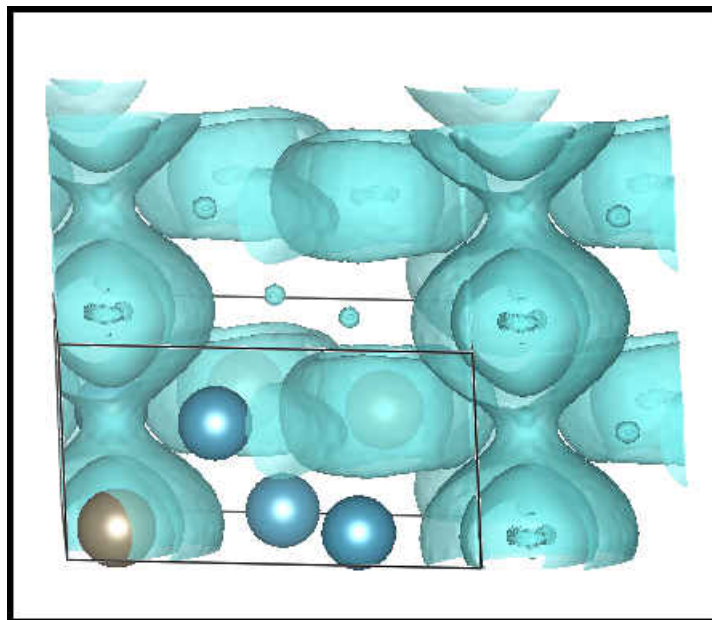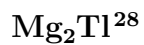
Figure A.16: Removing charge density loss and leaving only where the charge density has migrated to more clearly visualizes the bonding between the two types of thallium ions. Single thallium ions, separated by magnesium ions, show an increase of charge density. Likewise, the second type of thallium ion found by the corners have charge density built between Tl-Tl bonds to form linear chains Structure bonds and pack just like Mg_2In.
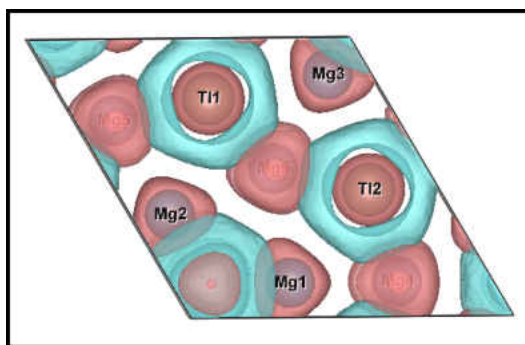
Figure A.17: Charge density is lost from the magnesium atoms, while accumulating between and around the thallium ions to form both chains and channels within the structure.

Appendix B

Oxides of Zintl Compounds

This appendix contains difference charge density maps for oxides of compounds classified as Zintl Compounds (many seen in Appendix A), which are structures that contain Group I and Group II metals (in this study Li, Na, K, Be, Mg & Ca), metals from Group XIII (Al, Ga, In, & Tl) and oxygen. All structures analyzed can be seen in table **??**. The color scheme is the same for all figures. The pink represents a loss of electron density and blue represents an increase in charge density. All of the structure's atoms show spherically gain or loss electron charge density, indicating that the crystal structures are ionic in nature. Similar to the unique behavior observed in the Zintl Compounds with calcium, in this appendix it is apparent that even with an even a more electronegative element (oxygen), in the crystal, calcium continues to accept charge density and is seen to polarized.

Oxides of Zintl-Klemm Compounds						
Oxides	Lithium	Sodium	Potassium	Beryllium	Magnesium	Calcium
$—Al_xO_y$	$LiAlO_2$ (92)	$NaAlO_2$ (33)	K_3AlO_3	$BeAl_2O_4$	$MgAl_2O_4$	$CaAl_4O_7$
	$LiAlO_2$ (166)	$NaAlO_2$ (92)				
	$LiAl_5O_8$					
$—Ga_xO_y$	$LiGaO_2$ (33)	$NaGaO_2$ (33)	K_3AlO_3		$MgGa_2O_4$	$CaGa_4O_7$
	$LiGaO_2$ (166)	$NaGaO_2$ (166)				
	$LiGa_5O_8$					
$—In_xO_y$	$LiInO_2$	$NaInO_2$			$MgIn_2O_4$	
		Na_5InO_4				
$—Tl_xO_y$		Na_3TlO_2				

Table B.1: List of Oxides found in this Appendix. The numbers in parenthesis indicate the different space groups.

B.1 Group I (Lithium) with Group XIII (Ga, In, & Tl) and Oxygen

B.1.1 —Ga$_x$O$_y$

LiGaO$_2$[113] (33)
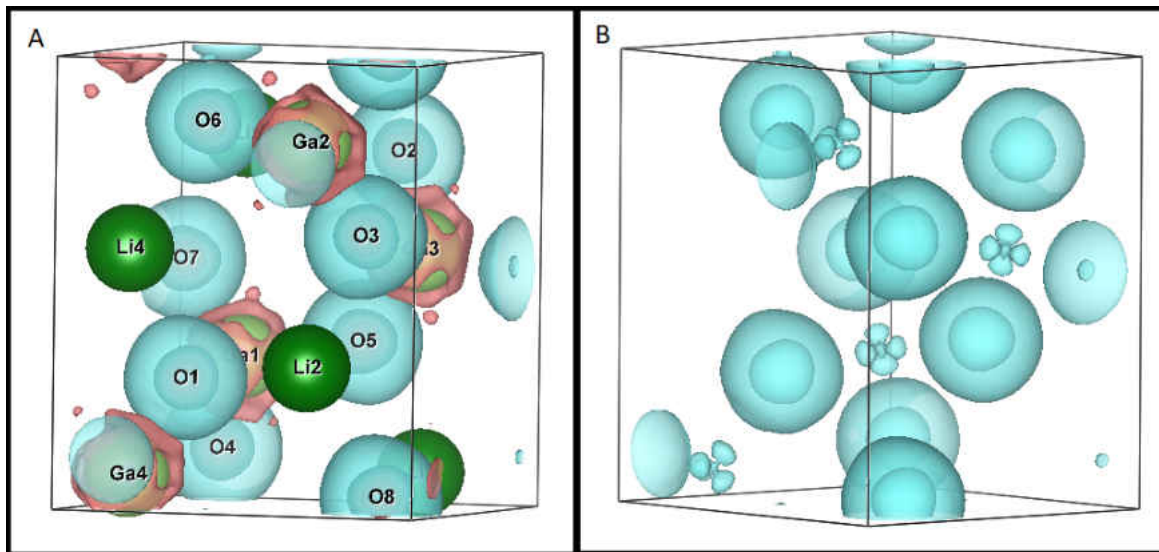
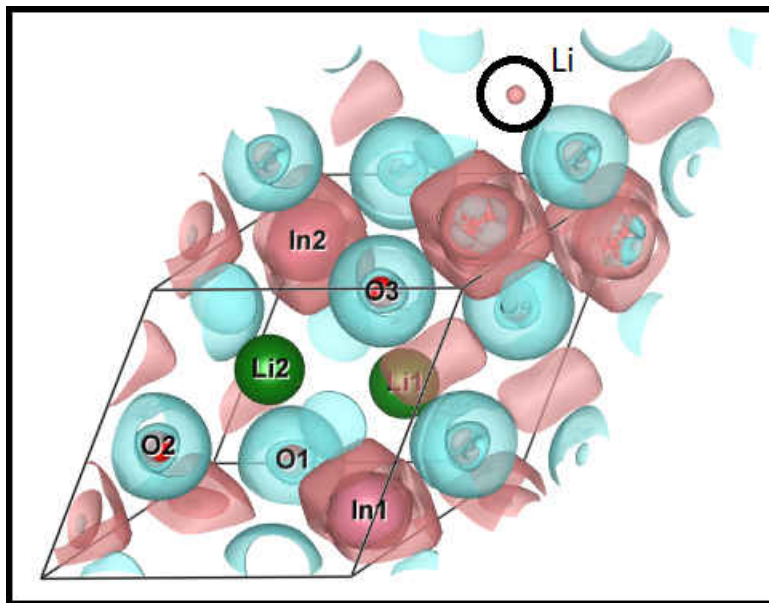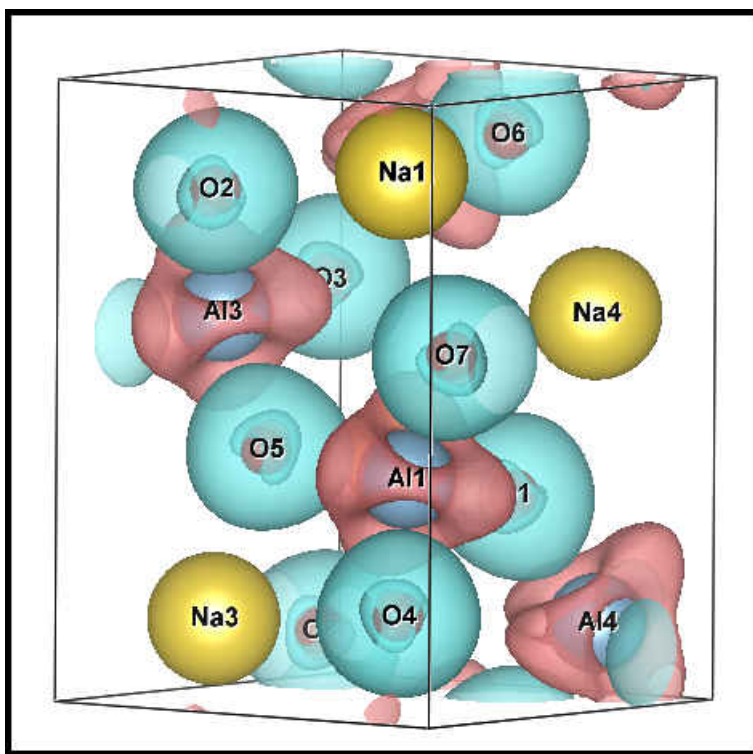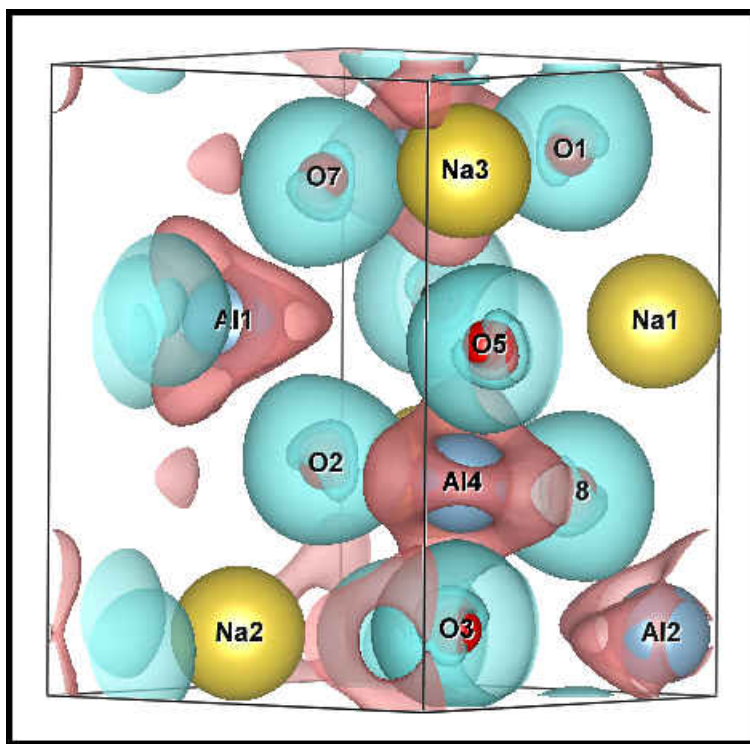Figure B.1: (A) oxygen atoms have gained charge density, spherically, while the gallium atoms and lithium atoms have lost charge density. (B) Removing the placement atoms, the figure shows no charge build up between Ga-Ga or Ga-O, though the gallium ions do seem to polarized towards the oxygen atoms.
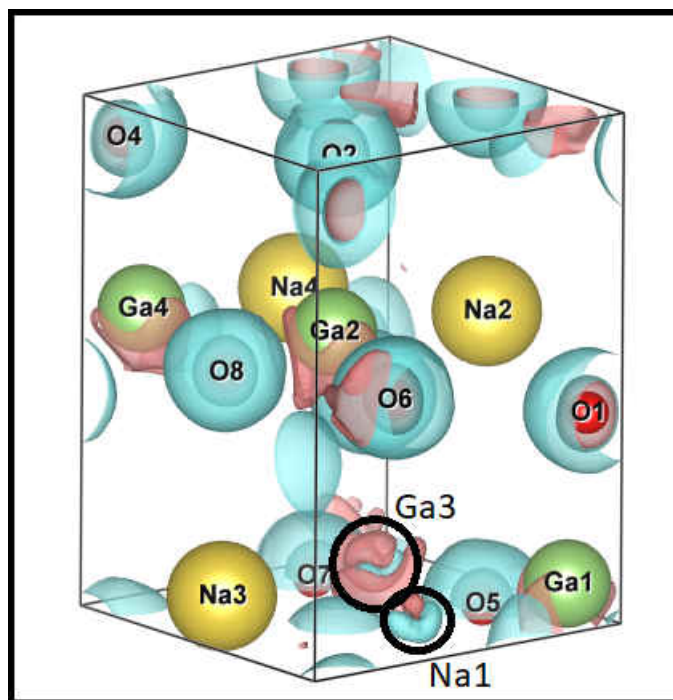
LiGaO$_2$[113] (166)
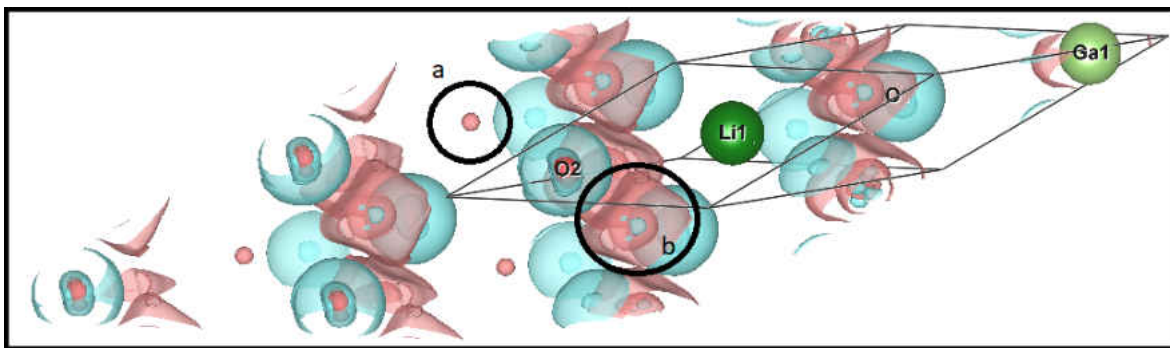
Figure B.2: oxygen atoms have gained charge density, spherically, while the (a) lithium atoms and (b) gallium atoms have lost charge density. The figure shows no charge build up between Ga-Ga or Ga-O.

LiGa$_5$O$_8$[74]
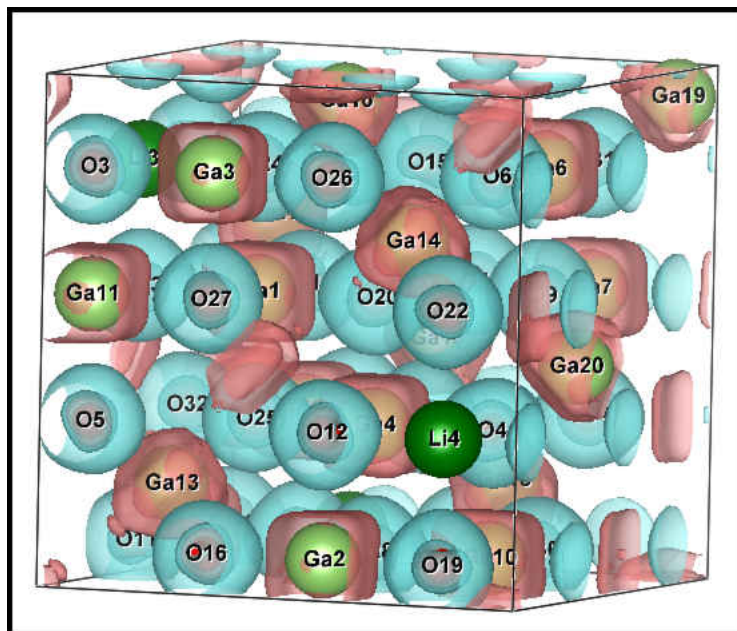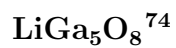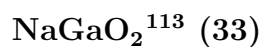

Figure B.3: oxygen atoms have gained charge density spherically while gallium atoms and lithium atoms has lost charge density.
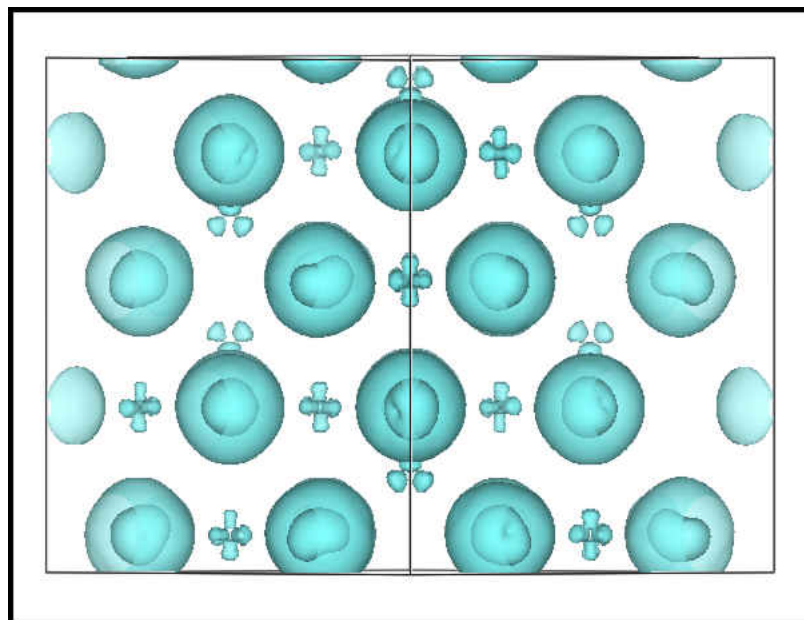
Figure B.4: Viewing only where there was charge density gain there is no charge density build up between either gallium atoms, oxygen atoms, or gallium-oxygen atoms. However, gallium ions seem to be polarized towards oxygen atoms.
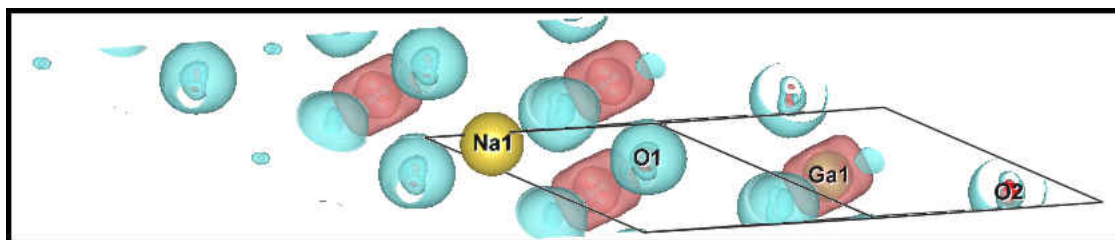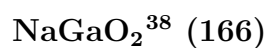
B.1.2 —In$_x$O$_y$

LiInO$_2$[30]

Figure B.5: oxygen atoms have gained charge density, spherically, while gallium atoms and lithium atoms have lost charge density. The figure shows no charge build up between Ga-Ga or Ga-O. However, the indium ion seems to be polarized towards the oxygen atoms.

B.2 Group I (Sodium) with Group XIII (Al, Ga, In, & Tl) and Oxygen

B.2.1 —Al_xO_y

$NaAlO_2$[27] (13)

Figure B.6: oxygen atoms have gained charge density, spherically, while gallium atoms and sodium atoms have lost charge density. The figure shows no charge build up between Al-Al or Al-O.
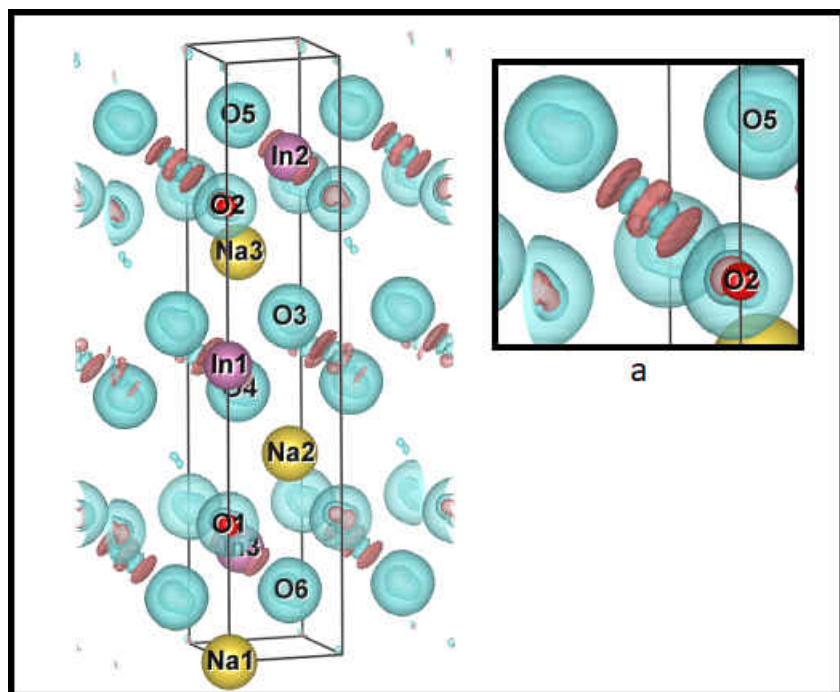
NaAlO$_2$^{91} (92)

Figure B.7: oxygen atoms have gained charge density, spherically, while gallium atoms and sodium atoms have lost charge density. The figure shows no charge build up between Al-Al or Al-O.

B.2.2 —Ga_xO_y

$NaGaO_2$[113] (33)

Figure B.8: oxygen atoms have gained charge density, spherically, while gallium atoms and sodium atoms have lost charge density. The figure shows no charge build up between Ga-Ga or Ga-O, however sodium does show its charge density has been polarized.

$NaGaO_2$[38] (166)

Figure B.9: oxygen atoms have gained charge density, spherically, while gallium atoms and sodium atoms have lost charge density. The figure shows no charge build up between Ga-Ga or Ga-O.

B.2.3 —In_xO_y

$NaInO_2$[111]

Figure B.10: oxygen atoms have gained charge density, spherically, while indium atoms and sodium atoms have lost charge density. (a) The close up of indium ions between two oxygen atoms show that the charge density of indium has been polarized toward and bridging the oxygen atoms.
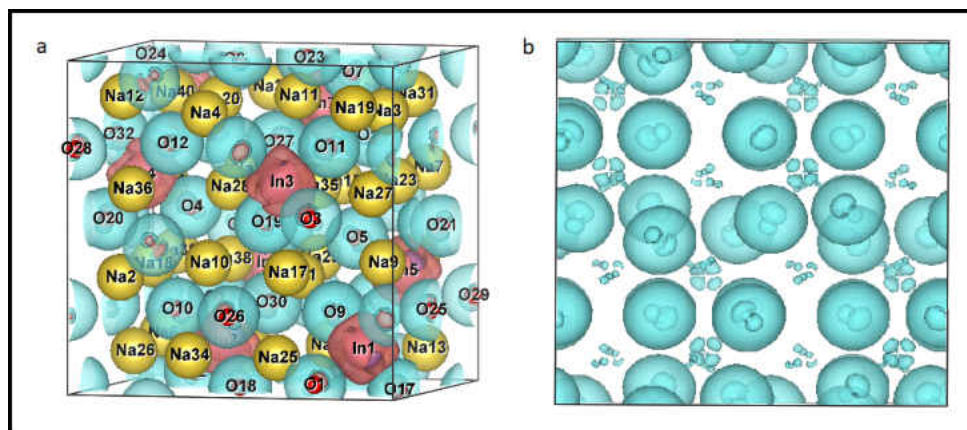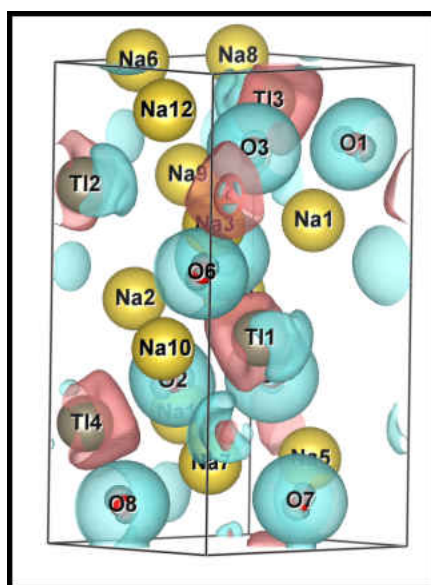
Na_5InO_4 [104]

Figure B.11: (a) oxygen atoms have gained charge density, spherically, while indium atoms and sodium atoms have lost charge density. (b) Looking at only the charge density gain the indium's charge density has been polarized tetrahedrally toward oxygen.
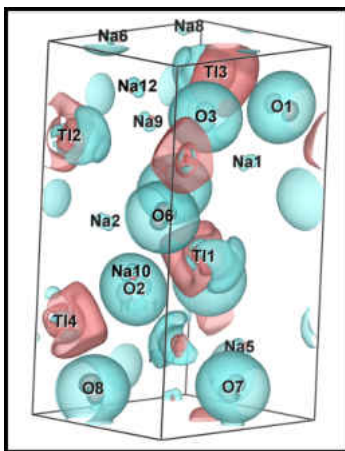
B.2.4 —Tl_xO_y

Na_3TlO_2 [103]

Figure B.12: oxygen atoms have gained charge density, spherically, while thallium atoms and sodium atoms have lost charge density.

Figure B.13: Looking at only the charge density, without the placement atoms, reveals that the thallium's charge density has been polarized away from oxygen atoms and toward the more positive sodium atoms.

B.3 Group I (Potassium) with Group XIII (Al, Ga, In, & Tl) and Oxygen
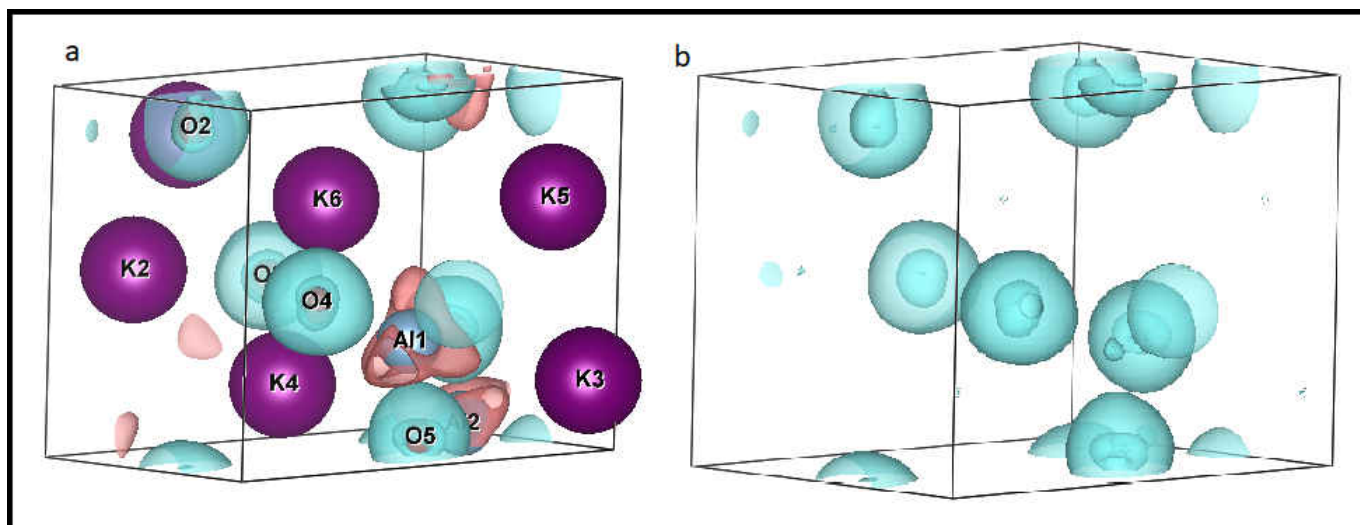
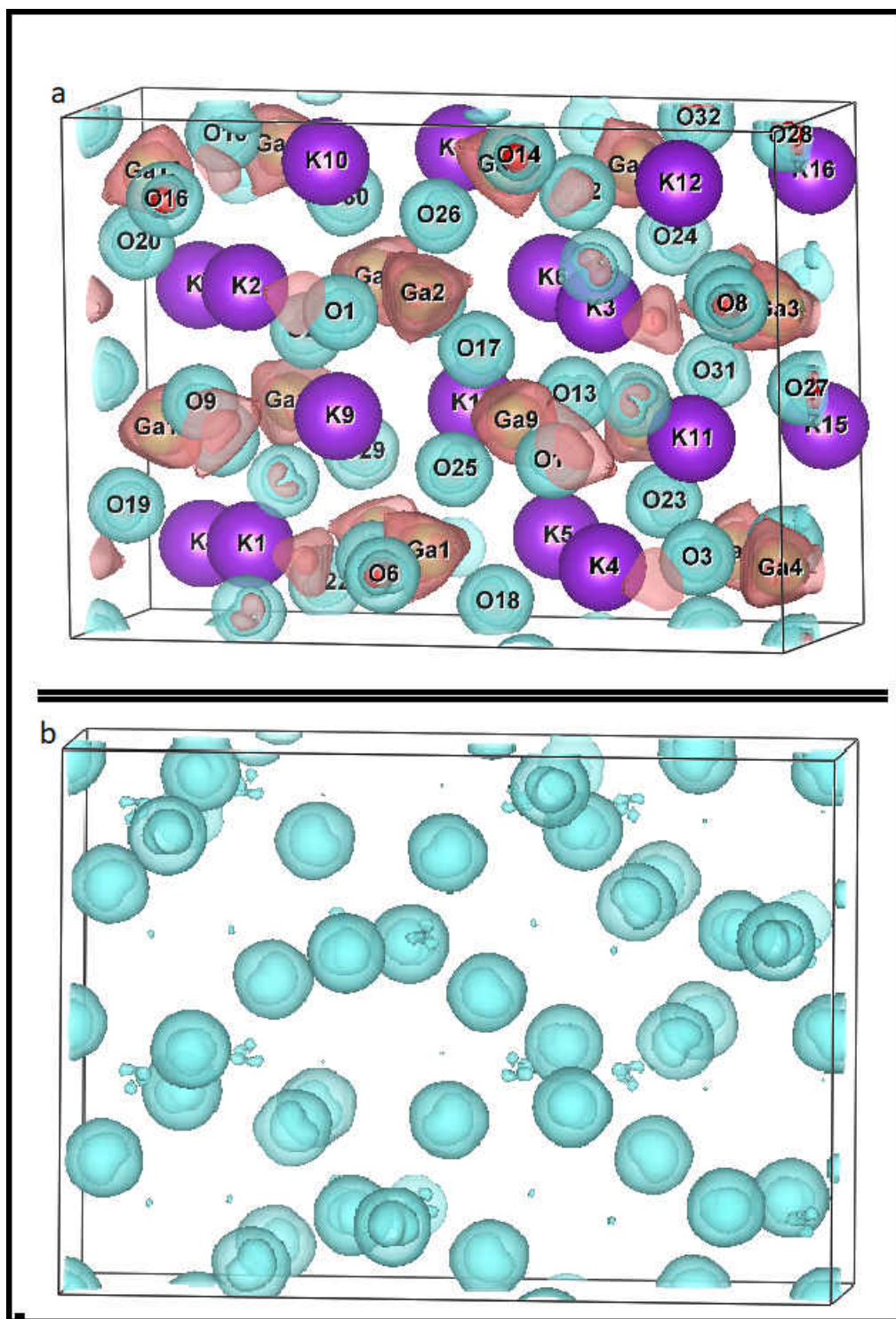### B.3.1 —Al$_x$O$_y$

K$_3$AlO$_3$[9]

Figure B.14: (a) oxygen atoms have gained charge density spherically and aluminum atoms and potassium atoms have lost charge density. (b) Removing the placement atom, the figure shows that aluminum has lost charge density spherically and that there are no polarization or Al-O or Al-Al bonds.

B.3.2 —Ga$_x$O$_y$

KGaO$_2$[112]

Figure B.15: (a) oxygen atoms have gained charge density spherically and aluminum atoms and potassium atoms have lost charge density. (b) Removing the placement atom, the figure shows that aluminum atoms have lost charge density spherically, as well and there are no polarization or Ga-O or Ga-Ga bonds.   144

B.4 Group II (Beryllium) with Group XIII (Al, Ga, In, & Tl) and Oxygen

B.4.1 —Al_xO_y
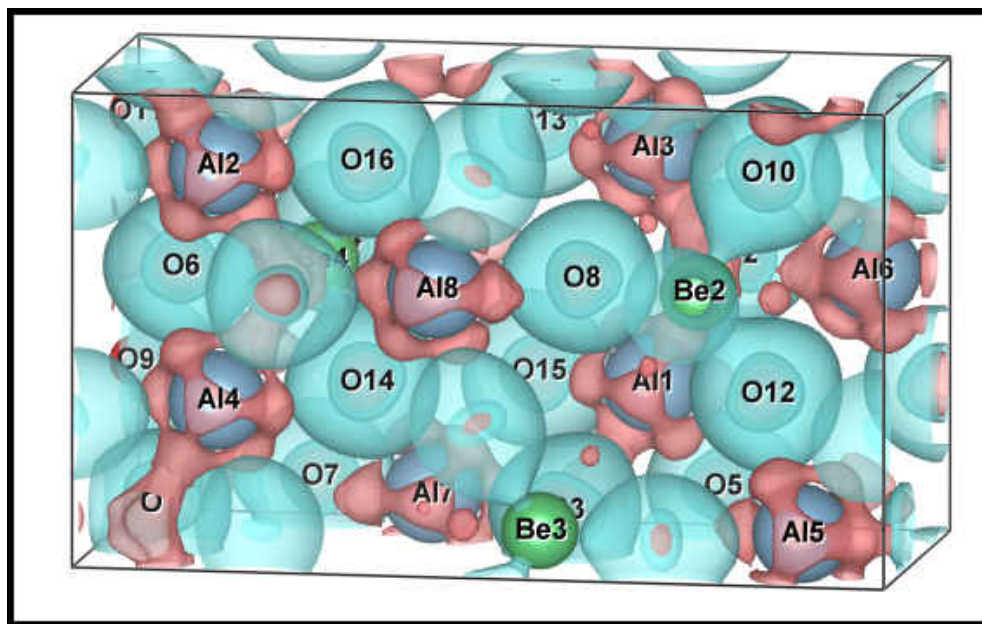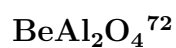
$BeAl_2O_4$[72]

Figure B.16: oxygen atoms have gained charge density while aluminum atoms and beryllium atoms have lost charge density. The charge density of oxygen atoms seem highly polarized toward beryllium atoms.
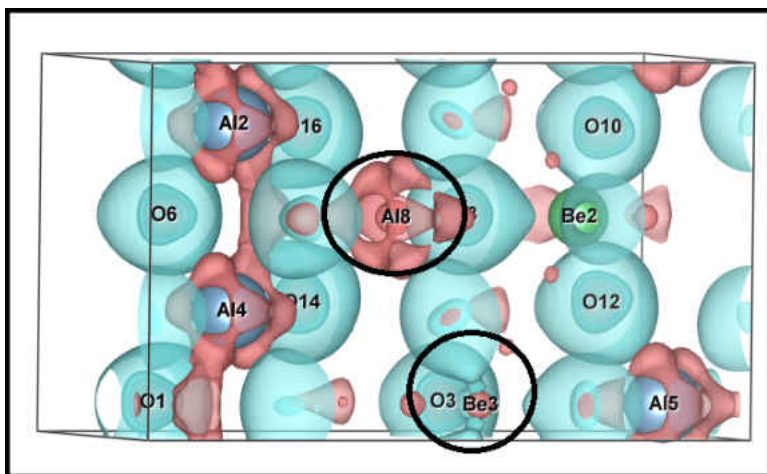
Figure B.17: Al8 and Be3's placement atoms have been removed for easier viewing. The aluminum has lost charge density and while Beryllium has lost charge density it appears that it has bonded or has a high charge density between three oxygen atoms in a trigonal planar formation. One can also see the formation of channels where charge density is lost.

B.5 Group II (Magnesium) with Group XIII (Al, Ga, In, & Tl) and Oxygen

B.5.1 —Al$_x$O$_y$
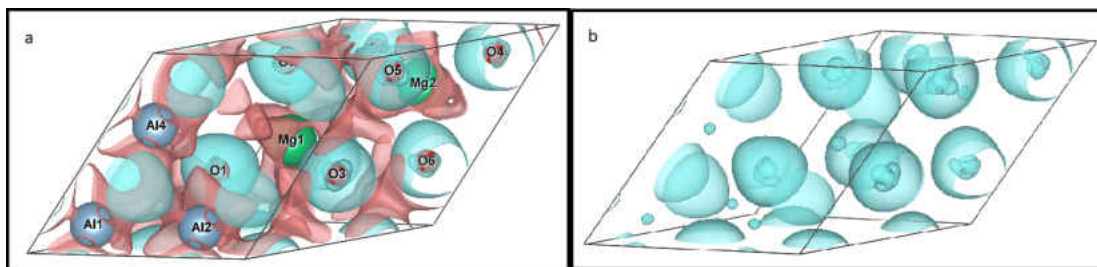
MgAl$_2$O$_4$[5]

Figure B.18: (a) oxygen atoms have gained charge density spherically. (b) Removing the placement atom, the figure shows that the aluminum atoms and magnesium atoms have lost charge density, spherically as well.
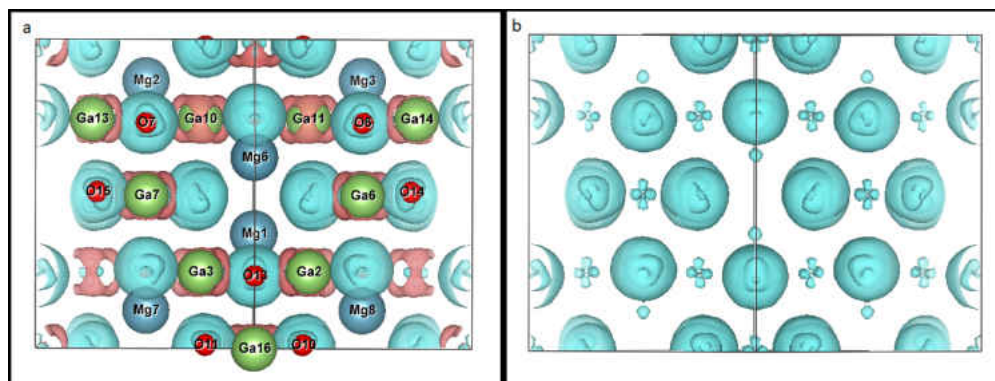
B.5.2 —Ga$_x$O$_y$

MgGa$_2$O$_4$[29]

Figure B.19: (a) oxygen atoms have gained charge density spherically. (b) Removing the placement atom, the figure shows that the gallium atoms and magnesium atoms have lost charge density. The charge density of gallium is polarized towards the oxygen atoms.

B.5.3 —In$_x$O$_y$
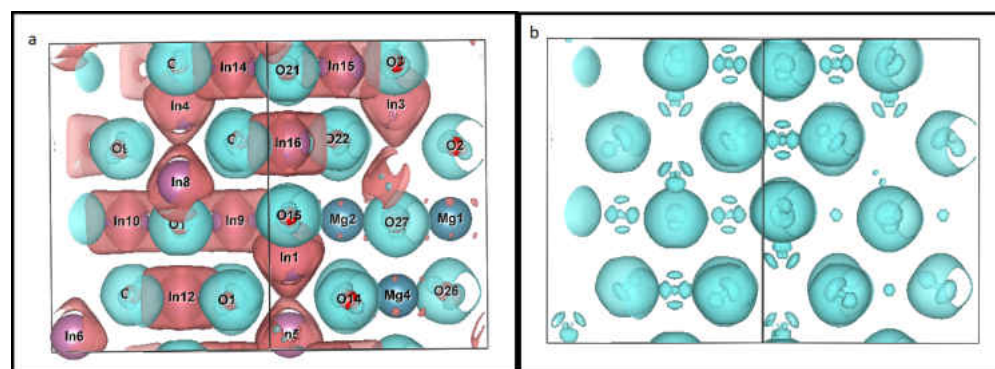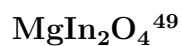
MgIn$_2$O$_4$[49]

Figure B.20: (a) oxygen atoms have gained charge density spherically. (b) Removing the placement atom, the figure shows that the indium atoms and magnesium atoms have lost charge density. The charge density of indium is polarized towards the oxygen atoms.

B.6 Group II (Calcium) with Group XIII (Ga, In, & Tl) and oxygen

B.6.1 —Ga$_x$O$_y$
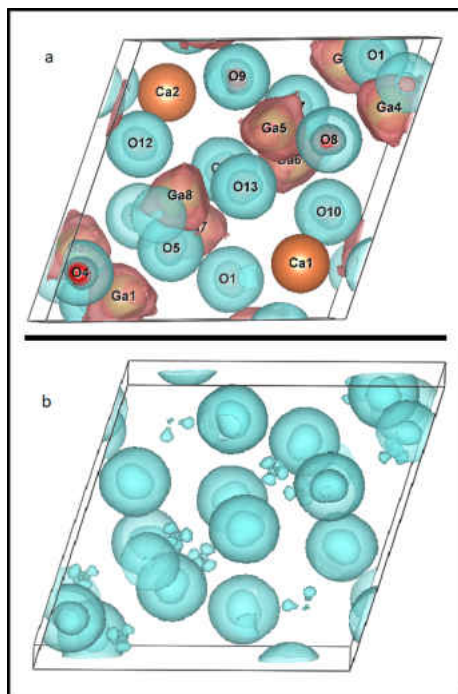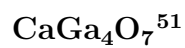
CaGa$_4$O$_7$[51]

Figure B.21: (a) oxygen atoms have gained charge density spherically. (b) Removing the placement atom, the figure shows that aluminum atoms have large charge density spherically while calcium atoms have have lost some charge density, it is polarized towards the oxygen atoms.

CURRICULUM VITAE

Sandra M. Simon

EDUCATION

Ph.D. in Chemistry [2011-2017]
University of Wisconsin – Milwaukee

B.S. in Chemistry (ACS Approved) & Criminal Justice [2006-2010]
University of Wisconsin – Milwaukee

SKILLS
Experienced in computational programs in both Windows and Linux OS:
- General computer software as well as: Microsoft office, Word, Excel, PowerPoint, Publisher, SPSS, VASP, FLAIR, CRYSTAL, OriginLabs, VESTA, Matlab, CrystalMaker, DPlot, LaTeX, LoggerPro

Experienced in the following Instrumentation and Analytical Chemical techniques:
- UV-VIS Spectroscopy, IR- Spectroscopy, Atomic Force Microscopy, Atomic Absorption, HPLC
- General sample preparation, Sample digestion, liquid-liquid separation, Filtration, distillation, sublimation, surface preparation (both manually and mechanically polished to various degrees of roughness), metal sublimation and deposition
- Chemical synthesis: inorganic and organic
- Ion-Exchange Chromatography, Column Chromatography, Thin Layer Chromatography,
- Titrations: acid-base reactions, complexation reactions, redox reactions, precipitation reactions

Administrative Skills:
- Communication: technical/non-technical writing, editing, presentations (oral/written), phone skills, scheduling, making travel and accommodation arrangements, excellent customer service
- Ordering, organizing, and maintaining inventory: chemicals, office supplies and equipment

RESEARCH
Lead Researcher (advisor Dr. Dennis Bennett) [2010-Present]
  Dissertation: "Theoretical Analysis of the Zintl-Klemm Concept and Its Extensions"
- Organized and Analyzed Complex Data Sets
- Performed Statistical Analyses on data from varying programs to verify data veracity
- Utilized Abstract Theories to verify whether connections and trends were present
- Effectively Visualized data to make connections easily discernible

EXPERIENCE
Lab Supervisor at UW-Milwaukee (Quantitative Chemistry and Seminar STEM Course) [Spring 2013-December 2016]
- Supervised and Instructed students in performing various techniques for quantitative analysis of unknown samples, while following all safety regulations (EPA Standards)
- Organized and Prepared laboratory materials, unknown samples, and pertinent equipment required for the analytical technique being taught that week
- Taught the concepts and math behind each analytical technique and prepared testing material
- "Laboratory Safety Training" Current

Chemistry Supplemental Instructor at UW-Milwaukee [Spring 2016-Present]
- Designed differentiated instructional material for Introductory Chemistry and Engineering University Students

- Taught sessions of non-required supplemental instruction with student overall turnout close to 1200 for Fall 2016 alone, increasing attendance 400% in the first two weeks of the semester
- Encouraged student success, at-risk students displaying a significant grade increase among the students that consistently attended my sessions
- Worked with Students & Veterans from varying socioeconomic backgrounds, cultures, and ages

Lead Project Organizer at UW-Milwaukee [Summer 2016]
- Consolidated and digitized chemistry supplemental instruction material for Introductory Chemistry, Chemistry for Engineers, and Chemistry for Clinical Nursing Students

Guest Lecturer at UW-Milwaukee [2009-Present]
- Requested by multiple Professors to lecture in both introductory & intermediate chemistry courses

Teaching Assistant at UW-Milwaukee [2009-2017]
- Designed tailored learning material for Taught Introductory Chemistry, Chemistry for Non-Science Majors, Quantitative Analysis, Chemistry for Engineering
- Assisted in Exam Development and Created Grading Rubrics for Course Material
- Co-Supervised five teaching assistants and Organized, Consolidated and Processed their Grades for Quantitative Analysis

COMMUNITY OUTREACH
Graduate Student Council of Chemistry and Biochemistry [2012-2013]
- President

COMPASS Mentor [2009-2010]
- For freshmen who were first generation college students in one of the STEM fields

Chemistry and Math Tutoring [2010-2015]
- For high school students, college students and veterans

Wisconsin Science Olympiad [2017]
- Assistant Event Supervisor

CULTURAL EXPERIENCES (Eager to Relocate within US and/or Abroad)
Traveling has let me experience the culture, customs, and traditions found within the people of each country
- Lived and visited multiple countries within Central and South America (Belize, Guatemala, Honduras, El Salvador, Nicaragua, Costa Rica, Ecuador, Uruguay, and Argentina); Recently visited China
- Spent more than half my life abroad and hope to continue traveling

AWARDS & HONORS
- Chancellor's Graduate Student Award [2011-2016]
- Frederick C. Hoppe Memorial Award [2011, 2012]
- Student Success Award [2014]
- Life Impact Scholarship [2006-2010]
- Durward Layde Memorial Fellowship [2008, 2009]